ALLUVIAL FAN SURFACES IN THE ATACAMA DESERT: IMPLICATIONS FOR SURFACE MODIFICATION RATES, THE EARTHQUAKE CYCLE, AND MARS

A Dissertation

Presented to the Faculty of the Graduate School

of Cornell University

in Partial Fulfillment of the Requirements for the Degree of

Doctor of Philosophy

by

Amanda Marie Baker

May 2012

ALLUVIAL FAN SURFACES IN THE ATACAMA DESERT: IMPLICATIONS FOR SURFACE MODIFICATION RATES, THE EARTHQUAKE CYCLE, AND MARS

Amanda Marie Baker, Ph.D.

Cornell University 2012

The Atacama Desert of Northern Chile is one of the oldest and driest landscapes on Earth. Many studies have referred to this landscape as relict, equating hyperaridity with abandonment as far as landscape modification is concerned. The presence of 26Ma boulders and 13Ma nitrate deposits do highlight landscape elements that have been unmoved due to a lack of precipitation since the onset of hyperaridity at least 10Ma. Evidence for more recent surface modification has caused some researchers to question the persistence of hyperaridity throughout the late Cenozic, emphasizing the potential for wetter and drier periods or even a delayed onset of hyperaridity overall.

A series of recent studies, however, have called this perspective into question. One of the predominant criticisms is the sampling of boulders as representative landscape features for surface activation. Present day mudflows and massive mobilizations of sediment during cm-scale rain events provide evidence that, despite the current hyperarid climate, significant landscape modification events can occur. The work of this thesis focuses on two sets of precipitation-driven alluvial fans in the Coastal Cordillera of the Atacama Desert, first determining a base level of activity and then using those activations to study long-term records of coseismic surface deformation and potential implications for the presence of similar features in young craters on Mars.

BIOGRAPHICAL SKETCH

Amanda Marie Schroeder grew up in northeast Ohio in the suburbs of Cleveland. As one of twenty-nine cousins, she was never lacking for company or competition. She started her schooling at St. Martin of Tours, where she was one in a class of fewer than twenty until the sixth grade. Midway through that year, she moved to Solon to join a class of over 400. Through dance, theater, writing, and Science Olympiad she eventually found her place. For undergrad she headed to Pennsylvania for Bucknell University, where she triple-majored in geology, psychology, and German. Between working as a TA, Chief Copy Editor for the Bucknellian, and studying abroad in Hamburg, her time there was as occupied as it was satisfying. While there, she met Kris Baker. The two married in August of 2007 and started graduate school at Cornell two weeks later. After a year of graduate school during which cooking and laundry were counted as free time, the two started studying at C.W. Taekwondo with Master Han Cho. Between classes and research at Cornell, fieldwork in Chile, and time at the dojang, Amanda lived her life in Ithaca fully. She and Kris tested for their black belts in January of 2011 and have been teaching Taekwondo since. She is looking forward to completing her dissertation and using her skills to move into a career that highlights her love of teaching and writing.

DEDICATION

To Kris. For everything.

To Sabumnim. For a little less.

To my family. For the rest.

ACKNOWLEDGEMENTS

My time at Cornell would not have been as productive or meaningful without the input of my mentors, students, and peers. I would like to thank my committee for doing their best to support me financially, intellectually, and emotionally throughout this process. First I must thank Rick Allmendinger for serving as my advisor. He pushed me to grow as a researcher, always maintaining high standards for my work, whether I was preparing for a national conference of simply a department seminar. I cannot thank him enough for allowing me to take the time to teach a first year writing seminar, which helped me grow both as an educator and communicator. Matt Pritchard served as a valuable sounding board and reality check when I all too often got stuck in my own head. He was an excellent listener and was always willing to provide advice on how to reach my goals, whatever those goals may be. Jim Bell has been a fresh perspective and supportive mentor, even from across the country. I cannot than him enough.

I must also acknowledge Jason Rech and Lewis Owen for the roles they played both during my fieldwork and after. Having both of them be a part of my first field season not only made it more productive, but also started a meaningful collaboration that would fill the rest of my time at Cornell. Lewis welcomed me into his lab and provided expertise and advice ever since. Jason has gone continuously out of his way to be available for advice and direction about my research and the academic world. I also want to thank Marc Caffee for the help and guidance has provided for the TCN work conducted at the PRIME lab. Thanks to Terry Spell completing the Ar-Ar dating for the

Punta de Lobos tuffs. Though none of these men were at Cornell, they played important roles in making the research I conducted here a success.

I must also send out some hearty thanks to my two field assistants: Brad Lipovsky and Chris House. Brad proved an invaluable ally and fellow food enthusiast that made the long days productive and enjoyable. Chris brought a fresh energy to my second field season. Pushing dead truck through the desert may have been terrible, but it would have been significantly worse without his strength, stamina, and positive attitude. I believe that I can speak for Chris and I both when I send our thanks to Miguel, for driving down an abandoned road, stopping to help, and driving us to Antofagasta in the middle of the night. Thank you.

I am grateful to the faculty of the Earth and Atmospheric Sciences Department, but I owe a particular debt to Chris Andronicos and Muawia Barazangi. No matter what the need or concern, Chris's door has been open to me. His advice and encouragement have been brutally honest and never once felt patronizing. Muawia has served as an example of how one person can have unyieldingly high standards for science and a truly compassionate human heart. His visits to the office always left it better than before.

My time in Snee would also have been significantly lacking if it hadn't been for the fellow graduate students I had the opportunity to share it with. In particular I must thank Chao for his honesty, Naomi for her compassion, Louise for her commitment, and Bill for his unpretentious but sincere love of science. Ryan Anderson for coming to my

rescue. Phoebe, after spending five years at desks no more than five feet apart, there isn't enough thanks in the world.

Of all of my work at Cornell, the most exhausting and most fulfilling was my time as an instructor for a first year writing seminar. I gratefully acknowledge the Knight Writing Institute for their funding and faith in my ability to create a new course. That thanks must also be shared with Rick, for allowing me to devote a semester to teaching. Katy Gottschalk, Joe Martin, Louise, and Deborah provided me with the tools to succeed. My students made the experience unforgettable.

I cannot conclude without thanking the support provided outside of my academic life. My parents have been dedicated and constant supporters since the start of my academic career at St. Martin of Tours elementary school. My brother has been brutally honest about both his standards for academic work and his faith in my abilities, a true supporter in the best way he knows how. Han Cho, forever my Sabumnim, for trusting me and pushing me harder than I ever thought possible. And Kris, for everything.

I also gratefully acknowledge the generous sources of my funding throughout my time at Cornell. Thanks to the Earth and Atmospheric Sciences faculty, for selecting me for the McMullen Fellowship and the NASA Space Sciences Graduate Fellowship. Thanks to the Knight Writing Institute for their funding during my semester of teaching. I also would like to thank Rick for the three years of support from NSF grant EAR 0738507. This funding made my time and success at Cornell possible.

TABLE OF CONTENTS

LIST OF FIGURES

LIST OF TABLES

0 INTRODUCTION

The Atacama Desert of Northern Chile is one of the oldest (Dunai et al., 2005; Nishiizumi et al., 2005) and driest (Houston and Hartley, 2003) landscapes on Earth. Many studies have referred to this landscape as relict, equating hyperaridity with abandonment as far as landscape modification is concerned. The presence of 26Ma boulders (Dunai et al., 2005) and 13Ma nitrate deposits (Rech et al., 2003) do highlight landscape elements that have been unmoved due to a lack of precipitation since the onset of hyperaridity at least 10Ma (Houston and Hartley, 2003; Nishiizumi et al., 2005; Hoke et al., 2004; Rech et al., 2006; Kober et al., 2007). The hyperarid climate of the Atacama Desert is the result of a combination of factors, including the Humboldt current and Hadley circulation to the west and the Andean rain shadow in the east. Hyperiaridity here is defined in the context of both precipitation and potential evapotranspiration (Houston & Hartley, 2003; Ewing et al., 2006).

Evidence for more recent surface modification has caused some researchers to question the persistence of hyperaridity throughout the late Cenozic, emphasizing the potential for wetter and drier periods (Placzek et al., 2009) or even a delayed onset of hyperaridity overall (Hartley & Chong, 2002). A series of recent studies, however, have called this perspective into question (Evenstar et al., 2009; Hall et al., 2008; González et al., 2006; Plazcek et al., 2010). One of the predominant criticisms is the sampling of boulders as representative landscape features for surface activation (Hall et al., 2008; Placzek et al., 2010). Present day mudflows and massive mobilizations of sediment during cm-scale rain events provide evidence that, despite the current hyperarid

climate, significant landscape modification events can occur (e.g. Ramirez & Perez, 2011).

The Atacama also provides an important record of the tectonic history of the South American subduction zone. This plate boundary has generated some of the largest earthquakes ever recorded. The Atacama spans three rupture segments in northern Chile, including the well-known seismic gap near Iquique (e.g. Loveless et al., 2009). These segments have produced earthquakes Mw ~8 every 100-150 years (Comte & Pardo, 1991). The magnitude of these earthquakes is often attributed to the sediment-starved nature of the trench resulting in particularly strong coupling of the plates (Hackney et al., 2006). Developing a greater understanding of sediment transport within a hyperarid environment plays a key role in being able to address potential links between climate and tectonics within this system. Located in the forearc of the South American subduction zone, the Coastal Cordillera contains a particularly important record. The Coastal Cordillera is bounded to the west by ~1000m escarpment and grades gradually to the central valley in the east. Its hyperarid landscape and tectonically important location make it an ideal location for studying the mobilization of sediment within a hyperarid regime. The work of this thesis focuses on two sets of precipitation-driven alluvial fans in the Coastal Cordillera of the Atacama Desert, first determining a base level of activity and then using those activations to study long-term records of coseismic surface deformation and potential implications for the presence of similar features in young craters on Mars.

Chapter one of the dissertation focuses on the Terrestrial Cosmogenic Nuclide (TCN) surface age dating of the alluvial fan surfaces using ^{10}Be and ^{26}Al. We discuss the age and frequency of the activations in the context of other surfaces throughout the Atacama that have been dated using smaller clasts and discuss the level surface modification that can be expected in a hyperarid environment. Chapter two uses the ages of the fan surfaces in conjunction with the extensive coseismic crack population in the Coastal Cordillera to determine a long-term strain rate due to cracking as well as cracking from single earthquake events. We compare those strains to the coseismic extension recorded by GPS from recent nearby earthquakes to assess the potential role permanent surface deformation may be playing in the supposedly elastic geodetic rebound signal. The third chapter highlights attributes of the Atacama Desert that contribute to the extremely efficient mobilization of sediment that occurs during decade-to-century, cm-scale rain events. Using visual and nighttime Thermal Emission (THEMIS) imagery, we search for evidence of these characteristics on young Martian fans and discuss potential implications for fleeting precipitation versus broader climate sources of rain on Mars.

WORKS CITED

Comte, D. and Pardo, M. 1991. Reappraisal of great historical earthquakes in the northern Chile and southern Peru seismic gaps. Natural Hazards 4, 23-44.

Dunai, T.J., Gonzáles López, G.A., and Juez-Larré, J., 2005. Oligocene-Miocene age of aridity in the Atacama Desert revealed by exposure dating of erosion-sensitive landforms. Geology 33, 321-324.

Evenstar, L.A., Hartley, A.J., Stuart, F.M., Mather, A.E., Rice, C.M., and Chong, G., 2009. Multiphase development of the Atacama planation surface recorded by cosmogenic 3He exposure ages: Implications for uplift and Cenozoic climate change in western South America. Geology, 37, 27-30.

González, G.L., Dunai, T., Carrizo, D., and Allmendinger, R., 2006. Young displacements on the Atacama Fault System, Northern Chile from field observations and cosmogenic ^{21}Ne concentrations. Tectonics 25, TC3006.

Hackney, R.I., Echtler, H.P., Franz, G., Götze, H.J., Lucassen, F., Marchenko, D., Melnick, D., Meyer, U., Schmidt, S., Tasarova, Z., Tassara, A. and Weinecke, S. 2006. The segmented overriding plate and coupling at the south-central Chilean margin (36-42ºS). In *The Andes: Frontiers in Earth Sciences.* Springer, Part III. 355-374.

Hall, S.R., Farber, D.L., Audin, L., Finkel, R.C., and Mériaux, A.-S., 2008. Geochronology of pediment surfaces in southern Peru: implications for quaternary deformation of the Andean forearc. Tectonophysics 459, 186-205.

Hartley, A.J. and Chong, G., 2002. Late Pliocene age for the Atacama Desert: implications for the desertification of western South America. Geology 30, 43-46.

Hoke, G.D., Isacks, B.L., Jordan, T.E. and Yu, J.S., 2004. Groundwater-sapping origin for the giant quebradas of northern Chile. Geology 32, 605-608.

Houston, J. and Hartley, A., 2003. The central Andean west-slope rainshadow and its potential contribution to the origin of hyper-aridity in the Atacama Desert. International Journal of Climatology 23, 1453-1464.

Loveless, J.P., Allmendinger, R.W., Pritchard, M.E., Garroway, J.L. and González, G.

2009. Surface cracks record long-term seismic segmentation of the Andean margin. Geology 37, 23-26.

Kober, F., Ivy-Ochs, S., Schlunegger, F., Baur, H., Kubik, P.W., and Wieler, R., 2007. Denudation rates and a topography-driven rainfall threshold in northern Chile: multiple cosmogenic nuclide data and sediment yield budgets. Geomorphology 83, 97-120.

Nishiizumi, K., Caffee, M.W., Finkel, R.C., Brimhall, G., and Mote, T., 2005. Remnants of a fossil alluvial fan landscape of Miocene age in the Atacama Desert of northern Chile using cosmogenic nuclide exposure age dating. Earth and Planetary Science Letters 237, 499-507.

Placzek, C.J., Matmon, A., Granger, D.E., Quade, J., and Niedermann, S., 2010. Evidence for active landscape evolution in the hyperarid Atacama from multiple terrestrial cosmogenic nuclides. Earth and Planetary Science Letters 295, 12-20.

Placzek, C., Quade, J., Betancourt, J.L., Patchett, J.P., Rech, J.A., Latorre, C., Matmon, A., Holmgren, C., and English, N.B., 2009. Climate in the dry central Andes over geologic, millennial, and interannual timescales. Annals of the Missouri Botanical Garden 96: 386-397.

Ramirez, F.J. and Perez, P.C., 2011. Passing volume calculation system (PVCS): computer software for managing data on watersheds that produce mud flows and the case of Quebrada La Cadena, Antofagasta, Chile. Natural Hazards, doi: 10.1007/s11069-011-9744-5.

Rech, J.A., Currie, B.S., Michalski, G., and Cowan, A.M., 2006. Neogene climate change and uplift in the Atacama Desert, Chile. Geology 34, 761-764.

Rech, J.A., Quade, J., and Hart, W.S., 2003. Isotopic evidence for the source of Ca and S in soil gypsum, anhydrite and calcite in the Atacama Desert, Chile. Geochimica et Cosmochimica Acta 67, 575-586.

CHAPTER 1

1 ACTIVE ALLUVIAL FANS IN A HYPERARID LANDSCAPE: ATACAMA DESERT, CHILE

1.1 Introduction

The Atacama Desert (Figure 1.1) is considered one of the oldest (Dunai et al., 2005; Nishiizumi et al., 2005) and driest (Houston and Hartley, 2003) landscapes on Earth. The hyperaridity in this region has resulted in the formation of gypsum soils and thick accumulations of nitrates (Rech et al., 2003). In addition, boulders and cobbles on pediments, alluvial fans, and terraces yield some of the world's oldest terrestrial cosmogenic nuclide (TCN) surface exposures ages (Dunai et al., 2005; Nushiizumi et al., 2005). This suggests that surfaces and the landscapes throughout the Atacama Desert are extremely old and possibly inactive, and that they have been very dry for at least the last 10 Ma (Houston and Hartley, 2003; Nishiizumi et al., 2005; Hoke et al., 2004; Rech et al., 2006; Kober et al., 2007). Some researchers have questioned the persistence of hyperaridity throughout the late Cenozic, emphasizing the potential for wetter and drier periods (Placzek et al., 2009) or even a delayed onset of hyperaridity overall (Hartley & Chong, 2002). Hyperaridity in this case can be qualified by the ratio of precipitation to potential evapotranspiration (Ewing et al., 2006). The conflicting interpretations might reflect the different methods used, and the surfaces and sample examined. To help examine whether a particular climate event has influenced landscape stability, we report on new TCN and Ar-Ar ages for alluvial fan surfaces showing their development during the Quaternary, and together with compiled regional TCN surface

Figure 1.1: Regional location shown on inset of South America. Location of study areas shown on digital elevation model of the Atacama Desert region. Study Area 1 refers to the Punta de Lobos fault region and Study Area 2 refers to the Mititus fault region. Major morphologic zones include the Coastal Cordillera, Central Depression, Cordillera Domeyko, and the Western Slope.

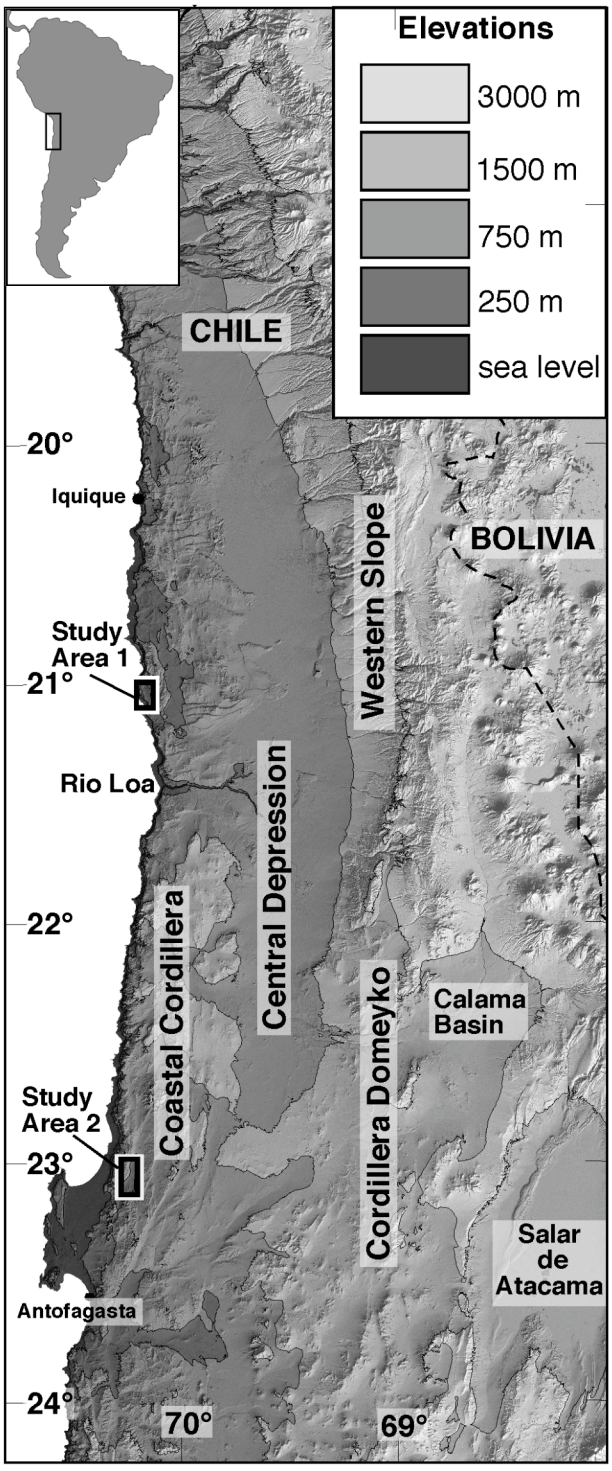
Elevations
3000 m
1500 m
750 m
250 m
sea level
CHILE
BOLIVIA
20°
Iquique
Study Area 1
21°
Rio Loa
22°
Study Area 2
23°
Antofagasta
24°
70°
69°
Western Slope
Central Depression
Coastal Cordillera
Cordillera Domeyko
Calama Basin
Salar de Atacama

ages we constrain what level of surface activity and modification is characteristic of a hyperarid environment. Determining what climatic and geomorphic characteristics are representative of the Atacama Desert for the last 10 Ma is difficult, particularly given that the region stretches for 1000 km N-S and 200 km E-W and because of the paucity of geomorphic data. Despite the expanse, groups of ages can provide insight into patterns of activity throughout the region, and then allow for the identification of potential exceptions to those patterns. For example, the occurrence of multiple 500 ka old boulders on what was considered a 5 Ma landscape redefined perceptions of activity in the region (Plazcek et al., 2010). Such instances are often written off as examples of local influences, such as tectonic stresses (Hall et al., 2008, González et al., 2006), groundwater input (Hall et al., 2008), or even localized influxes of atmospheric moisture (Plazcek et al., 2010). However, when taken together a pattern of landscape modification < 1.2 Ma begins to emerge. By measuring TCNs on low-angle, precipitation-driven alluvial fan deposits in the driest latitudes of the Coastal Cordillera, near landforms that have yielded 5-10 Ma ages, we explore whether Quaternary landscapes in the central latitudes of the Atacama were actively being modified by geomorphic processes in a landscape that was formally considered essentially inactive. Surface activation in the current work refers to the mobilization of and deposition of sediment on that surface. The surfaces we date, however, do not negate the persistence of hyperaridity throughout the Quaternary, but rather they begin to highlight that active modification of surfaces that can take place within the confines of a hyperarid climate regime.

1.2 Regional Setting

1.2.1 Geologic Setting

The Atacama Desert extends from southern Peru to northern Chile and from the Pacific Ocean to the western flank of the Andes (Figure 1.1). From west to east, the area can be divided longitudinally into four major morphologic zones: 1) the Coastal Cordillera; 2) the Central Valley; 3) the Sierra de Domeyko; and 4) the Western Andean Flank (Figure 1.1). As the westernmost of these zones, the Coastal Cordillera is bounded by the coastal escarpment that rises ~1000 m from the narrow coastal platform. To the east it grades down more gently into the Central Valley, serving as a potential barrier for Pacific moisture to the desert's slightly lower-lying core. The entire region is dominated by saline soils, which blanket most surfaces with a meter-scale crust, but the extent and thickness of these soils vary by region (e.g., Rech et al., 2003; Ewing et al., 2006). Transect studies show that the input of water for these soils varies from groundwater in the east to marine aerosols in the west (Rech et al., 2003).

Most of the Coastal Cordillera is within 150 km of the Peru-Chile trench of the South American-Nazca Plate boundary and is subject to Pliocene to Recent tectonic activity. Studies such as Comte and Pardo (1991) and Pritchard et al. (2006). document modern and historical seismic activity in the region. González et al. (2006) and Allmendinger and González (2010) document activation and reactivation of faults throughout the Coastal Cordillera. Some faults cut smaller depositional surfaces such as alluvial fans (González et al., 2006), while others can be seen offsetting the coastal escarpment itself (Carrizo et al., 2008). Marine terraces record a continued history of uplift, further

indicating the developing nature of what is often considered a relict landscape (Hartley & Jolley, 1995).

1.2.2 Climate Setting

The hyperarid climate of the Atacama Desert is the result of a combination of factors, including the Humboldt current and Hadley circulation to the west and the Andean rain shadow in the east. Much of the desert can be qualified as hyperiarid, based on both precipitation and potential evapotranspiration (Houston & Hartley, 2003; Ewing et al., 2006). Slightly more humid areas are present at the base of the Western Andean Flank and along the lower elevations of the coastal escarpment. The vegetation on the Western Flank is probably supported primarily by rare summer precipitation that is sourced from over the Andes (Latorre et al., 2002). This intermittent precipitation that does not reach the core of the desert, where extremely soluble soil nitrates have been accumulating for more than 13 Ma (Rech et al., 2006).

The Coastal Cordillera is isolated from the moisture sourced over the Andes and, despite its proximity to the Pacific, is largely unable to support vegetation. The current moisture in the Coastal Cordillera stems from the cold air fronts that form over the Pacific Ocean during the winter months, yielding sparse rainfall that affects mostly lower elevations and a thick coastal fog affecting elevations between ~300 m and ~1000 m above sea level (asl) (Rech et al., 2003). Much of the Coastal Cordillera is above ~1000 m asl and does not experience rainfall but is influenced by the fog. This fog, known locally by as camanchaca, plays an integral role in the formation of the crusty soil salts that are responsible for the durability and preservation of geomorphic surfaces (Rech et

al, 2003). Both modern and geologic records track a history of rare, punctuated precipitation events throughout the Atacama (e.g., Houston & Hartley, 2003; Houston, 2006; McKay et al., 2003). The potential significance of such events, which seldom amount to > 30 mm per event, will be addressed more thoroughly in the discussion.

1.3 Terrestrial cosmogenic nuclides methods

TCNs can be used to determine the exposure age or erosion rate within a geomorphic system (Gosse & Phillips, 2001). The methods assume that rocks have experienced a constant rate of erosion since exposure, have not been buried, and have not changed elevation enough to affect the production rates (Gosse & Phillips, 2001). For sediments and clasts in a depositional system, such as an alluvial fan, the TCN concentrations can be produced before erosion, during transport, and/or after deposition. TCNs produced before erosion and transportation are considered as derived TCNs and can result in overestimates of the age of sediments and clasts. To provide an estimate of the possible inheritance, we sampled an incised alluvial fan channel. In addition, we sampled sediments from a bajada and bedrock to provide data on how quickly the bedrock may be eroded and how long sediment is stored in the bedrock-alluvial fan system. It was not possible to collect samples from depth profile work to test for inheritance because the alluvial fans were so highly indurated it was not possible to dig into them.

Samples for TCN determination were collected from alluvial fan surfaces, bedrock and an alluvial fan channel. Sampling on alluvial fan surfaces was undertaken after a relative morphostratigraphy was developed using a combination of IKONOS imagery

and fieldwork to be more thoroughly described later (Figure 1.2). Samples for each of the fan surfaces included fist-sized clasts of vein quartz that were processed individually and pebble-sized clasts of vein quartz that were amalgamated and processed together (Table 1.1). Where large clasts were not available, on the bajada and in the active channel, multiple amalgamation samples of the vein quartz pebbles were taken. Sediment samples were also taken from within the active channel. Granodiorite bedrock samples were taken from three points within the source drainage for Channel 1. No outcrop of the quartz vein was found in the source drainage area. In total, samples included 8 individual clasts, 8 amalgamated samples, 3 sediment samples, and 3 samples of granodiorite bedrock (Table 1.1).

Isolation of quartz, chemical separation of Be and Al, and preparation of BeO were undertaken in the geochronology laboratories at the University of Cincinnati. Samples from clasts were crushed and sieved to obtain the 250–500 μm size fraction. Sand samples were sieved to collect the 250-500 μm size fraction. This fraction was chemically leached with a minimum of four acid leaches: aqua regia for >9 h; two 5% HF/HNO_3 leaches for ~ 24 h; and one or more 1% HF/HNO_3 leaches each for ~24 h. Acid-resistant and mafic minerals were removed from the residue after the first 5% HF/HNO_3 leach by a heavy liquid separation with lithium heteropolytungstate (density 2.7 g/cm^3). A low-background Be carrier ($^{10}Be/^{9}Be = 3.09x\ 10^{-15}\pm1.52x10^{-15}$) and Al carrier ($^{26}Al/^{27}Al = 28.82x10^{-15}\pm-24.45x10^{-15}$) were added to the pure quartz, which was then dissolved in concentrated HF and fumed with perchloric acid to remove fluorine atoms. Approximately fifteen grams of quartz was assumed for determining acid volumes

Figure 1.2: Location and sample sites of Study Area 1 (Punta de Lobos) plotted on IKONOS imagery. Sample collection sites shown in while ovals, with larger ovals encompassing regions over which amalgamated samples were collected. Surfaces are labeled by their relative ages where cross-cutting relationships were clear from S1 (oldest) to S5 (youngest). The place of B1 in that timeline is unclear. Colors simply serve to differentiate surfaces.

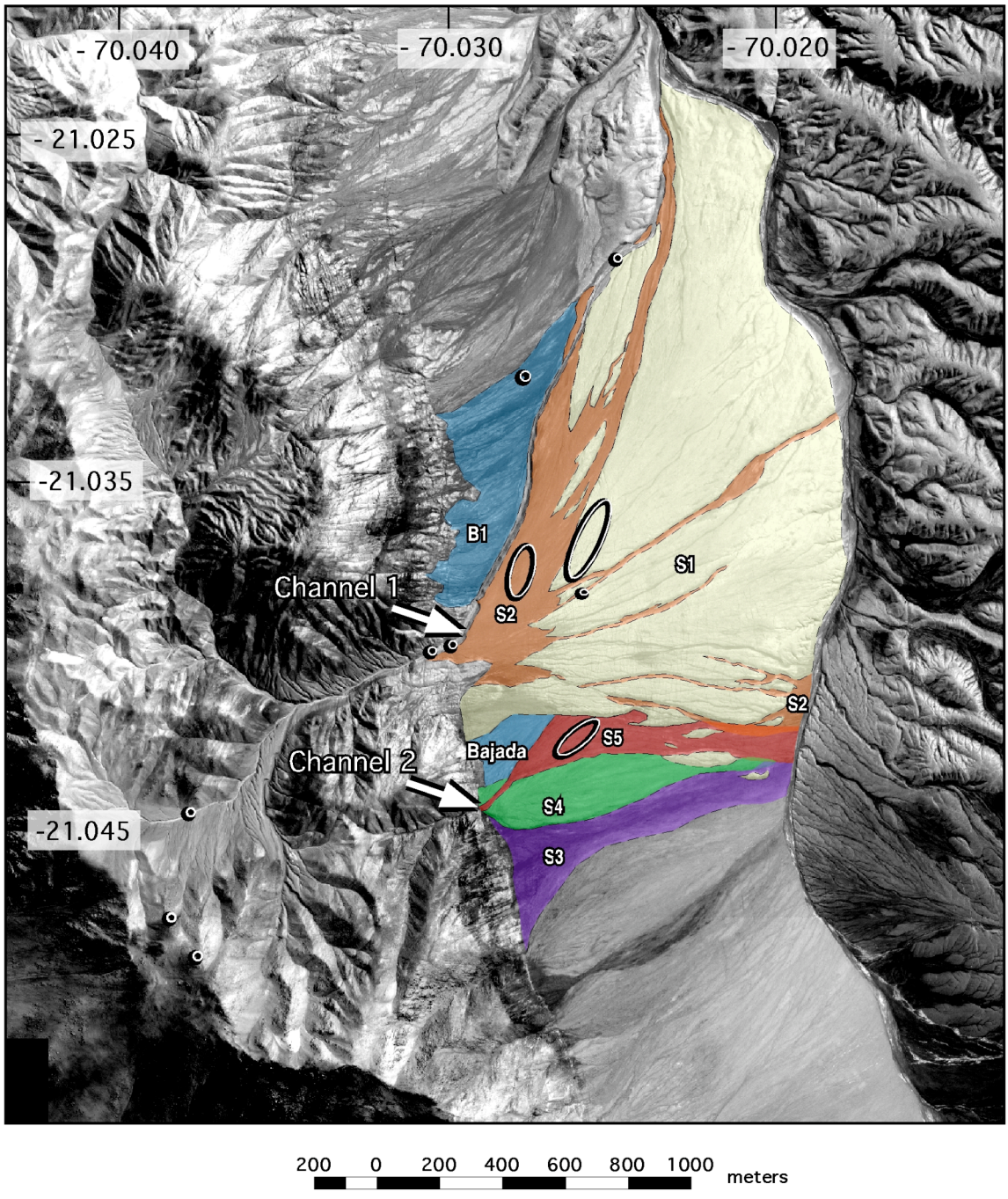
- 70.040
- 70.030
- 70.020
- 21.025
-21.035
-21.045
B1
S1
S2
S2
S3
S4
S5
Bajada
Channel 1
Channel 2
200 0 200 400 600 800 1000
meters

Table 1.1: Nuclide concentration of ^{10}Be and ^{26}Al and calculated ages for Northern Chile

Sample Name	Latitude (°S)	Longitude (°W)	Elevation (m)	Thickness (cm)	Sample Material	Concentration 10Be (106 Atoms/g)	+/-	Concentration 26Al (Atoms/g)	+/-	26Al/10Be ratio	Minimum 10Be exposure age (Myr) *	+/-	Minimum 26Al exposure age (Myr) *	+/-
Surface 1														
S1CA	-21.038	-70.126	609	4.5	quartz cobble	4.55	0.17	22.05	0.75	4.85+-0.24	1.09	0.15	0.90	0.15
S1CB	-21.038	-70.126	609	5	quartz cobble	4.77	0.11	22.76	1.42	4.77+-0.32	1.17	0.16	0.90	0.17
S1CC	-21.038	-70.126	609	4	quartz cobble	5.02	0.60	21.45	0.89	4.27+-0.54	1.24	0.27	0.85	0.14
S1P	-21.038	-70.126	609	4.5	composite quartz	4.20	0.10	18.54	0.85	4.41+-0.23	0.99	0.13	0.69	0.11
											1.12*	**0.09**	**0.83**	***0.07***
Surface 2														
S2CA	-21.038	-70.128	624	6.5	quartz cobble	3.04	0.11	15.54	0.62	5.11+-0.28	0.67	0.08	0.54	0.08
S2CB	-21.038	-70.128	624	7.5	quartz cobble	1.48	0.08	8.36	0.30	5.63+-0.38	0.29	0.04	0.25	0.03
S2C3	-21.038	-70.128	624	8	quartz cobble	1.47	0.17	8.56	0.46	5.81+-0.73	0.29	0.05	0.26	0.03
S23D	-21.038	-70.128	624	7	quartz cobble	1.54	0.05	8.72	0.50	5.65+-0.36	0.30	0.03	0.26	0.03
S2P	-21.038	-70.128	624	4.5	composite quartz	2.03	0.12	10.29	0.53	5.08+-0.39	0.41	0.05	0.31	0.04
S2Ch	-21.03755	-70.12571	611	3	composite quartz	1.74	0.07	9.97	0.48	5.75+-0.37	0.34	0.04	0.30	0.04
											0.38*	**0.02**	**0.32**	***0.02***
Surface 5												0.15		
S5CA	-21.042	-70.126	617	6	quartz cobble	1.23	0.05	7.38	0.31	5.99+-0.35	0.24	0.03	0.22	0.03
S5CB	-21.042	-70.126	617	8	quartz cobble	0.09	0.01	0.42	0.09	4.68+-1.26	0.02	0.00	0.01	0.00
S5P	-21.042	-70.126	617	2	composite quartz	0.53	0.03	3.39	0.38	6.40+-0.79	0.10	0.01	0.09	0.01
											0.12	**0.01**	**0.10**	***0.01***
Active Channel														
AC1	-21.03969	-70.13058	645	3	composite quartz	0.82	0.02	2.72	0.26	3.30+-0.33	0.15	0.02	0.07	0.01
AC2	-21.04432	-70.138	741	3	composite quartz	1.28	0.13	5.14	0.47	4.01+-0.55	0.22	0.03	0.12	0.02
AC3	-21.02844	-70.12486	541	4	composite quartz	1.20	0.13	5.57	0.32	4.63+-0.58	0.24	0.04	0.17	0.02
											0.20	**0.01**	**0.12**	***0.01***
Bajada														
B1	-21.03175	-70.12771	578	4	composite quartz	1.26	0.06	7.13	0.36	6.65+-0.39	0.25	0.03	0.21	0.03
Sedmient														
SS1	-21.02844	-70.12486	541	2	sediment	1.50	0.06	6.37	0.37	4.25+-0.30	0.30	0.03	0.19	0.02
SS2	-21.03952	-70.13007	635	2	sediment	1.33	0.06	5.28	0.38	3.97+-0.33	0.25	0.03	0.14	0.02
SS3	-21.04432	-70.138	741	2	sediment	1.53	0.07	6.55	0.85	4.27+-0.59	0.26	0.03	0.16	0.03
											0.27	**0.01**	**0.16**	**0.01**
Bedrock														
MT1	-21.04845	-70.13783	857	1.5	granodiorite bedrock	0.55	0.03	3.60	0.27	6.52+-0.62	0.09	0.01	0.08	0.01
MT2	-21.04845	-70.13783	857	2	granodiorite bedrock	0.46	0.05	2.71	0.23	5.93+-0.86	0.07	0.01	0.06	0.01
MT3	-21.04734	-70.13862	814	3	granodiorite bedrock	1.30	0.12	6.26	0.34	4.82+-0.53	0.21	0.03	0.15	0.02
											0.12	**0.01**	**0.10**	**0.00**

* Note: These surfaces are abandoned and should be accommodated for inheritance.
Ages and scaling factors are calculated using CRONUS Earth Online calculator version 2.2 (Lifton et al., 2005; Balco et al., 2008). Normalized to 07KNSTD for ^{10}Be and KNSTD for ^{26}Al.

used in the processing of chemical blanks. The samples were then passed through anion and cation exchange columns to separate and collect the Be and Al fractions. Ammonium hydroxide was added to the Be and Al fractions to precipitate beryllium hydroxide and aluminum hydroxides. The hydroxides were oxidized by ignition at 750°C for 5 min in quartz crucibles. Beryllium and aluminum oxides loaded in steel targets for the measurement of the $^{10}Be/^{9}Be$ and $^{26}Al/^{27}Al$ ratios by accelerator mass spectrometry at the Purdue Rare Isotope Measurement (PRIME) Laboratory at Purdue University.

Ages were calculated using the scaling scheme of Lifton et al. (2005) on the CRONUS calculator version 2.2 (Balco et al., 2008). This method uses a sea level high latitude production rate of 4.8±0.4 atoms of ^{10}Be per gram of quartz per year and 32.7±2.5 atoms of ^{26}Al per gram of quartz per year. No corrections were made for erosion. Since we cannot adequately define altitudinal changes for our study areas, we assume no altitudinal change and use the present altitude of the sampling site to calculate TCN ages and erosion rates.

Measuring ^{10}Be and ^{26}Al TCNs helps determine any burial history for the sampled clasts. We have also collected samples from local granodiorite bedrock and the most recently active channels to account for potential inheritance. Determining the nuclide levels at these points in the system allow us to estimate the potential exposure clasts received before reaching their current location, either as part of the bedrock or during transport. Neon 21 analyses were only performed on a small subset of these samples, but several authors have reported ^{21}Ne ages for surfaces in the Coastal Cordillera (e.g. González et

al., 2006; Dunai et al., 2005; Placzek et al., 2010). Our ^{21}Ne analyses can be found in the appendices for comparison with published data.

1.4 Descriptions of field sites

1.4.1 Punta de Lobos

The Punta de Lobos alluvial fan system is located at 21.04°S and 70.12°W at an altitude of 600 m to 850 m asl and is bounded by the Punta de Lobos fault to its west (Figure 1.2). The drainage basin for the alluvial fan lies west of the fault, with the upper reaches of the source area truncated by the coastal escarpment. The alluvial fan is experiences coastal fog during the winter months. Salts are present in the upper few meters of the soils, forming a hard gypcrete crust that would require construction equipment for meaningful excavation, on the oldest surfaces, whereas the youngest surface has no discernable salt development. The alluvial fan surfaces are hardest on the oldest surfaces. In addition, the size of surface clasts decreases with relative alluvial fan age. All surfaces have NNE-trending decimeter-wide and many meter-long cracks, which Loveless et al. (2009) argues were formed during great earthquakes. Some cracks that cross-cut surfaces show greater opening in the older surface than the younger.

Using cross-cutting relationships, relative salt development, surface clast size, and surface hardness, we determine the relative ages of the five main alluvial fan surfaces, sourced from two neighboring drainages (Table 1.2). The oldest surface (S1) is heavily indurated, has ventifacts and streaks showing the prevailing wind direction, and has a

Table 1.2: Description of Surfaces at Punta de Lobos Study Area

Sample Name	Description of Surface			
	Morphostratigraphy	Notable Features	Level of Induration	Surface Material
S1	Oldest surface (Panels B and D in Fig. 1.3), originally sourced by Channel 1, abadoned	Fine desiccation cracks present, strong ventifacts	Heavily indurated surface difficult to break, cobbles need to be pried (sometimes with a hammer) to be removed, indurated with anhydrite	Fine grained and light in color; sparse coarse sands, pebbles, and small gravels litter the surface
S2	Second oldest surface, originally sourced by Channel 1, overlays S1, currently abandoned	Desiccation cracks clearly visible through thin covering of material	Only slightly less indurated than S1, almost all cobbles need to be pried out of the surface rather than picked up, indurated with gypsum	More extensive overlay of pebbles and coarse sand than S1, large cobbles on the surface are fist sized but can get up to head sized (Panel B in Fig. 1.3), slightly darker in appearance
S3	Sourced from a number of smaller, poorly-defined drainages along the slope (Fig. 1.2)	Desiccation cracks visible beneath thick overlay of pebbles and cobbles	Less coherent than the above (older) surfaces, some material moves when walked upon, some cobbles can be easily removed	The surface contains many dark volcanic clasts, and some silt and sand is present and mobile
S4	Originally sourced by Channel 2 (Fig. 1.2), surface incised at the apex by S5, most distributary channels strongly degraded	Less pronounced desiccation cracks and subtle ventifacts, thin overlay	The cobbles need to be pried from the indurated sediment	Thin overaly of pebbles and gravel with little coarse sand (Panels C and D in Fig. 1.3), larger gravels with some clasts up to 10 cm in diameter also present butconcentrated exclusively channels
B1	Numerous coalescing units forming a single surface	No visible desiccation cracks	Mildly indurated, most clasts require only minor prying to remove (Panel D of Fig. 1.3)	Varied clast composition and size, generally coarser than S1-S4, the few clasts of vein quartz <4cm in diameter
S5	Sourced by Channel 2, surface appears active, it is incised into S4 near the source, spills out over other fan surfaces in a thin sheet to the East	No visible desiccation cracks	Primarily large clasts, what sand sized grains are present are not significantly indurated	Highly angluar fist- to head-sized clasts dominate the surface near its source, sand-sized grains present, occasional small boulders up to 50 cm in diameter near the mouth (Panels C and D in Fig. 1.3)

sparse population of pebble- and even fewer cobble-sized clasts (Figure 1.3). In contrast, the youngest surface has no discernible salt formation and is made up of primarily angular, cobble-sized clasts. Photos of each of surface can be seen in Figure 1.3. Overall, older surfaces are more heavily indurated, more finely grained, and have a sparser distribution of large clasts. All surfaces become more finely-grained farther from the front, with the boundaries between surfaces becoming less clear as distal deposits overlap in thin overlays.

Two of the fans are sourced by the northern drainage (Channel 1 in Figure 1.2) and two by the southern (Channel 2 in Figure 1.2). The modern channel of the northern drainage, Channel 1, is incised into the main fan complex by 6-8 m, leaving behind two abandoned fan surfaces. Channel 2 sourced two fans, one of which is still active. The younger fan is fed by a channel that is slightly incised (2-4 m) into the older fan/bajada deposits near the mountain front. The intersection point, where the fan spreads out over the older deposits, is located about 135 m east of the mountain bounding fault. A number of distributary paleodrainages can be identified in the abandoned and inactive fan surfaces.

The Punta de Lobos fan complex is underlain by two closely spaced tuffaceous beds that lie about 3 m below the current fan surface. These tuffaceous beds are exposed in the incised channel on the northern side of the fan complex and can be seen at both the head and near the toe of the fan. The two beds show evidence of significant reworking

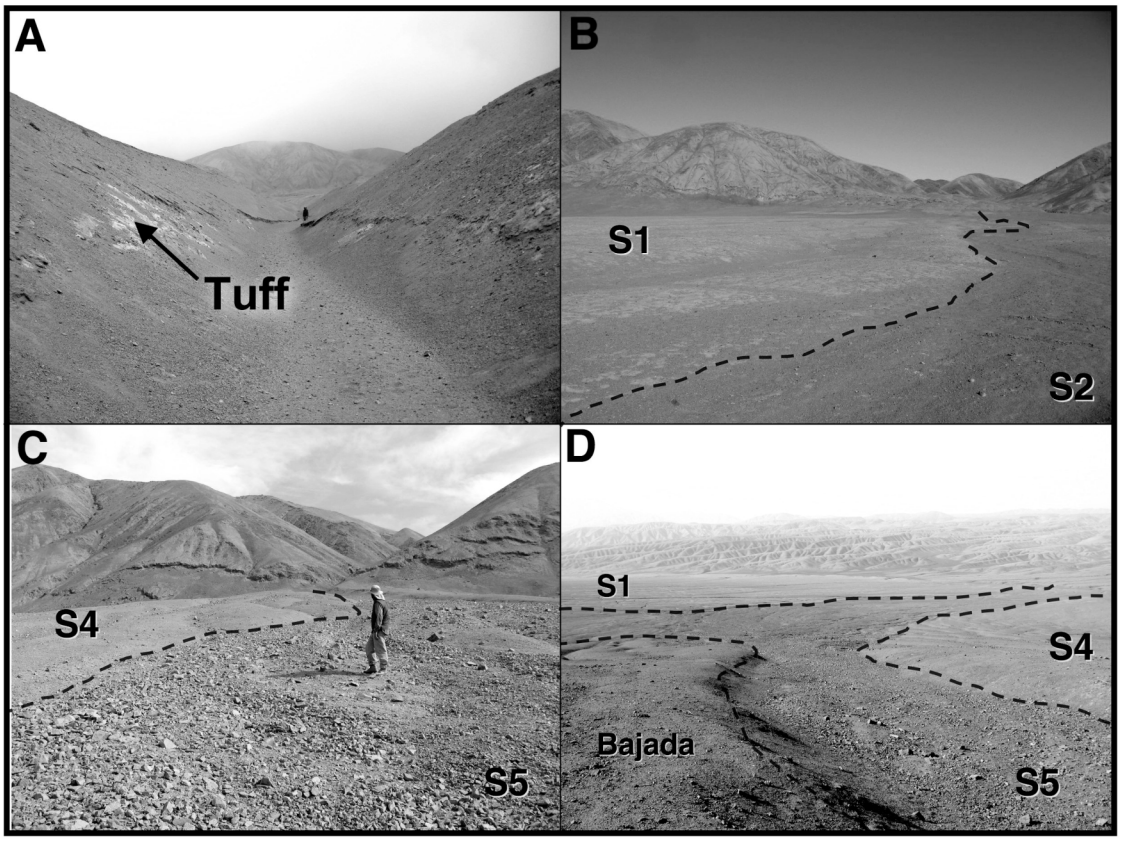

Figure 1.3: Photos of surfaces and cross-cutting relationships at Study Area 1. A) Channel 1 incised into S2; reworked tuff visible ~3m below surface. B) Boundary between S1 and S2. C) Coarser material of S5 spilling over onto S4. D) Incision of S5 near source drainage into bajada and S1, overflow onto S4.

and locally contain transported bedrock clasts up to a few centimeters in diameter. Despite this inauspicious setting, given the importance of constraining the ages of the deposits underlying the surfaces dated cosmogenically, we collected samples of the upper, and somewhat more pristine of the two tuffaceous beds in exposures at the head of the fan.

The samples lack sufficient sanidine, so biotite separates were dated by $^{40}Ar/^{39}Ar$ stepwise heating at the Nevada Isotope Geochronology Laboratory at the University of Nevada Las Vegas. The age spectrum lacks a plateau and there is a suggestion of excess argon. The total gas age of 10.09 ± 0.04 Ma is likely an overestimate. An isochron age determined from about 36% gas release between heating steps 11 and 15, is well defined and yields an age of 3.99 ± 0.06 Ma (see appendices). While this can hardly be considered a robust result, it is consistent with the surface ages as well as dated fans in similar settings elsewhere in the Coastal Cordillera and very tentatively suggests that at the head of the fan, ~3 m of coarse clastic sediment accumulated in about the last 4 million years.

1.4.2 Mititus

The study area (Figure 1.4) at 23.07°S and 70.19°W is more laterally extensive and at lower elevation than the Punta de Lobos fans 225 km to the north. Though the Mititus (Study Area 2) fans are technically farther inland, that is only due to the presence of the Mejillones Peninsula to the west. These fans are at a comparable distance to the coastal escarpment as those at Punta de Lobos, though the escarpment here is less pronounced. Mititus is

Figure 1.4: Mititus (Study Area 2) A) Fan surfaces overlain on QuickBird Imagery from GoogleEarth Pro. Numbers correlate to order in which surfaces were mapped. Colors correspond to relative ages of surfaces, yellow being the oldest surfaces, orange the intermediate, and red the youngest. B) Larger map area shown in white rectangle. Sample locations from Placzek et al. (2010) shown as white dots.

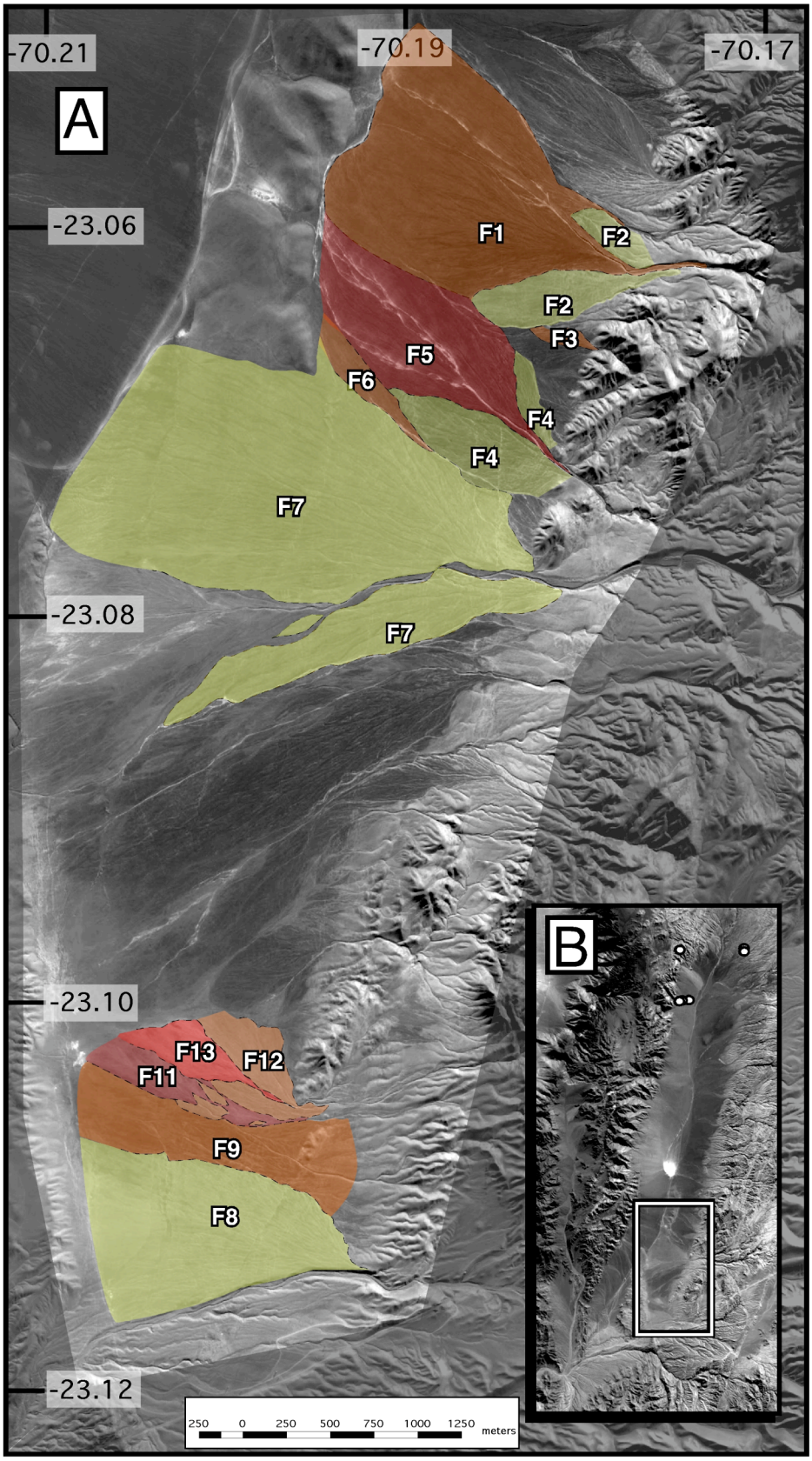
-70.21
-70.19
-70.17
A
-23.06
F1
F2
F2
F3
F5
F6
F4
F4
F7
-23.08
F7
B
-23.10
F13
F12
F11
F9
F8
-23.12
250 0 250 500 750 1000 1250
meters

still within the zone consistently affected by the coastal fog, but has less extensive induration of the soils overall. To the west, the fans abut the Mititus fault, which has normal displacement and is part of complex of domino style normal faults that characterize this part of the Coastal Cordillera. All of the fan surfaces are populated by cracks striking NNE.

The fans at this location cover more than 7 km from north to south and receive sediment from at least seven separate drainages. All of the fan surfaces are low angle and tributary systems suggestive of a precipitation-driven system. The lateral extent and the possibility of simultaneous activations make it difficult to form a single timeline of relative ages across the system. Instead, based on morphology, level of induration, and cross-cutting relationships, we divide the fans into three primary groups (Table 1.3). Naturally, some variation in grain size and composition exist within groups due to variations in source material.

1.5 TCN ages

The fans we describe here do not have boulders incorporated into them, the largest clasts are fist-sized, and the unique weathering style in the Coastal Cordillera results in higher erosion rates and younger ages for bedrock than neighboring alluvial surfaces (Nishiizumi et al., 2005). Based on the findings of Placzek et al. (2010), described more thoroughly in the discussion, we are confident that sampling the available quartz clasts in the fans at Punta de Lobos will provide a representative age.

Table 1.3: Description of Surfaces at Mititus Study Area.

Sample Name	Description of Surface			
	General Appearance	Level of Induration	Drainages	Surface Material
Oldest Surfaces	Typically light in color and more densly cracked than those surrounding it. Fine grained material appears flaky on top and sometimes forms meter-scale polygons with a few centemeters of vertical difference between the peaks ans lows. Shown in yellow in Fig. 1.5.	Well-indurated, fine-grained material overlain with a spase cover of small gravel.	Drainages are wide and subtle, and have the same general characteristics of the rest of the surface. Incised at their source by channels of younger deposits that have intersection points at least 0.75 km from the mountain front.	Very few clasts >10 cm in diameter, and the clasts present need to be pried out of the surface. Up-to-fist-sized pieces of hard gypsum disributed througout the surfaces.
Intermediate Surfaces	Nearly completely covered with gravel and finer material, with sparse patches revealing indurated material. Indurated material exposures lack polygonal structure, flaking, and clumps of gypsum of the older surfaces. Shown in Orange in Fig. 1.5.	Moderately indurated with some larger clasts needing to be pried out, and finer-grained indurated material can be seen through the cover. Stepping on surface leaves minor indentation.	Clear braiding of channels, bars of coarser material still visible in many channels. Incision extends to mountain front, sometimes backfilling into the drainage.	Few clasts >10 cm, though more than in the older surfaces. Clasts are also easier to pry out.
Youngest Surfaces	Consistent cover of gravel, sand, and silt, lacks the patchiness of the older surfaces. Shown in red in Fig. 1.5.	Thin, gravelly crust which is easily broken to reveal >10cm of unconsolidated fine-grained material, surface difficult to walk on.	Typically travel much of the fan in a narrow channel, intersecting the surface 0.7-1.5 km from the mountain front.	The few larger clasts in these surfaces are easily removed.

1.5.1 Punta de Lobos

TCN exposure ages for samples can be found in Table 1.1 and $^{26}Al/^{10}Be$ ratios in Figure 1.5. The $^{26}Al/^{10}Be$ ratio of clast (dashed ovals) and sediment (dotted ovals) samples from the active channel fall below the line for steady-state erosion, suggesting a complex burial history (Figure 1.5). Knowing this, we can interpret the mean ~200ky age from the Active Channel samples as one potential measure of inheritance as a minimum. Similarly, the sediment samples suggest a minimum exposure ages of ~270ky. Even with potential burial, these ages provide a minimum amount of inheritance that should be removed from the surface ages of the two surfaces (S1 and S2) that were abandoned by the incision of that drainage. The $^{26}Al/^{10}Be$ ratios for the granodiorite bedrock samples fall closer to the curve for steady-state erosion (Figure 1.5) and yield younger ages, ranging from 210ky to 70ky. These findings are consistent with Nishiizumi et al. (2005) suggesting that bedrock surfaces in the Atacama erode more quickly and have higher erosion rates than surrounding surfaces.

Though only approximations, these inheritance measures provide context for the minimum surface exposure ages for the other surfaces. Consider the relative youth of both the Bajada (B1) and S5 surface samples. The clasts collected on these surfaces yielded minimum exposure ages the same or younger than the active channel and bedrock samples. All but one of the $^{26}Al/^{10}Be$ ratios fall near the curve for steady-state erosion, suggesting a minimal role of burial (Figure 1.5). This suggests that these surfaces are as active as can be measured by these methods, with clasts being deposited as recently as they have weathered out of the bedrock.

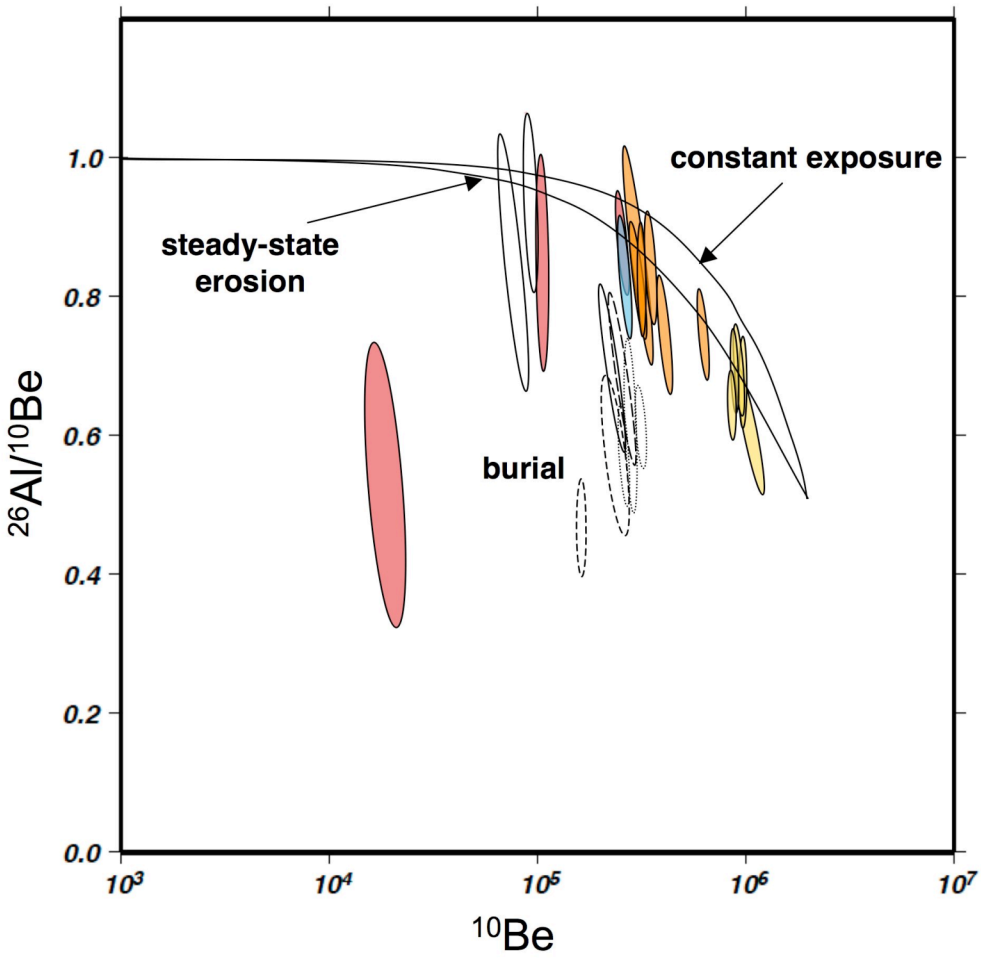

Figure 1.5: Ratios of $^{26}Al/^{10}Be$ fall largely between lines of constant exposure and steady-state erosion. Yellow ovals represent samples from S1, orange from S2, blue from B1, and red from S5. The unfilled ovals represent samples taken for measures of inheritance, including active channel sediment (dotted), active channel clasts (dashed), and bedrock (solid).

The other two surfaces, S1 and S2, have been abandoned by the downcutting of the source drainage and should thus be considered minus the inheritance suggested by samples in the active channel. The nuclide ratios for the samples from both surfaces fall along the curve for steady-state erosion, with few exceptions suggesting some potential burial. The nuclide levels for S2 suggest ages of ~380ky and those for S1 suggest 1.12my. Removing the ~200ky inheritance suggested by the active channel, these ages become 180ky and 920ky respectively (Table 1.1).

1.5.2 Mititus

We did not collect quartz samples for dating at Mititus. However, there are dated surfaces only 20 km to the north within the same basin (Placzek et al., 2010). See inlay B in Figure 4 for location. These ages are part of a transect study to compare landscape modification levels and rates across a swath of the central Atacama. Placzek et al. (2010) found evidence of <1.2 Ma surfaces throughout the transect. At this location, ages range from 86 ka to 1.5 Ma (Placzek et al., 2010). It is likely that the fans at Mititus fall within the same general age range, which is quite comparable to those found at Punta de Lobos. This suggests that this precipitation-driven deposition on low-angle fan surfaces is likely occurring throughout the Coastal Cordillera, despite hyper-arid conditions overall.

1.6 Discussion

Our surface exposure ages for low-angle, precipitation-driven alluvial fans in the Coastal Cordillera are much younger than many that have been found in the Atacama.

Nonetheless, they fit well with a number of recently published ages from within the last million years from a variety of landforms and locations (Dunai et al., 2005; Nishiizumi et al., 2005; Carrizo et al., 2008; Kober et al., 2007, Evenstar et al., 2009; Hall et al., 2008; González et al., 2006; Plazcek et al., 2010). Placzcek et al. (2010) found numerous examples of younger surfaces across the southern latitudes of the Atacama spanning from the coast to the base of the Andes. Additional examples have been found along the Salar del Carmen fault zone (González et al., 2006) up to southern Peru (Hall et al., 2008).

Evidence for significantly older surfaces can be found throughout the same geographical expanse (e.g., Dunai et al., 2005), thus begging the question of how to reconcile these disparities. Other authors have acknowledged that while the core of the Atacama has remained within the bounds of "hyperarid" for millions of years, the intensity of that aridity may have varied in both location and time (Houston, 2006; Houston & Hartley, 2003; McKay et al., 2003). In order to tease out some of these differences, it is important to consider two primary influences: location and sampling practices.

Location clearly plays a role in the attempt to identify any broader climate patterns over such a large area. Broadly, the annual rainfall in the dry core is within the confines of "hyperarid" as defined by Ewing et al. (2006) (Houston & Hartley, 2003). This is largely due to the fact that these annual averages reflect one or only a few storms. The core is particularly stable because of topographic protection from atmospheric variations over the Andes or from the Pacific (Figure 1.6). We initially compare our findings with others

in the Coastal Cordillera (Figure 1.6) and find a range of ages, the most extreme being greater than 20 Ma (Dunai et al., 2005), but most remaining within the last 2 Ma (Appendices). Our ages clearly fall in the latter group, but together all of these ages paint a changing picture of what hyperaridity has looked like over time. With the exception of the few older ages (Dunai et al., 2005), many of the surface ages summarized here suggest an earlier period of more readily available surface water 3-5 Ma (e.g. Carrizo et al., 2008). The extensive paleochannel networks throughout the Coastal Cordillera are a likely remnant of this period (Figure 1.7). Many of these channels were more than 100 m across and, when obstructed by uplifting fault blocks, created playa lakes (Allmendinger et al., 2005; Carrizo et al., 2008). Deposition and erosion, however, did not cease with the end of this period; they merely slowed down. Plazcek et al. (2010), Hall et al. (2008), González et al. (2006), Kober et al. (2007), and our work demonstrate the slow but continued modification of surfaces after that time.

Similar challenges must be considered for differences in the material sampled. Numerous authors have actively debated which landforms and methods are the most representative for trying to discern patterns in paleoclimate (e.g. Rech et al., 2006; Hartley, 2007; Rech et al., 2007). Even restricting this debate to TCN dating specifically, traditional practices are starting to be drawn into question for the Atacama (e.g. Plazcek et al., 2010; Hall et al., 2008). For

Figure 1.6: DEM of northern Chile with average annual precipitation contours (mm/year) based on Houston and Hartley (2006). Each dot represents a surface age from this and previous work, with age corresponding to the color bar (Placzek et al, 2010; Dunai et al, 2005; Nishiizumi et al, 2005; Carrizo et al, 2008; Kober et al, 2007; González et al, 2006; Evenstar et al, 2009; current work).

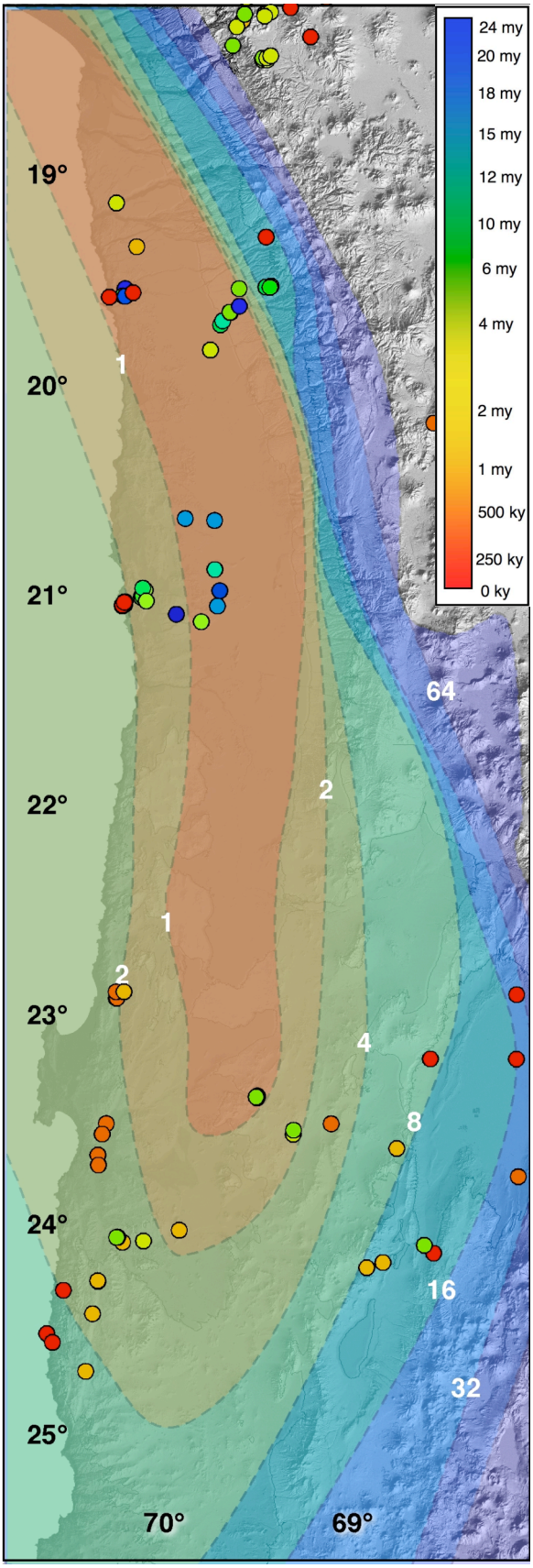
24 my
20 my
18 my
15 my
12 my
10 my
6 my
4 my
2 my
1 my
500 ky
250 ky
0 ky
19°
20°
21°
22°
23°
24°
25°
70°
69°
1
2
1
2
4
8
16
32
64

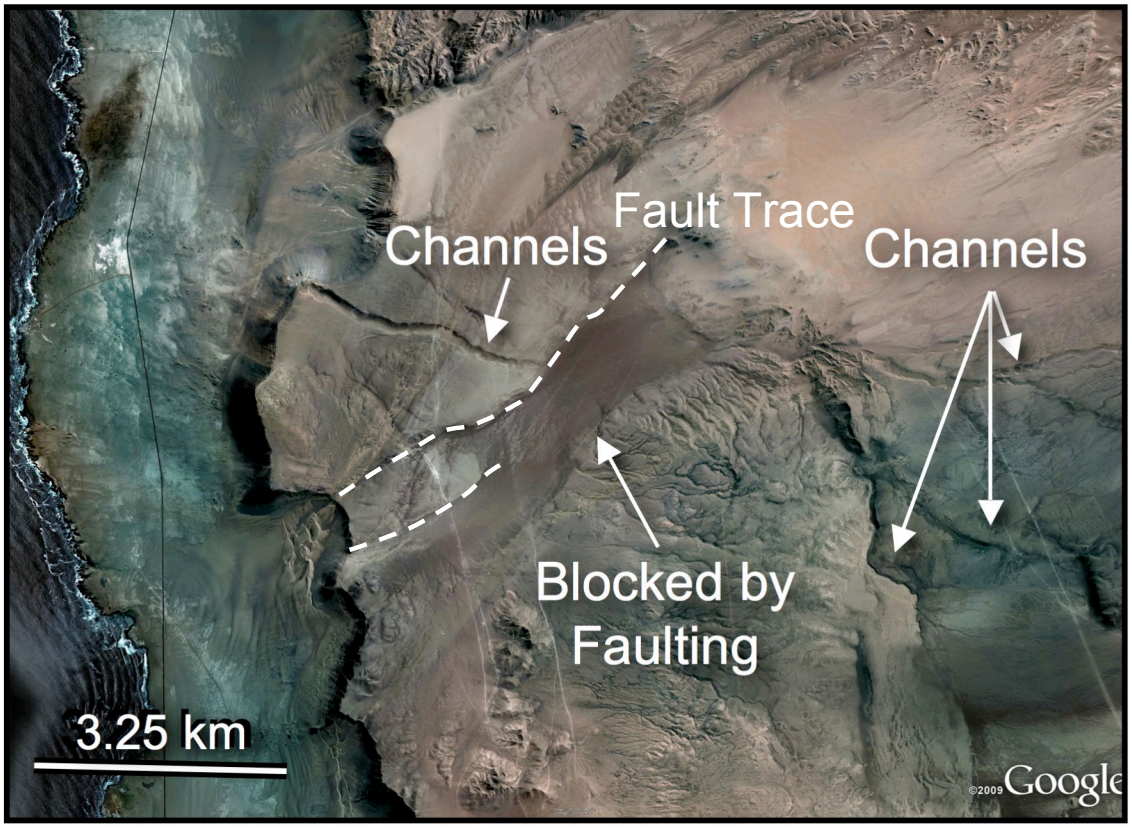

Figure 1.7: Examples of abandoned and offset channel networks in the Coastal Cordillera. Clear formation of playa lake after truncation by faulting. Quickbird Imagery from GoogleEarth Pro.

example, boulders have traditionally been preferred as sampling sites. Their size makes them less likely to have complex burial histories. In the Atacama, however, boulders are commonly lacking on many of the lower-angle, fluvial surfaces, and our fans. The second limiting factor, particularly in the Coastal Cordillera, is the high level chemical and mechanical weathering that results from the sulfur-rich fog. In many cases, boulders have been observed in various stages of disintegration, suggesting they break down into gravel-sized pieces where they lie instead of breaking down during transport. Comparisons of ages and erosion rates for boulders and the sediment around their bases have even suggested that the boulders may be relicts that no longer interact with the younger and more active landscape (Plazcek et al., 2010). When compared to other sample types across a number of studies, boulders yield generally older ages than either bedrock or smaller clast samples, supporting the notion that the boulders are an expression of an older landscape (e.g. Plazcek et al., 2010; Hall et al., 2008). This does not question the existence of older landscape elements, but it does support the argument that more recent, albeit slower, modification is still occurring.

One way to put our observations into context is to look at the mobilization of sediment under the current climate as a reference. Modern records provide insight into precipitation rates throughout the Atacama, both in amount and frequency. In the core, rain is less than 1mm annually and parts of the coastal cities register 3-4 mm per year (Houston & Hartley, 2003). Many of these averages, however, are reflective of single events once per year or even decade (Houston & Hartley, 2003; Houston, 2006; McKay et al., 2003) (Figure 1.6). The punctuated events, combined with the general lack of vegetation in the region, make these storms capable of mobilizing significant amounts

of sediment (Ramirez & Perez, 2011). When records of rainfall events were compared to the amount of liquid that would be likely to mobilize deposits found on fans with sub-kilometer lengths in the Coastal Cordillera, Haug et al. (2010) found that such sheet-flood activations could be happening reliably on the year-to-decade timescale. As our fans from this study are both larger and of lower-angle than those in Haug et al. (2010), precipitation events large enough for activation likely occur only from more severe events that happen after longer intervals. In the case of the fans at Punta de Lobos, there appear to have been only a few major activation events within the last million years, including some in the recent past. The 1991 rain event, during which 42 mm of rain in 3 hours caused mudslides near Antofagasta, may have been an example of such an event (Ramirez & Perez, 2011).

The mounting evidence for punctuated precipitation events with lasting morphological signatures within a hyperarid regime highlights the extreme care that must be taken when using such features to draw broader implications regarding climate and tectonics. Given the evidence that boulders and other larger landscape features may be recording a relict environment, more work needs to be done to investigate the history recorded in clasts with smaller deposits. Such work will not negate the persistence of hyperaridity throughout the Quaternary, but rather highlight the active modification of surfaces that can take place within the confines of a hyperarid climate regime.

1.7 Conclusion

The alluvial fans dated in this study have TCN surface exposure ages similar to many recent studies but significantly older than those based on boulders and large channels. These deposits appear to express a few, catastrophic precipitation events in an otherwise hyperarid regime rather than broad changes in climate. The fans dated in this study have been activated multiple times within the last million years, and at least one fan appears still to be active. Dating smaller clasts in alluvial deposits provides a record of a more recent and slowly changing landscape where previous work suggested that surfaces were inactive.

WORKS CITED

Allmendinger, R. W., and González, G. G., 2010, Neogene to Quaternary Tectonics of the Coastal Cordillera, northern Chile: Tectonophysics, 495, 93-110, doi: 10.1016/j.tecto.2009.04.019.

Allmendinger, R. W., González, G., Yu, J., Hoke, G. D., and Isacks, B. L., 2005. Trench-parallel shortening in the northern Chilean forearc: Tectonic & climatic implications. Geological Society of America Bulletin 117(1), 89-104.

Balco, G., Stone, J.O., Lifton, N.A., Dunai, and T.J., 2008. A complete and easily accessible means of calculating surface exposure ages or erosion rates from ^{10}Be and ^{26}Al measurements. Quaternery Geochronology 3, 174-195.

Carrizo, D., González, G., and Dunai, T., 2008. Constricción neógena en la Cordillera de la Costa, norte de Chile: neotetónica y datación de superficies con ^{21}Ne cosmogénico. Revista Geológica de Chile 35(1), 1-38.

Comte, D. and Pardo, M., 1991. Reappraisal of great historical earthquakes in the Northern Chile and Southern Peru seismic gaps. Natural Hazards 4, 23-44.

Dunai, T.J., Gonzáles López, G.A., and Juez-Larré, J., 2005. Oligocene-Miocene age of aridity in the Atacama Desert revealed by exposure dating of erosion-sensitive landforms. Geology 33, 321-324.

Ewing, S.A., Sutter, B., Owen, J., Nishiizumi, K., Sharp, W., Cliff, S.S., Perry, K., Dietrich, W., McKay, C.P., and Amundson, R., 2006. A threshold in soil formation at Earth's arid-hyperarid transition. Geochimica Cosmochimica Acta 70, 5293-5322.

Evenstar, L.A., Hartley, A.J., Stuart, F.M., Mather, A.E., Rice, C.M., and Chong, G., 2009. Multiphase development of the Atacama planation surface recorded by cosmogenic 3He exposure ages: Implications for uplift and Cenozoic climate change in western South America. Geology, 37, 27-30.

González, G.L., Dunai, T., Carrizo, D., and Allmendinger, R., 2006. Young displacements on the Atacama Fault System, Northern Chile from field observations and cosmogenic ^{21}Ne concentrations. Tectonics 25, TC3006.

Gosse, J.C. and Phillips, F.M., 2001. Terrestrial in situ cosmogenic nuclides: theory and application. Quaternary Science Reviews 20, 1475-1560.

Hall, S.R., Farber, D.L., Audin, L., Finkel, R.C., and Mériaux, A.-S., 2008. Geochronology of pediment surfaces in southern Peru: implications for quaternary deformation of the Andean forearc. Tectonophysics 459, 186-205.

Hartley, A.J., 2007. Neogene climate change and uplift in the Atacama Desert, Chile: COMMENT. Geology, doi: 10.1130/G23709C.1.

Hartley, A.J. and Chong, G., 2002. Late Pliocene age for the Atacama Desert: implications for the desertification of western South America. Geology 30, 43-46.

Hartley, A.J. and Jolley, E.J., 1995. Tectonic implications of Late Cenozoic sedimentation from the Coastal Cordillera of northern Chile (22-24°S). Journal of the Geological Society 152(1), 51-63.

Haug, E.W., Kraal, E.R., Sewall, J.O., Van Dijk, M. and Chong Diaz, G., 2010. Climatic and geomorphic interactions on alluvial fans in the Atacama Desert, Chile. Geomorphology 121 (3-4), 184-196.

Hoke, G.D., Isacks, B.L., Jordan, T.E. and Yu, J.S., 2004. Groundwater-sapping origin for the giant quebradas of northern Chile. Geology 32, 605-608.

Houston, J., 2006. The great Atacama flood of 2001 and its implications for Andean hydrology. Hydrological Processes 20, 591-610.

Houston, J. and Hartley, A., 2003. The central Andean west-slope rainshadow and its potential contribution to the origin of hyper-aridity in the Atacama Desert. International Journal of Climatology 23, 1453-1464.

Kober, F., Ivy-Ochs, S., Schlunegger, F., Baur, H., Kubik, P.W., and Wieler, R., 2007. Denudation rates and a topography-driven rainfall threshold in northern Chile: multiple cosmogenic nuclide data and sediment yield budgets. Geomorphology 83, 97-120.

Latorre, C., Betancourt, J.L., Rylander, K.A., and Quade, J., 2002. Vegetation invasions

into absolute desert: a 45,000-yr rodent midden record from the Calama-Salar de Atacama basins, northern Chile (lat 22-24°S). Geological Society of America Bulletin 114, 349-366.

Lifton, N.A., Bieber, J.W., Clem, J.M., Duldig, M.L., Evenson, P., Humble, J.E., Pyle, R., 2005. Addressing solar modulation and long-term uncertainties in scaling secondary cosmic rays for in situ cosmogenic nuclide applications. Earth and Planetary Science Letters 239, 140-161.

Loveless, J.P., Allmendinger, R.W., Pritchard, M.E., Garroway, J.L., and González, G., 2009. Surface cracks record long-term seismic segmentation of the Andean margin. Geology 37, 23-26.

McKay, C.P., Friedmann, E.I., Gómez-Silva, B., Cáceres-Villanueva, L., Andersen, D.T., and Landheim, R., 2003. Temperature and moisture conditions for life in the extreme arid region of the Atacama Desert: four years of observations including the El Niño of 1997-1998. Astrobiology 3(2), 393-406.

Nishiizumi, K., Caffee, M.W., Finkel, R.C., Brimhall, G., and Mote, T., 2005. Remnants of a fossil alluvial fan landscape of Miocene age in the Atacama Desert of northern Chile using cosmogenic nuclide exposure age dating. Earth and Planetary Science Letters 237, 499-507.

Placzek, C.J., Matmon, A., Granger, D.E., Quade, J., and Niedermann, S., 2010. Evidence for active landscape evolution in the hyperarid Atacama from multiple terrestrial cosmogenic nuclides. Earth and Planetary Science Letters 295, 12-20.

Placzek, C., Quade, J., Betancourt, J.L., Patchett, J.P., Rech, J.A., Latorre, C., Matmon, A., Holmgren, C., and English, N.B., 2009. Climate in the dry central Andes over geologic, millennial, and interannual timescales. Annals of the Missouri Botanical Garden 96: 386-397.

Pritchard, M.E., Ji, C., and Simons, M., 2006. Distribution of slip from 11 M_w>6 earthquakes in the northern Chile subduction zone. Journal of Geophysical Research 111, B10302, doi:10.1029/2005JB004013.

Ramirez, F.J. and Perez, P.C., 2011. Passing volume calculation system (PVCS): computer software for managing data on watersheds that produce mud flows and the case of Quebrada La Cadena, Antofagasta, Chile. Natural Hazards, doi: 10.1007/s11069-011-9744-5.

Rech, J.A., Currie, B.S., Michalski, G., and Cowan, A.M., 2006. Neogene climate change and uplift in the Atacama Desert, Chile. Geology 34, 761-764.

Rech, J.A., Currie, B.S., Michalski, G., and Cowan, A.M., 2007. Neogene climate change and uplift in the Atacama Desert, Chile: COMMENT REPLY. Geology doi: 10.1130/G23810Y.1.

Rech, J.A., Quade, J., and Hart, W.S., 2003. Isotopic evidence for the source of Ca and S in soil gypsum, anhydrite and calcite in the Atacama Desert, Chile. Geochimica et Cosmochimica Acta 67, 575-586.

CHAPTER 2

2 PERMANENT COSEISMIC EXTENSION IN THE COASTAL CORDILLERA, NORTHERN CHILE: IMPLICATIONS FOR GEODETIC INTERPRETATIONS OF ELASTIC REBOUND

2.1 Introduction

Earthquakes, due to the potential hazard they pose to both local populations from shaking and more distant coastal cities from tsunamis, have long been a primary focus within the geoscience community. Our current understanding of these events is the combined result of numerous field studies, geophysical and remote sensing data sets, and numerical models. Recently, an increase in available records of real-time, cm-scale surface displacements from GPS and InSAR for modern earthquakes has allowed for the development of more sophisticated models of the various components of the seismic cycle. These geophysical data sets, however accurate, provide only a snapshot of the most recent events and interpretations depend heavily on the validity of such assumptions as the bulk elastic behavior of the crust during the seismic cycle (e.g. Reid, 1910; Okada, 1985; Okada, 1992). To better connect modern geophysical measurements to the long-term behavior of a system, we must turn to the geologic record.

In trying to find an area to study the long-term record of surface deformation from plate boundary earthquakes, the Atacama Desert of Northern Chile serves as an ideal setting. Situated on the western coast of Chile where the Nazca plate is being subducting beneath the South American Plate at ~79mm/yr (Angermann, et al., 1999;Kendrick et al., 2001), the Atacama lies along the plate boundary that has experienced some of the

largest earthquakes ever recorded (Figure 2.1). The desert spans 200 km E-W and 1000 km N-S and receives <1mm of rain annually (Houston & Hartley, 2003) and surface features have been remarkably preserved since the onset of hyperaridity 10Ma (Houston and Hartley, 2003; Nishiizumi et al., 2005; Hoke et al., 2004; Rech et al., 2006; Kober et al., 2007). In the Coastal Cordillera, many of these ancient surfaces are pervasively fractured by numerous tension cracks. Though the cracks originate from a variety of mechanisms ranging from soil process and topographic effects to drainage events to tectonics, a specific subset is linked directly to large seismic events in the region. These coseismic cracks, which cut topography and can reach hundreds of meters to kilometers long, have been observed to open during earthquakes (Keefer & Moseley, 2004; Loveless et al., 2005; Loveless et al., 2009). These cracks have been interpreted as a record of the long-term segmentation of the Chilean margin (Loveless et al., 2009), but the rate of cracking remained elusive due to lack of suitable material to date the crack fill.

Here we circumvent this problem by dating alluvial fan surfaces in which the cracks occur and measuring the strain on scanlines (as described later) perpendicular to the cracks. This work uses populations of coseismic cracks across alluvial fan surfaces in the Coastal Cordillera of the Atacama to investigate the longevity and consistency of surface deformation from plate boundary earthquakes. Our work yields three primary results: the strain rate due to coseismic cracking for the last ~900ky, the amount of strain due to cracking from a single event, and the comparison of these strains to GPS measurements of coseismic displacement from recent earthquakes. These results are

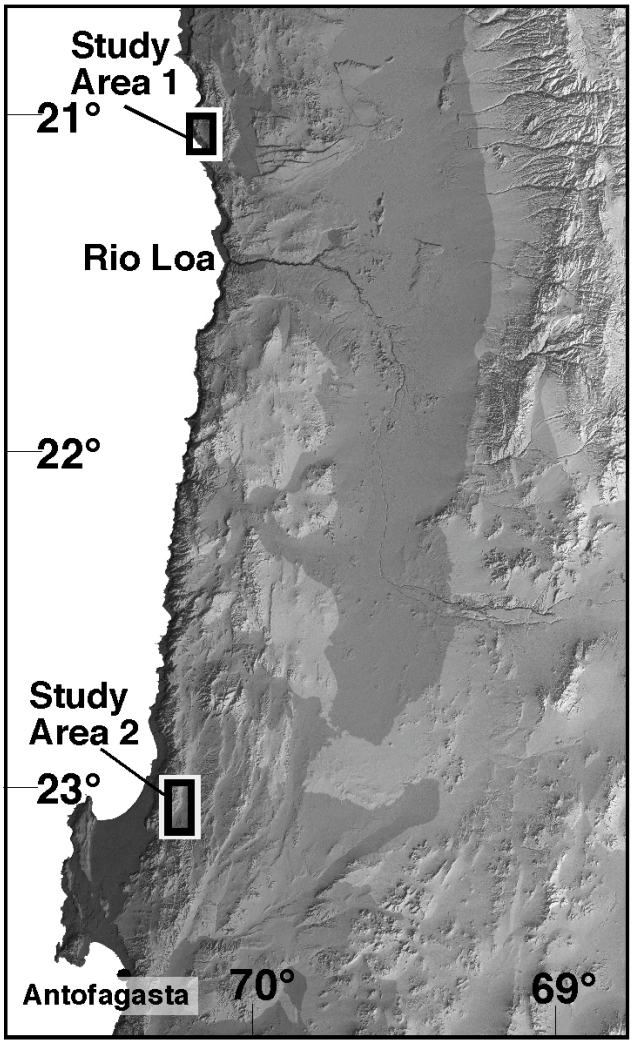

Figure 2.1: Regional location shown on inset of South America. Location of study areas shown on digital elevation model of the Atacama Desert region.

important not only for the potential longevity of plate boundary processes, but also shed light on the nature of coseismic extension.

2.2 Plate boundary seismicity and previous work

Historic records of earthquakes in northern Chile indicate that the subduction zone is divided into distinct rupture segments that rupture with relative consistency both in time and magnitude (Comte & Pardo, 1991). In the region of the Atacama, there are three distinct segments: one that extends south of the Mejillones Peninsula, a second from the Mejillones Peninsula north approximately to Tocopilla, and a third from Tocopilla to the northern border of Chile (Comte & Pardo, 1991). The third, referred to here as the Iquique segment, is a seismic gap that last ruptured in 1877 with an approximate magnitude of 8.8 (Comte & Pardo, 1991). The central segment was a part of that seismic gap that had last ruptured with the northern segment in 1877 until the Mw 7.8 earthquake that occurred in 2007 (e.g. Béjar-Pizarro et al., 2010). The expected recurrence interval for both segments is ~100-200 years (Comte & Pardo, 1991). The segment near Antogafasta last ruptured in 1995 with a Mw=8.0 (e.g. Klotz et al., 1999). Though all three segments are located clearly within a convergent tectonic setting, extensional structures can be found throughout the forearc (e.g. Loveless et al., 2010; Allmendinger & González, 2010). Many of the normal faults in the Coastal Cordillera display reverse motion, complicating the deformational signature of the region relative to seismic events (e.g. Loveless et al., 2010; Allmendinger & González, 2010).

Also characteristic of the region are pervasive tension cracks, with tens to hundreds of meters of length and millimeters to meters of opening (Loveless et al., 2005). Though the

cracks originate from a variety of mechanisms ranging from soil process and topographic effects to drainage events to tectonics, the specific subset discussed in this paper is linked directly to large seismic events in the region. Multiple studies have determined that these features, which cut across topography and maintain orientation for tens to hundreds of meters, are activated coseismically (Loveless et al., 2005; Loveless et al., 2009; Keefer & Moseley, 2004). Loveless et al (2005) determined that the extensional strain associated with a great earthquake as recorded by GPS would be orders of magnitude too weak to produce these features in a single event. This notion is strongly supported by field evidence of reactivation, including fresh cracking in well-preserved older features and the vertical backing of gypsum progressively filling cracks as they form (Loveless et al., 2009). While Loveless et al (2005) suggest that the cracks potentially record hundreds of seismic cycles, they lack absolute ages to find the rate or longevity of cracking in this region.

2.3 Description of crack and fan morphology

The two fan systems we use in this study are located within the Coastal Cordillera. The Punta de Lobos alluvial fan system (Study Area 1 in Figure 2.1) is located at 21.04°S and 70.12°W at an altitude of 600 m to 850 m (asl) and is bounded by the Punta de Lobos fault to its west. The drainage basin for the alluvial fan lies west of the fault, with the upper reaches of the source area truncated by the coastal escarpment. Terrestrial cosmogenic nuclide (TCN) surface exposure ages provide absolute ages from ~900ky to recent (Chapter 1 of this work). The Mititus fans (Study Area 2 in Figure 2.1) at 23.07°S and 70.19°W are more laterally extensive and at lower elevation than the Punta de

Lobos fans 225 km to the north. Though the Mititus fans are technically farther inland, that is only due to the presence of the Mejillones Peninsula to the west. These fans are at a comparable distance to the coastal escarpment as those at Punta de Lobos, though the escarpment here is less pronounced. To the west, the fans abut the Mititus fault, which has normal displacement and is part of complex of domino style normal faults that characterize this part of the Coastal Cordillera. TCN ages for these surfaces are not available, but ages from the northern end of the same basin yield ages ~1.2My and younger (Plazcek et al., 2010). The alluvial fans in both areas experience coastal fog during the winter months, resulting in the induration of the soil with surface salts. Salts are present in the upper few meters of the soils, forming a hard gypcrete crust. The fans at Mititus have less extensive induration of the overall.

Both locations are also cut by extensive coseismic tension cracks that are pervasive throughout the Coastal Cordillera (Loveless et al., 2005). The cracks cut topography, maintaining orientation for tens to hundreds of meters and ranging from millimeters to meters of opening. The heavily indurated soil helps to preserve the surface expression of the cracks, but measurements have shown that cracks can extend at least 12m into the underlying bedrock (Loveless et al., 2005). Crack morphologies vary throughout the Coastal Cordillera, some remaining open and others developing a gypsum fill. This fill provides a glimpse into the cumulative nature of the cracks, with mm-scale vertical banding of gypsum from each subsequent coseismic activation (Loveless et al., 2009). Fresh cracks were observed directly following the 2007 Tocopilla event, both down the center of previously existing cracks and in the surrounding material. Both fan surfaces have NNE-trending dm-wide and meter- to hundreds-of-meters long cracks cutting

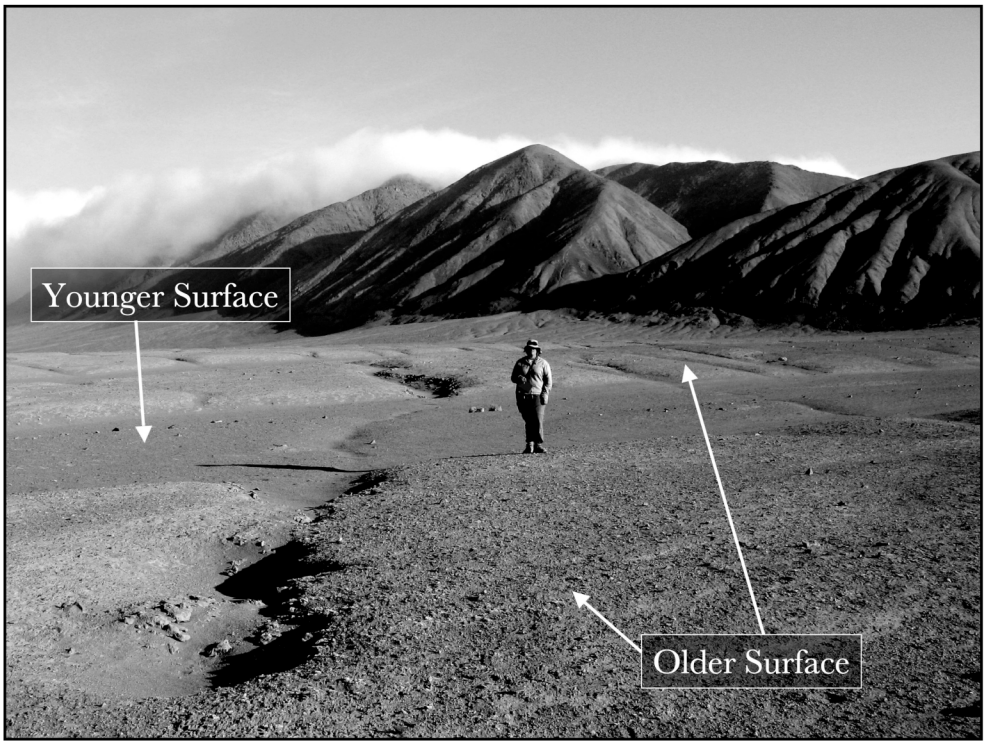

Figure 2.2: Field photograph showing crack expression on two neighboring surfaces. Note that the cracks that extend across both surfaces are wider and more pronounced on the older surface than on the younger surface. Also note that some of the cracks found in the older surface are not expressed in the younger surface at all. Photo by Rick Allmendinger.

their surfaces. The expressions of the cracks change as they cut across neighboring surfaces of differing ages, with more and larger cracks cutting the older fan surfaces. In many cases, individual cracks can be traced between surfaces, displaying more opening on the older surface than the younger (Figure 2.2).

2.4 Strain as Determined by Field Measurements

Quantifying this apparent difference in opening between surfaces required us to estimate aperture from the degraded surface expression of the crack profiles. Ideally, we would trench each crack and measure the opening in profile, but the heavily indurated gypsum soils would require the use of excavation equipment to do so. Instead we approximate the strain using the halfwidth, which is the perpendicular width of the crack at half of the depth (Figure 2.3). To assess the representativeness of this approximation, we trenched 81 cracks where conditions made such trenching possible (Appendix B). As shown in Figure 2.4, halfwidth is a highly representative approximation of the true width of a crack measured at depth. Using halfwidth to approximate opening, we measured ~18.5km of scanlines over 17 surfaces at the two study areas.

Paths for scanlines were selected to be approximately perpendicular to the crack population and provide one of the longest possible transects along the length of the fan. Walking along these paths, we measured the orientation, halfwidth, level of degradation, estimated length and sinuosity, and presence of fresh cracking for each crack we passed. Halfwidths were measured using a tape measure, with error varying with level of degradation of the cracks. Fresh cracks with well-preserved edges were

accurate within a few centimeters, but measurements the most degraded cracks could vary by ~10cm. The opening due to cracking for each scanline was totaled and the extension was calculated as the change in length of the transect (the sum of the openings) divided by the original length (i.e., the final length minus the sum of the openings). There is a clear variation of accumulated strain with age of the surface, increasing from 0.003% on the youngest surfaces to 3.52% on the oldest.

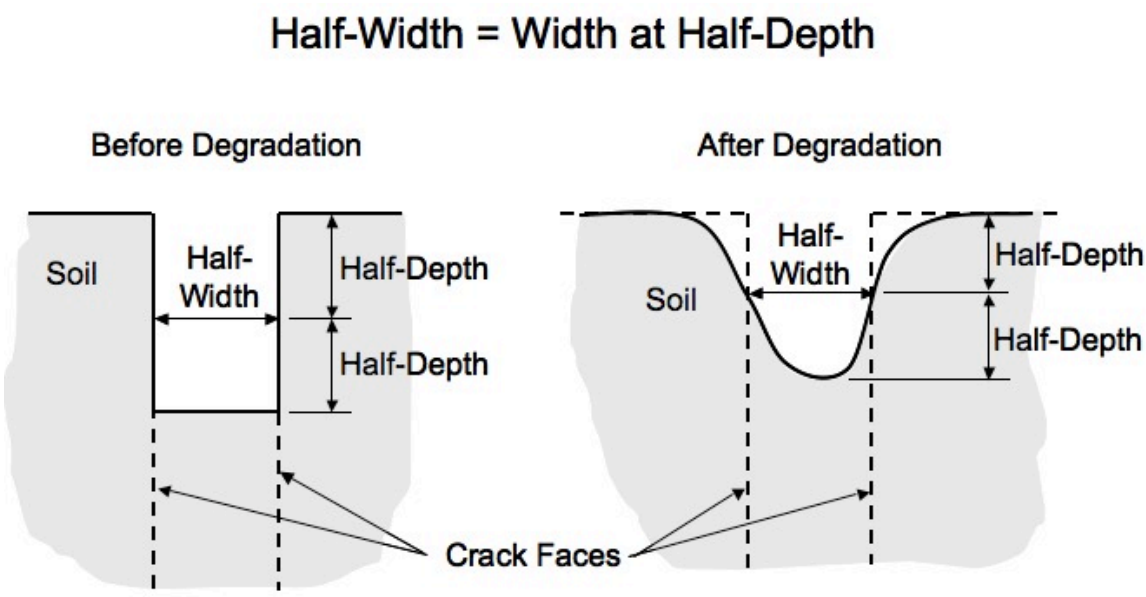

Figure 2.3: Cartoon depicting the field method employed for approximating the true aperture of a crack from its degraded profile.

We can quantify strain rate by using three surface exposure ages determined from terrestrial cosmogenic nuclide levels of ^{10}Be and ^{26}Al at study area 1 (Chapter 1 of this work). These ages do not measure the ages of the cracks directly, but rather the surfaces

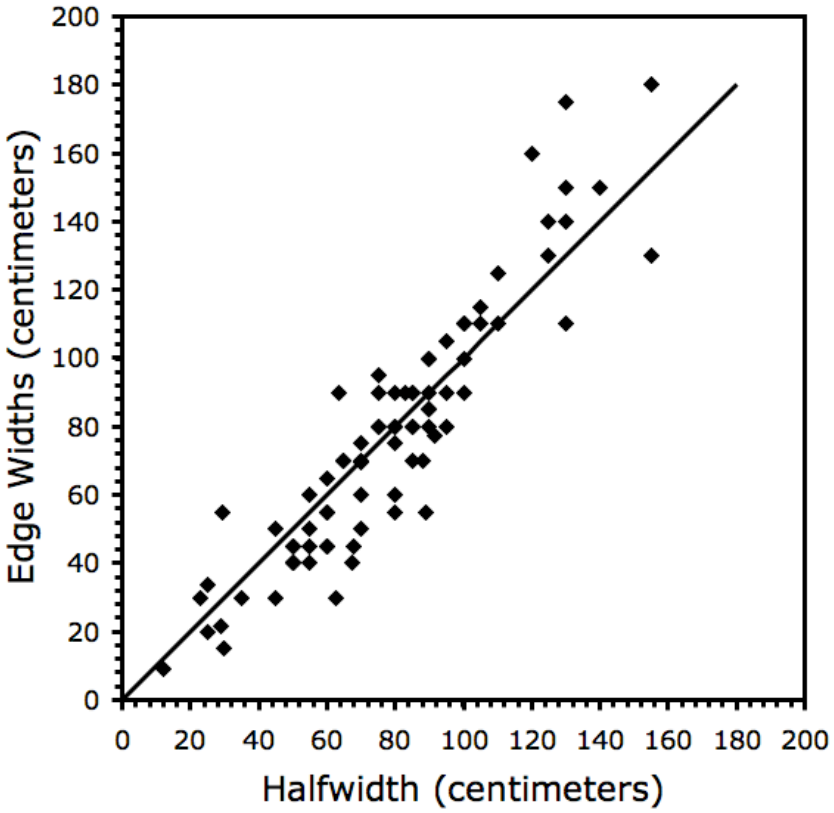

Figure 2.4: Comparison of halfwidth measurements with the true widths of the cracks once excavated. The exhibited 1:1 ratio makes this an excellent approximation for true width where excavation is not possible. Error in the halfwidth measurements is at most ±4cm and the edge width measurements ±2cm.

in which the cracks occur. Because more than one surface was dated, we can determine both bulk strain rate over the span of time since the oldest surface was deposited and see how strain rate varies with time between formation of the different surfaces. Using both calculations for ^{10}Be and ^{26}Al, we find strain rates ranging from 9.8×10^{-16}/s to 2.4×10^{-15}/s. This strongly suggests that the strain rate due to cracking in this region has been consistent for at least the last ~900ky (Figure 2.5).

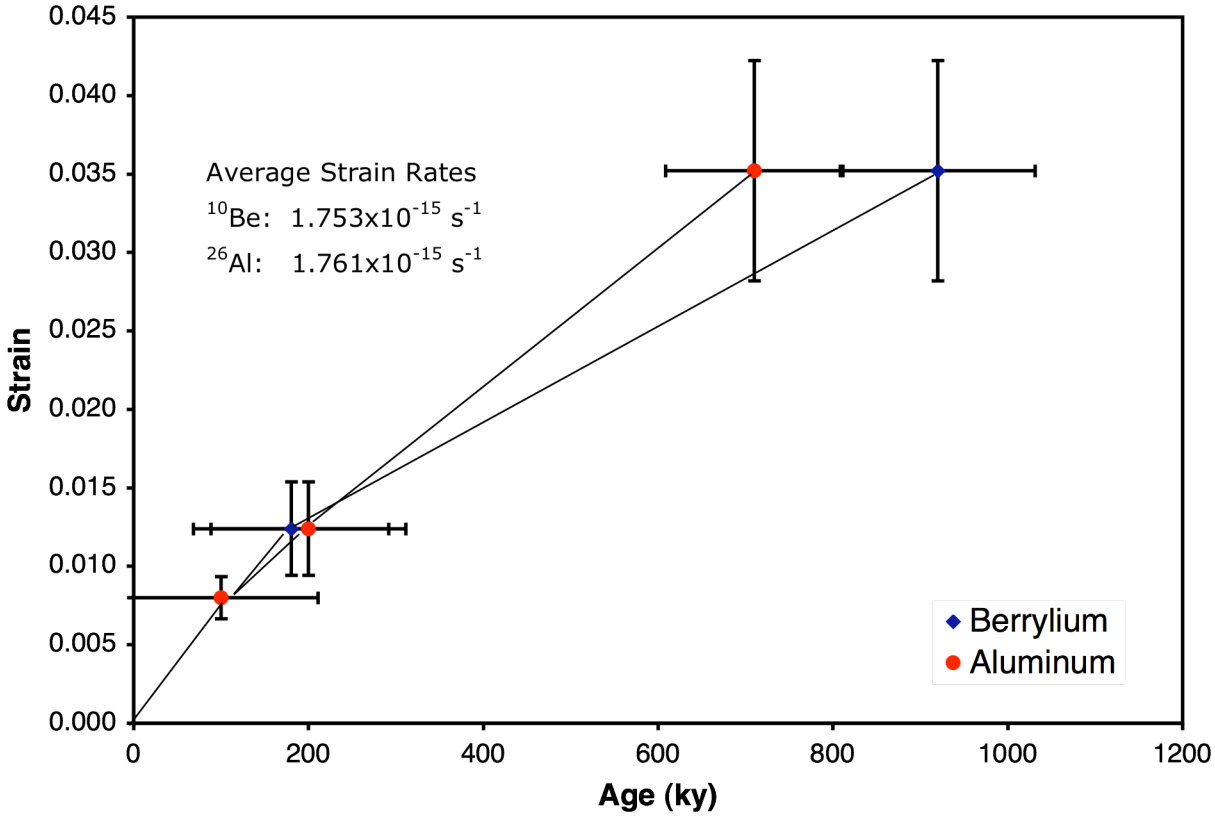

Figure 2.5: Strain as determined by scanline measurements of crack apertures on fan surfaces as a function of TCN surface exposure ages for those surfaces. Note the linear nature of the relationships, suggesting a consistent strain rate for the last ~900ky. The lines serve as a visual aid for changes in strain rate over time for both nuclides.

The other key question is how much strain due to cracking occurs during a single event. This is important not only to assess the representativeness of the long-term record from Study Area 1, but also to assess how much of the surface displacement recorded by GPS is potentially taken up by permanent deformation. The southern area is located only 75km from the epicenter of the 2007 Tocopilla earthquake (e.g. Béjar-Pizarro, 2010). We visited the site only months after the event; it was clear that in addition to the pervasive older cracks there was a clear population of fresh cracks across all the surfaces, both in isolation and within the previously existing cracks. By measuring the millimeter-scale openings from the fresh cracks over 11.4 km of scanlines over 11 surfaces, we

determined an average surface strain of $5.5 \times 10^{-6} \pm 2.8 \times 10^{-6}$ associated with Tocopilla coseismic extension.

2.5 GPS Strain

In order to compare these strains and rates with coseismic geodetic data, we calculated the extensional strain for three recent events: the 2001 Mw 8.1 Antofagasta earthquake, the 2007 Mw 7.8 Tocopilla earthquake, and the 2010 Mw 8.8 Maule earthquake. As there has not been an earthquake on the Iquique segment for the past 135 years, these events serve as the best possible proxies. By determining the coseismic signal of extension as recorded by surface displacements and comparing it to the strain due to cracking, we determine what proportion of this supposedly elastic signal is being produced with permanent deformation. Obviously, one cannot characterize an entire earthquake using a single strain value. Strain varies with the exact nature of the earthquake slip, meaning that even two earthquakes with the same magnitude and epicenter may not produce the same strain at a given point. Nonetheless, the coseismic extension as recorded by the GPS displacements discussed below provides a meaningful comparison for the permanent deformation recorded by the cracks.

Using the Klotz et al. (1999) GPS displacements, we constructed a 1-D strain profile projected along the mean displacement vector. We then calculated the strain recorded by stations in the Coastal Cordillera, thus focusing on the part of the profile where cracking is known to occur. This yields a coseismic strain of $5.6 \times 10^{-6} \pm 3.3 \times 10^{-8}$ from a Mw 8.1 event. Using a similar process, we selected a well-instrumented transect of GPS

stations from the Mw 8.8 Maule event, determined the mean-slip vector, and calculated a 1-D coseismic strain of $2.2 \times 10^{-5} \pm 5.6 \times 10^{-8}$ (Vingny et al., 2011). These two events bookend the anticipated magnitude for an event on the Iquique segment, where Study Area 1 is located.

The coverage of GPS stations near the Tocopilla event is not as extensive, thus making the construction of a meaningful profile more difficult (e.g. Béjar-Pizarro, 2010). Three of the stations, however, form a triangle around Study Area 2, where the strain due to fresh cracking for the Tocopilla event was measured. Using Delaunay triangulation, we determine a coseismic strain of $2.0 \times 10^{-6} \pm 1.6 \times 10^{-8}$. This allows for a nearly direct comparison of surface displacement from GPS with the field expression of strain due to permanent cracking. Again these strain values provide only one characterization of the earthquakes measured, but those values provide important context for the permanent coseismic strains recorded by the cracked surfaces.

2.6 Discussion

The concept of elastic rebound has dominated thinking about the seismic cycle since Reid's (1910) classic study of the 1906 San Francisco earthquake. In this view, elastic strain in the blocks on either side of a locked fault accrues as far field displacement of the blocks continues. During an earthquake, the fault slips and the accumulated elastic strain in blocks on either side of the fault is released, producing elastic rebound. At subducting plate boundaries, this process produces interseismic shortening and coseismic extension in the upper plate. Geophysicists use elastic models that integrate

surface displacement data, such as GPS and InSAR, to determine the distribution of slip on the fault at depth. By definition, elastic deformation is non-permanent; cracks and other forearc coseismic extensional features like normal faults, however, are permanent deformation.

By comparing the amount of strain rate due to cracking over the last ~900ky (Chapter 1 of this work) and the strain due to cracking from a single seismic event to the coseismic extension from recent events as recorded by GPS, we obtain a measure of how much of the coseismic extension signal is made up of permanent deformation (Figure 2.6). To compare the strain rate from the Punta de Lobos fans, we apply the determined strain rate to the expected recurrence interval for the Iquique segment 150 ± 50 years, and we calculate a coseismic extensional strain of $8.0 \times 10^{-6} \pm 2.5 \times 10^{-6}$ per event. This is remarkably consistent with the strain due to cracking from a single event as measured near the Mititus fans from the Tocopilla earthquake. A can be seen in Figure 2.6, these two measures of strain due to coseismic cracking are also remarkably similar to the coseismic extensions as recorded by GPS from recent events.

The coseismic extension from GPS of the 1995 Mw 8.1 Antofagasta earthquake falls in the overlapping range of strain-per-event recorded in both the long-term and single event records, suggesting that the permanent cracking from coseismic extension formed during similar events. The Mw 8.8 Maule event coseismic GPS recorded greater coseismic extensions than the long-term or single event crack records, suggesting that an event of this magnitude may exceed those that produced the cracks seen in the

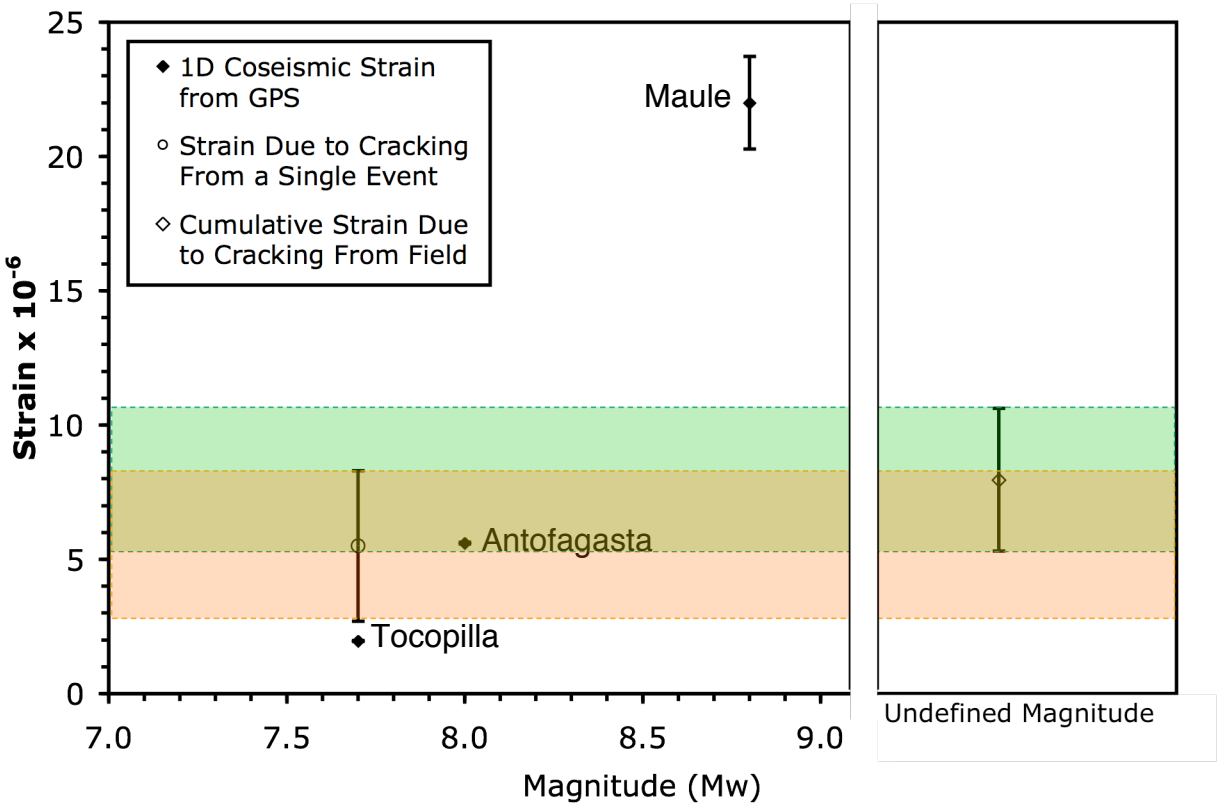

Figure 2.6: Comparison of coseismic extensional strains from GPS and field measurements of coseismic cracks. The orange bar indicates the range of strains suggested by the strain due to fresh cracking that formed during the Tocopilla earthquake and was measured on the Mititus fans. The green bar contains the range of extensional strains per earthquake as inferred from the long-term strain rate from the cracks at Punta de Lobos applied to the 100-200 year recurrence interval expected for the Iquique segment. The black diamonds and error bars are coseismic extensional strain for the named earthquakes as recorded by GPS. The events are separated by magnitude on the horizontal axis for visual clarity.

northern Atacama. The strain due to cracking from the Tocopilla earthquake actually exceeds the coseismic strain from GPS for that event. This may be the result of error from original field measurements, concentration of strain in one small region, or the time between the event and the time the measurements were taken. It is also possible that this is expressing a meaningful critique of the ability of GPS to represent smaller, spatially varying strain fields within a broadly instrumented region. It is also important to note that the orientation of the cracks at Mititus (study area 2) are oblique to the strain field indicated by the GPS, making it possible that the measurements of the fresh cracks perpendicular to their strike may, in fact, underestimate the amount of permanent opening. Additionally, our measures of permanent coseismic extension do not include displacements from any of the numerous normal faults throughout the Coastal Cordillera, making it possible that an even greater component of the extensional signal may be made up of permanent deformation. In any of these cases it is clear that a very significant portion of the coseismic extension recorded by GPS is actually the result of permanent surface deformation.

Considering that the seismic cycle is commonly modeled elastically based on surface displacement data, finding evidence for any significant portion of the coseismic surface displacement signal being taken up permanently is problematic. In the broadest sense it draws the validity of using surface displacement data as representative of processes happening at greater depth into question. More specifically to northern Chile, this provides the logistical question of whether the forearc is getting wider with time or there is permanent interseismic shortening accommodating the difference. Possible mechanisms exist for both possibilities. If we assume that interseismic deformation is

entirely elastic, then the forearc must be widening. We know however, that the coastline is not moving west, but is, in fact, being consumed via subduction erosion (e.g. von Huene et al., 1999). It is possible that this coseismic extension is one way the crust is being thinned for the subduction erosion process. At the other end of the spectrum, assuming that the bulk behavior at large is still elastic, there must be some permanent interseismic surface shortening in the Coastal Cordillera to make up the difference. One excellent possibility is the abundance of reactivated normal faults with recent reverse motion documented throughout the region (e.g. Loveless et al., 2010; Carrizo et al, 2008; Allmendinger & González, 2010). Though widely documented, no satisfactory explanation has yet to be given for the mechanism behind the shortening. Our findings may provide just that mechanism. While it may be tempting to argue that this permanent failure at the surface is not representative of bulk processes at depth, the surface is where displacement measurements put into the geophysical models of that deformation are taken. This does not negate the possible elastic behavior of the crust during the seismic cycle, but it does draw the use of surface displacements recording permanent deformation as inputs for such elastic models into question.

WORKS CITED

Allmendinger, R. W. and González, G. G. 2010, Neogene to Quaternary Tectonics of the Coastal Cordillera, northern Chile: Tectonophysics, 495, 93-110, doi: 10.1016/j.tecto.2009.04.019.

Angermann, D., Klotz, J. and Reigber, C. 1999. Space-geodetic estimation of the Nazca-South America Euler vector. Earth and Planetary Science Letters 171, 329-334.

Béjar-Pizarro, M., Carrizo, D., Socquet, A., Armijo, R., Barrientos, S., Bondoux, F., Bonvalot, S., Campos, j., Comte, D., de Chabalier, J.B., Charade, O., Delorme, A., Gabalda, G., Galetzka, J., Genrich, J., Nercessian, A., Olcay, M., Ortega, F., Ortega, I., Remy, D., Ruegg, J.C., Simons, M., Valderas, C. and Vigny, C. 2010. Asperities and barriers on the seismogenic zone in North Chile: state-of-the-art after the 2007 Mw 7.7 Tocopilla earthquake inferred by GPS and InSAR data. Geophysical Journal International 183(1), 390-406.

Carrizo, D., González, G., and Dunai, T., 2008. Constricción neógena en la Cordillera de la Costa, norte de Chile: neotetónica y datación de superficies con ^{21}Ne cosmogénico. Revista Geológica de Chile 35(1), 1-38.

Comte, D. and Pardo, M. 1991. Reappraisal of great historical earthquakes in the northern Chile and southern Peru seismic gaps. Natural Hazards 4, 23-44.

Hoke, G.D., Isacks, B.L., Jordan, T.E. and Yu, J.S., 2004. Groundwater-sapping origin for the giant quebradas of northern Chile. Geology 32, 605-608.

Houston, J. and Hartley, A., 2003. The central Andean west-slope rainshadow and its potential contribution to the origin of hyper-aridity in the Atacama Desert. International Journal of Climatology 23, 1453-1464.

Keefer, D.K. and Moseley, M.E. 2004. Southern Peru desert shattered by the great 2001 earthquake: implications for paleoseismic and paleo-El Niño-Southern Oscillation records. PNAS 101(30), 10878-10883.

Kendrick, E., Bevis, M.G., Smalley, R. and Brooks, B.A. 2001. An integrated crustal velocity field for the central Andes. Geochemistry Geophysics Geosystems 2. DOI: 10.1029/2001GC000191.

Klotz, J., Angermann, D., Michel, G.W., Porth, R., Reigber, C., Reinking, J., Viramonte, J., Perdomo, R., Rios, V.H., Barrientos, S., Barriga, R. Cifuentes, O. 1999. GPS-derived deformation of the Central Andes including the 1995 Antofagasta M_w=8.0 earthquake. Pure and Applied Geophysics 154, 709-730.

Kober, F., Ivy-Ochs, S., Schlunegger, F., Baur, H., Kubik, P.W., and Wieler, R., 2007. Denudation rates and a topography-driven rainfall threshold in northern Chile: multiple cosmogenic nuclide data and sediment yield budgets. Geomorphology 83, 97-120.

Loveless, J.P., Allmendinger, R.W., Pritchard, M.E., Garroway, J.L. and González, G. 2009. Surface cracks record long-term seismic segmentation of the Andean margin. Geology 37, 23-26.

Loveless, J.P., Allmendinger, R.W., Pritchard, M.E. and González, G. 2010. Normal and reverse faulting in the northern Chilean fore arc. Tectonics 29, TC2001, doi: 10.1029/2009TC002465.

Loveless, J.P., Hoke, G.D., Allmendinger, R.W., González, G., Isacks, B.L. and Carrizo, D.A. 2005. Pervasice cracking of the northern Chilean Coastal Cordillera: new evidence for forearc extension. Geology 33, 973-976.

Nishiizumi, K., Caffee, M.W., Finkel, R.C., Brimhall, G., and Mote, T., 2005. Remnants of a fossil alluvial fan landscape of Miocene age in the Atacama Desert of northern Chile using cosmogenic nuclide exposure age dating. Earth and Planetary Science Letters 237, 499-507.

Okada, Y. 1985. Surface deformation due to shear and tensile faults in a half-space. Bulletin of the Seismological Society of America 75(4), 1135-1154.

Okada, Y. 1992. Internal deformation due to shear and tensile faults in a half-space. Bulletin of the Seismological Society of America 82(2), 1018-1040.

Placzek, C.J., Matmon, A., Granger, D.E., Quade, J., and Niedermann, S., 2010. Evidence for active landscape evolution in the hyperarid Atacama from multiple terrestrial cosmogenic nuclides. Earth and Planetary Science Letters 295, 12-20.

Rech, J.A., Currie, B.S., Michalski, G., and Cowan, A.M., 2006. Neogene climate change and uplift in the Atacama Desert, Chile. Geology 34, 761-764.

Reid, H.F. 1910. The mechanics of the earthquake, in *The California Earthquake of April 18, 1906,* vol. 2, 192 pp., Carnegie Institute of Washington, Washington, D.C.

Vigny, C., Socquet, A., Peyrat, S., Ruegg, J. –C., Métois, M., Madariaga, R., Morvan, S., Lancieri, M., Lacassin, R., Campos, J., Carrizo, D., Bejar-Pizarro, M., Barrientos, S., Armijo, R., Aranda, C., Valderas-Bermejo, M, -C., Ortega, I., Bondoux, F., Baize, S., Lyon-Caen, H., Pavez, A., Vilotte, J.P., Bevis, M., Brooks, B., Smalley, R., Parra, H., Baez, J. –C., Blanco, M., Cimbaro, S. and Kendrick, E. 2011. The 2010 M_w 8.8 Maule mega-trhrust earthquake of central Chile, monitored by GPS. Scienceexpress, 10.1126/science.1204132. retrieved from www.scienceexpress.org.

Von Huene, R., Weinrebe, W. and Heeren, F. 1999. Subduction erosion along the north Chile margin. Geodynamics 27, 345-358.

CHAPTER 3

3 ACTIVATION OF ALLUVIAL FANS IN THE HYPER-ARID ATACAMA DESERT: IMPLICATIONS FOR INTERPRETING MARTIAN FANS

3.1 Introduction

Though the current Martian climate is unable to sustain liquid water, there is an extensive geomorphic record of periods when water played a more prominent role (e.g. Carr & Clow, 1981; Baker, 2001; Hyneck & Phillips, 2003). Attempts to utilize analogs to interpret these fluvial deposits have spanned many of the Earth's coldest and driest landscapes (e.g. Breed et al., 1982; Hauber et al., 2009; Kochel & Trop, 2008). Recently, attention has shifted to features reminiscent of terrestrial alluvial fans found in numerous Martian craters. Alluvial fans often preserve one of the only records of flooding events or fluvial activity in arid to hyperarid regions, since the water supply may not be great enough to make it to the main fluvial channels (Harvey, 1997; Hooke, 1967). This is particularly important on Mars, where various models suggest that the surface-water supply may have been punctuated or fleeting (Baker, 2001). Most analogs for large Martian alluvial fans have depended on melt-water or ground water as the primary sources for fluid, with precipitation playing only a peripheral role in potential groundwater recharge any later than the Noachian (Kraal et al., 2008; Moore & Howard, 2005). The discovery of sub-kilometer alluvial fans with higher-order tributaries in the Later Hesperian-Amazonian Mojave Crater (Williams & Malin, 2008) renewed questions about the presence and duration of potential precipitation on the more recent Martian surface.

Using terrestrial features as Martian analogs can be difficult, due to differences in major governing forces (e.g. Baker, 2001), but comparing similar depositional environments on both planets can provide insight into Martian environments that will remain inaccessible for at least the near future. The alluvial fans of the Atacama Desert (Figure 3.1) serve as a compelling analog, the Quaternary-to-recent fans have formed and remained relatively active through a period of hyperaridity (e.g. Chapter 1 of this work). These fans provide an opportunity to study the morphologies of fans in a hyperarid environment, as well as the relationship of those morphologies to depositional mechanisms and water supply. The alluvial fans of the Coastal Cordillera are of similar scale and have similar morphologies to those in Mojave Crater on Mars (Figure 3.2). The higher-order tributary systems originating from topographic highs for the Martian fans strongly suggest precipitation as the primary source for water, further suggesting a post-Noachian presence of precipitation (Williams & Malin, 2008). Barring what broader implications this might have for Martian climate, more basic questions about the formation and preservation of these features remain.

Alluvial fans of the Atacama Desert present a record of a few influential events over an extended period of stability. The sedimentary and geomorphologic records these events left on the landscape were so profound due to the convergence of four primary factors: the presence of a heavily indurated crust during fan formation and preservation, the styles of weathering of the source material, the weathering of material after deposition, and the amount of water necessary to mobilize such a landscape. In combination, these factors result in the exceedingly efficient mobilization and transport

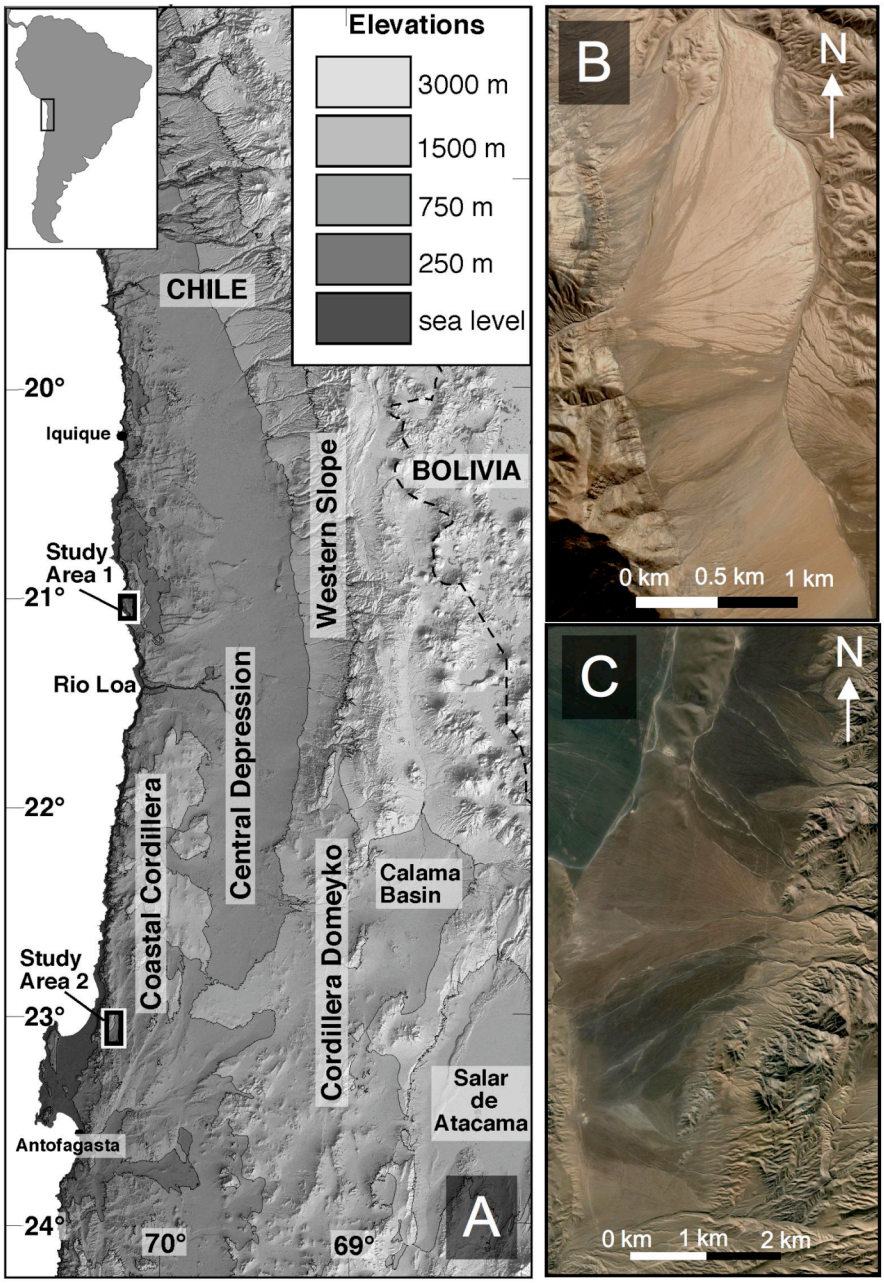

Figure 3.1. Location map of Atacama Desert and QuickBird imagery of analog features in the Coastal Cordillera. A) Major zones of Atacama Desert and locations of study areas. B) QuickBird imagery of Punta de Lobos fans from GoogleEarth Pro at 21.039°S 70.126°W. Location labeled as Study Area 1 in part A. C) QuickBird imagery of Mitius fans from GoogleEarth Pro at 23.076°S 70.196°W. Location labeled as Study Area 2 in part A.

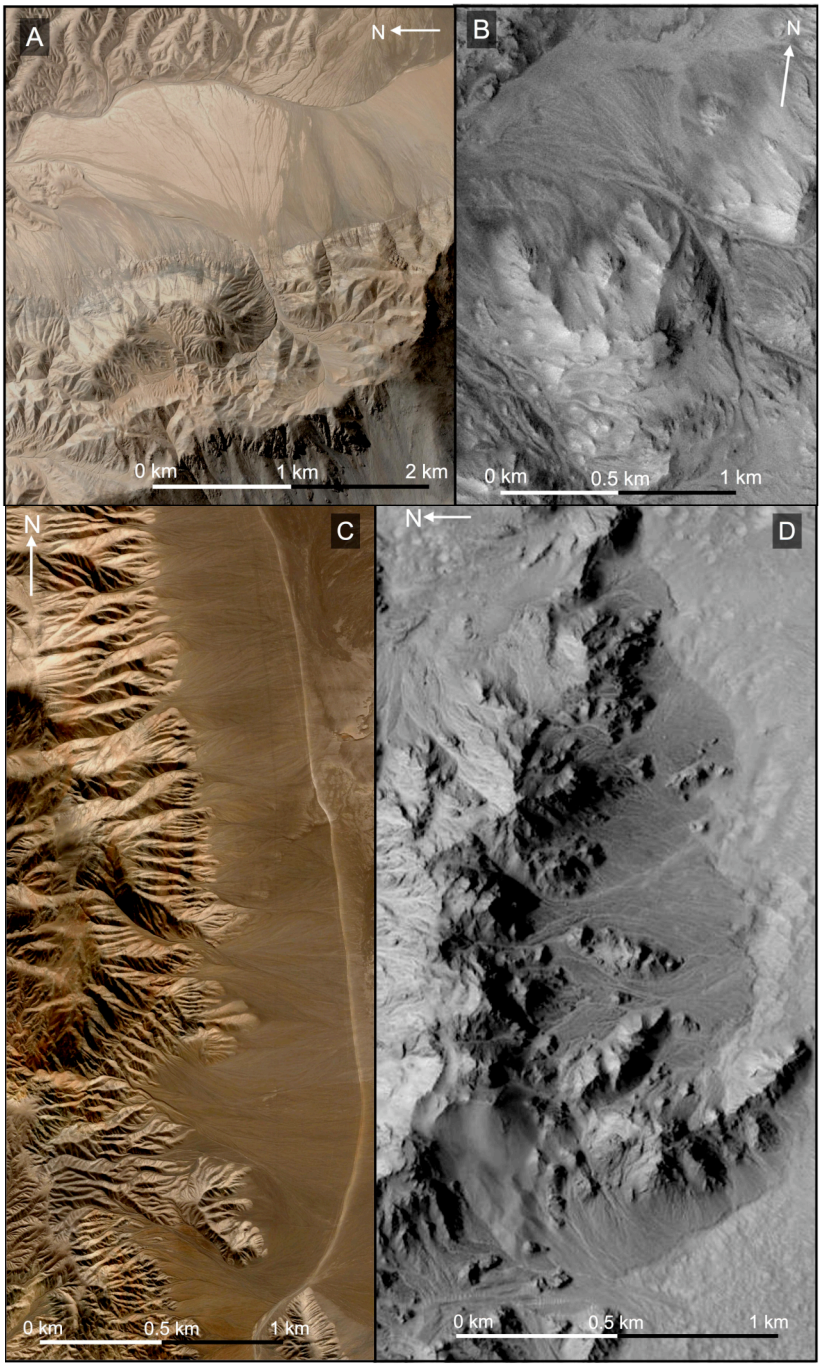

Figure 3.2. Comparison of Atacama fans with martian counterparts. A) QuickBird imagery of Punta de Lobos fan from GoogleEarth Pro at 21.039°S 70.126°W. B) MOC image of single fan in Mojave Crater. Located at 7.334°N 327.432°E in MOC image R0601306:MOC. C) QuickBird imagery of bajadas near Salar Grande at 21.057°S 70.087°W. Located within Study Area 1 box labeled on Figure 3.1A. D) HiRISE image of bajada in Mojave Crater. Located at 7.736°N 326.627°E on image PSP_002167_1880.

of sediment during what would be considered, in any landscape with less-extreme conditions, to be a minor precipitation event. These instances of sediment mobilzation and transport are what are referred to as activations throughout this chapter. We conduct a first-order assessment of whether the induration and weathering styles typical of the Atacama may be playing a role on small Martian fans using morphological comparisons of terrestrial and Martian fans, nighttime Thermal Emission Imaging System (THEMIS) imagery of select fans in Mojave crater, and known precipitation events and resulting sediment mobilizations in the Atacama as a baseline comparison for comparable features on Mars.

3.2 Alluvial Fans

Alluvial fans are depositional features, which form when the confined streams of high-relief environments are allowed to spread and lose velocity in the available space of an adjacent low-relief environment. In high-relief terrains, water tends to be confined to streams and catchments forming a network of tributaries, which leave the mountain front at one or relatively few points. Once the stream has passed through the mountain front, it is no longer confined to channels and stream power reduces significantly, resulting in deposition (Hooke, 1967). Though alluvial fans can be found in most climates, there are a number of conditions that can make formation more favorable. As the most basic level, alluvial fans require a sediment supply from highlands and a sudden decrease in stream power downstream (Harvey, 1997). These conditions do exist in humid and sub-humid environments (Kochel, 1990), but are made even more favorable in particularly dry regions. The lack of vegetation in arid to hyper-arid

environments leads to high storm sediment production as well as high rates of sediment transport in mountain streams. The episodic nature of sediment supply is more highly exaggerated when events are more rare, and high evaporation and infiltration rates lead to more abrupt decreases in stream power down slope (Harvey, 1997).

The formation of an alluvial fan, under the right conditions, is initially controlled by long-term environmental factors, such as tectonic setting and local geology (Harvey, 1997). Subsequent aggradation or dissection is often more highly influenced by shorter-term conditions like climate and vegetation (Harvey, 1997). Deposits ultimately take the form of debris flow, sheet flow, or channel deposits. In general, large source terrains result in fluvially dominated processes, whereas smaller and steeper basins are more likely to produce debris-flow-dominated fans (Harvey, 1997). Fans transition between fluvial and debris-flow processes as sediment and water supply change.

The cone shape typical of most alluvial fans is the result of numerous episodes of deposition, during which channels are cut, overflowed, and rerouted in order to take the easiest path down the fan (Hooke, 1967). The fan apex is the point where the channel system changes from tributary in the source terrain to distributary in the zone of deposition. If the fanhead is incised, the point at which the incised channel meets the fan surface and is able to spread is called the intersection point. If the incised channel cuts the entire fan, the fan surface itself is completely transected and is considered inactive (Harvey, 1997).

Identifying alluvial fans from satellite imagery presents its own difficulties, because alluvial fans are not the only features with a triangular signature in plan view. Martian features that have been identified as alluvial fans share the main morphological signatures of incised channels, a clear apex, and activations with on-lapping and cross-cutting relationships (Moore & Howard, 2005; Kraal et al., 2008; Williams & Malin, 2008). This distinguishes them from other fan-shaped features on Mars such as viscous flow fields, which lack a clear apex, deltas, which have marked breaks in slope and positive channeling, and planation surfaces, which lack channels and episodic formation (Moore & Howard, 2005; Kraal et al., 2008; Williams & Malin, 2008).

3.3 Using the Atacama as an Analog

In order to draw comparisons between Martian fans and their terrestrial counterparts, we focus on an environment long respected as one of the best Earth-analogs for the Martian surface: the Atacama Desert. As one of the oldest (Dunai et al., 2005; Nishiizumi et al., 2005) and driest (Houston and Hartley, 2003) landscapes on Earth, the Atacama exemplifies the powerful shaping influence that rare, punctuated events can have on an otherwise stable and dry landscape. Spanning over 200,000km^2, it extends from Northern Chile to Southern Peru and the Pacific Ocean to the Western Andean Flank (Figure 3.1). The current hyperarid conditions are the combined result of the Humboldt Current and Hadley Circulation to the west and the Andean rainshadow to the east. The resulting desert is categorized as hyperarid based both on levels of precipitation and potential evapotranspiration (Houston & Hartley, 2003; Ewing et al., 2006). Conditions have been hyperarid for at least the last 10 Ma (Houston & Hartley,

2003; Nishiizumi et al., 2005; Hoke et al., 2004, Rech et al., 2006; Kober et al., 2007), making the region an excellent comparison for Mars relative to other terrestrial landscapes. Slightly more humid regions exist along the fringes of the desert, including the lower elevations of the coastal escarpment and the Western Andean Flank. In the core, rain is less than 1mm annually and parts of the coastal cities register 3-4 mm per year (Houston & Hartley, 2003). Many of these averages, however, are reflective of single events over a year or even a decade (Houston & Hartley, 2003; Houston, 2006; McKay et al., 2003). The intermittent moisture of these peripheral regions does not reach the core of the desert, where highly soluble soil nitrates have been accumulating for at least 13 Ma (Rech et al., 2003).

Recent work focusing on Terrestrial Cosmogenic Nuclide (TCN) ages of Atacama surfaces has revealed that, despite the antiquity of the general landscape, including boulders dating back millions of years (e.g. Dunai et al., 2005), more recent activations of alluvial surfaces suggest a level of activity and modification as characteristic of a hyperarid environment (Plazcek et al., 2010; Hall et al., 2008; González et al., 2006; Kober et al., 2007; Chapter 1 of this work). Some of the work on features of the Coastal Cordillera are particularly compelling, as the activation can be attributed to precipitation rather than groundwater (e.g. Hartley et al., 2005; Haug et al., 2010). The Coastal Cordillera, which is bounded by the 1000m coastal escarpment to the west, is isolated from moisture sourced over the Andes and is above the elevations affected by the sparse winter rainfalls along the coast (Rech et al., 2003). The precipitation that does reach into the higher elevations of the Coastal Cordillera does so on timescales of decades to centuries and includes only <1 cm of rain over a 24-hour period (Houston &

Hartley, 2003). The greater governing influence in the Coastal Cordillera is the coastal fog, known locally as the *camanchaca*. This fog affects elevations between 300 and 1000m and plays an integral role in the formation of the crusty, durable soils characteristic of the region (Rech et al., 2003). Sulfur-rich aerosols and heavily indurated crusts are believed to play similar roles on Mars (e.g. Tosca et al., 2004; Banin et al., 1997; Settle, 1979), thus making these processes so important.

This chapter focuses on a set of key characteristics which likely have particular relevance to the formation and preservation of alluvial fans on Mars. The first is the sulfur-rich fog. The camanchaca not only plays a role in developing the heavily indurated soils of the Coastal Cordillera, comparable durable soils of which are also believed to exist on Mars (Quinn et al., 2005; Sutter et al., 2005; McLennan & Grotzinger, 2009; Tosca et al., 2004; Banin et al., 1997; Settle, 1979), but also impacts the general style of weathering in the coastal range. Aided by the general lack of water to transport material and the abundance of soil salts, boulders and bedrock often weather directly into smaller pieces in place, breaking down rather than transporting (Placzek et al., 2010). As a result, older surfaces tend to become more finely grained. The breakdown of boulders and clasts without transport has actually drawn into question the validity of traditional TCN sampling practices in the Atacama, as the boulders present appear to relicts of a previous landscape rather than expressions of recent surface modification (Placzek et al., 2010; Hall, et al., 2008). This is of particular importance when attempting to use clast size as a proxy for fluid availability for depositional units after hundreds of thousands to millions of years.

Also related, and also relevant, is the combined effect this style of weathering and induration of soils has on sediment transport during events when water is available. Decreased sediment size, lack of vegetation, and decreased potential for infiltration in heavily indurated soils leads to significantly higher sediment loads and transport rates than would be expected in other even slightly less arid environments (Reid & Frostick, 1997). It is acknowledged that arid environments are significantly more efficient at transporting sediment during a rain event of equivalent magnitude than their more humid counterparts (Reid & Frostick, 1997), and the extreme rarity of events in the Atacama paired with the hyperarid conditions in the interim make this environment likely to be extremely efficient. Since such factors are likely also relevant to Mars (e.g. Tosca et al., 2004; Banin et al., 1997; Settle, 1979), the amount and rate of sediment transport is likely to have as large of an impact shaping the surface during punctuated events as in the Atacama.

These conditions, while as similar as any on Earth are to Mars, are still orders of magnitude less severe than those on Mars. Precipitation is even more rare, periods of dormancy and longer, and temperatures make surface water even less stable. Though Mars is believed to have had a warmer, wetter period in its history, many argue that was prior to 3.5Gy (e.g. Baker et al., 1991). Mars also has a lower gravitational acceleration, lower atmospheric pressure, and prevailing temperatures below freezing, which can influence sediment transport, debris flows, and the role of ice (Baker, 2001). Comparisons of such systems are fruitful. As argued by Baker (2001), the use of analogies in the absence of other options at a minimum provides testable working hypotheses. Providing just such hypotheses is our goal in completing this work.

3.4 Alluvial Fans of the Coastal Cordillera

Despite the onset of hyperaridity 10Ma (Houston & Hartley, 2003; Nishiizumi et al., 2005; Hoke et al., 2004, Rech et al., 2006; Kober et al., 2007), surfaces of the Atacama have maintained a level of activity. Numerous studies of multiple landforms have shown activations within the last million years under the hyperarid climate regime (Plazcek et al., 2010; Hall et al., 2008; González et al., 2006; Kober et al., 2007; Chapter 1 of this work). In particular, alluvial fans throughout the Coastal Cordillera have remained active throughout the Quaternary - in some cases within the last 100ky (Hartley et al., 2005; Haug et al., 2010; Placzek et al., 2010; Chapter 1 of this work). Unlike the fans of the western slope, those in the Coastal Cordillera are not fed by snowmelt and are in many cases unlikely to be sourced by groundwater. The fans in this region range from numerous coalesced surfaces forming extensive bajadas along the eastern and western flanks of the cordillera to smaller more isolated fans within the coastal range. Morphologically the fans within the Coastal Cordillera are primarily fluvial, with distinct channels, and shallow slopes. Evidence points to precipitation as the most likely source of available water, based on higher order tributaries and high drainage densities in broader, shallower source basins, particularly with tributaries originating from local topographic highs. Based on the extreme paucity of rain events, the morphological indicators of precipitation highlight the rare and profound nature punctuated rain events have on forming alluvial fan deposits in this landscape. This work focuses on two sets of low-angle fans in the Coastal Cordillera with aprons 1-1.5km in length.

The Punta de Lobos alluvial fan system is located at 21.04°S and 70.12°W at an altitude of 600 m to 850 m asl and is bounded by the Punta de Lobos fault to its west (Figure 3.1B). The drainage basin for the alluvial fan lies west of the fault, with the upper reaches of the source area truncated by the coastal escarpment. The proximity to the escarpment makes it extremely unlikely that groundwater played any significant role in mobilizing the sediment deposited on the fans. The alluvial fan experiences coastal fog during the winter months. Salts are present in the upper few meters of the soils, forming a hard gypcrete crust that would require construction equipment for meaningful excavation, on the oldest surfaces, whereas the youngest surface has no discernable salt development. The alluvial fan surfaces are hardest on the oldest surfaces. In addition, the size of surface clasts decreases with relative alluvial fan age. The alluvial fan surfaces are hardest on the oldest surfaces. Additionally, the older surfaces, due to prolonged exposure to harsh weathering conditions, are also the most finely grained. TCN surface exposure ages reveal that the surfaces have been formed within the last 900ky and the youngest surface has likely currently active (Chapter 1 of this work).

The second focus area, at 23.07°S and 70.19°W, is more laterally extensive and at lower elevation than the Punta de Lobos fans 225 km to the north (Figure 3.1C). Though the Mititus fans are technically farther inland, that is only due to the presence of the Mejillones Peninsula to the west. These fans are at a comparable distance to the coastal escarpment as those at Punta de Lobos, though the escarpment here is less pronounced. Mititus is still within the zone consistently affected by the coastal fog, but has less

extensive induration of the soils overall. To the west, the fans abut the Mititus fault, which has normal displacement and is part of complex of domino style normal faults that characterize this part of the Coastal Cordillera. The fans at this location cover more than 7 km from north to south and receive sediment from at least seven separate drainages. This lateral extent and the possibility of simultaneous activations make it difficult to form a single timeline of relative ages across the system. Surfaces range from heavily indurated on the oldest to minor salt formation on the youngest surfaces (Chapter 1 of this work). Nearby TCN surface exposure ages (Placzek et al., 2010) suggest that there have been multiple activations within the last million years.

3.5 Alluvial Fans on Mars

3.5.1 Evidence of Water on Mars

Though the current Martian climate is unable to sustain liquid water, there is an extensive geomorphic record of periods when water played a more prominent role (see Baker, 2001 for summary). Beyond the well-known catastrophic outflows, there is mounting evidence for a more widespread role of surface water throughout Martian history. Evidence of well-developed meanders (Malin & Edgett, 2003; Pondrelli et al., 2005) draw particular attention, as it suggests that material must have become consolidated between activations. Controversies continue to abound, however, concerning the source, duration, and timing of many of the fluvially driven deposits. Disagreements of the nature of distributary deposits in Holden crater serve as excellent examples, with Malin and Edgett (2003) seeing evidence for short, catastrophic bursts of water and Moore et al. (2003) arguing for a more gradual formation on the scale of years

to decades based on the same imagery. Similarly, potentially Amazonian outflow events (Ivanov & Head, 2001) and 10^4-year persistent paleolakes in the Ebenswalde crater (Malin & Edgett, 2003; Ori et al., 2000), suggest dramatic changes in climate and result in equally dramatic levels of controversy.

As for timing, most fluvial features are divided into Noachian and post-Noachian, which refer to periods during and after greatest bombardment respectively. Erosion rates are believed to have dropped from 10^2-10^4 mm per 10^6 years (Hynek and Phillips, 2001) to 10^{-1}-10^{-2} mm per 10^6 year (Golombek & Bridges, 2000) between those two periods. Though this may seem like a dramatic change, erosion during the earlier, warmer, wetter period was likely to be more consistent and the colder, dryer post-Noachian as more punctuated episodes (Baker, 2001). This makes it possible that the nature of sediment transport did not fundamentally change, merely the frequency with which it occurred. Recent evidence for modern gully activation (Malin & Edgett, 2000) brings the debates about source and timing into the current day.

3.5.2 Investigation of Fan-Shaped Features

Because multiple features are triangular in plan view, studies have focused on features that lack the abrupt termini and frontal scarps at valley mouths characteristic of deltas and the highly variable grain size and lobes characteristic of debris-flow-dominated fans (Moore & Howard, 2005; Kraal et al., 2008; Williams & Malin, 2008). A primary investigation of such features by Moore and Howard (2005) was limited to between 0° and 30°S, based on the argument that the areas to the north and south would be obscured by the presence of a pervasive mantle over those terrains. They also limited

their study to fans longer than 10km from apex to toe. Using ~100m/pixel daytime thermal infrared (IR) Thermal Emission Imaging System (THEMIS) images, Moore and Howard (2005) identified fans in 18 craters, most of which had been sufficiently surveyed by the Mars Orbiter Laser Altimeter (MOLA) for topographic analyses. The fan-bearing craters all fell within the range of 18° and 29°S and were located in three distinct clusters, rather than randomly over the surface. These clusters were limited to three zones of the southern highlands: Southern Margaritifer Terra, Southwest Terra Sabaea, and Southwest Tyrrhena Terra (Moore & Howard, 2005).

A subsequent survey of the entire Martian surface by Kraal et al. (2008) revealed that almost all fans of $>40km^2$ in area fell within the three zones already identified by Moore and Howard (2005), with only a few outliers. Like Moore and Howard's (2005) survey, the fan population identified within this survey was limited to the resolution of the THEMIS imagery. The host craters fell in the distinctive diameter range of 30-150 km, with 65 fans being found in total (Kraal et al., 2008). The orientations of the fans themselves did not provide meaningful clusters, with fans emerging from crater rims in practically every orientation (Kraal et al., 2008). It remains unclear whether the clustering of fan-bearing craters is a result of formation or preservation, though Kraal et al. (2008) argue that the lack of partially buried fans in other areas makes it more likely that the Southern Highlands were more conducive to forming fans rather than just preserving them. The lack of clarity on this matter makes it difficult to try to draw any conclusions as far as relationship to, or origin of, water supply.

Williams and Malin (2008), in a more focused study, observed sub-kilometer fans that seem to be unique to Mojave Crater (Figure 3.2B,D). Since the Mojave Crater itself is believed to be Late Hesperian-Amazonian (Williams and Malin, 2008), these fans are likely to have formed in a different epoch and under different conditions than the larger fans of the previous studies. It is also possible that many of the features preserved in it may have existed elsewhere but have since been eroded or covered by mantling. Either possibility highlights the importance of studying these particular fans. Though age is difficult to approximate by crater counting, due to the small area of these features, the presence of only very few small craters further supports their youthful origin (Williams and Malin, 2008). Like the recent gully activity on Mars (Malin et al., 2000), these features bring the role of water into an extremely modern context.

Much smaller in scale, these fans range from ~100 to 1500m in length and originate from massifs on the crater walls (Williams and Malin, 2008). Some fan-like features appear to be viscid flow *fields* rather than distinct fans with a clear apex, but even such features would suggest a fluid-based reworking of the material involved (Williams and Malin, 2008). The most characteristic fans have channels and an apex, but also have the unique, higher-order tributary systems. Though they observe isolated fans (Figure 3.2B), many coalesce to form well-channeled bajadas (Figure 3.2D). Williams and Malin (2008) argue that the cross-cutting relationships present suggest incremental formation, with clear incision of channels and abandonment and on-lapping of older surfaces. Some channels intersect midfan and overflow in what appears to be sheetfloods onto the surface and other channels dissect older surfaces completely and terminate in smaller fan deposits beyond the edge of the older surface (Williams & Malin, 2008;

Williams et al., 2004; Williams et al., 2004b). As mentioned above, these fans have higher order tributary systems with first-order tributaries originating at topographic highs suggesting precipitation as the likely source for water (Williams & Malin, 2008). Subsequent toe erosion suggests potential reworking even after initial fan formation, and some of the craters on fan surfaces appear to have been degraded by flow (Williams & Malin, 2008).

3.6 Discussion

Young alluvial fans with indications of precipitation-sourced activation in Mojave crater beg questions about the role of localized precipitation events on Mars. The overall clustering of alluvial fans in the lower central latitudes of the Martian surface suggests that that surface is somehow more conducive to the formation or the preservation of alluvial fans than craters elsewhere on the planet (Moore & Howard, 2005; Kraal et al., 2008). Alluvial fans of similar scope and morphology have formed in Coastal Cordillera of northern Chile in a desert that has been hyperarid for at least 10Ma (Chapter 1 of this work). The fans of the Atacama form and are preserved due to the combined influences of extensive weathering and induration followed by rare, punctuated precipitation that may be relevant to Mars. These factors are: the presence of a heavily indurated crust during fan formation and preservation, the style of weathering of the source material, the weathering of material after deposition, and the amount of water necessary to mobilize such a landscape.

First to consider is the heavily indurated crust that is pervasive in the Atacama (Rech et al., 2003; Ewing et al., 2006), which plays an active role in both the formation and preservation of alluvial fans in the Coastal Cordillera. Forming a durable layer of soil salts up to meters thick, the crusts of the Coastal Cordillera are primarily indurated with gypsum sourced from marine aerosols present in the coastal fog (Rech et al., 2003). In older surfaces, the induration is so severe as to preclude excavation even with heavy equipment. The first role the induration plays in alluvial fan development is during formation. By significantly reducing the infiltration capacity of the soils, the flow volume and flow rate can remain higher further down the fan (Reid & Frostick, 1997). After deposition, induration helps to make the surface materials more cohesive and resistant than loose sediment. This helps not only in the preservation of the fan surfaces, but also serves as a mechanism for increasing the cohesiveness of fan material enough to allow for the formation of sinuous channels during subsequent activations. Both the preservation of fan surfaces and the presence of sinuous channels on Martian fans have been points of concern in the Martian research community (Malin & Edgett, 2003; Moore et al., 2003). The potential presence of indurated fan surfaces in Mojave Crater could help explain the presence of these features and is addressed more thoroughly in the analysis of two sets of nighttime THEMIS images at the end of the discussion section.

The second factor, the weathering of the source material, is linked both to the generally stable nature of the landscape and the coastal fog. In the Coastal Cordillera the fog not only interacts with the bedrock chemically, but also allows for the repeated hydration of salts that help to break down the material as well (Ewing et al., 2006). Studies of TCN

exposure ages reveal that the erosion rate for bedrock in the Atacama is frequently higher than that of sedimentary deposits (Nishiizumi et al., 2005). Though the bedrock breaks down efficiently, the lack of available surface water results in formation of a mantle of finer-grained pieces overlaying the bedrock rather than steep slopes with boulders at their bases (Figure 3.3). Due to the absence of vegetation or intermittent precipitation, this material is mobilized with extreme efficiency when the decade-to-century scale rain events do occur (Hartley et al., 2005). Pervasive mantling of bedrock and a general lack of precipitation events are both also present on Mars, albeit to more extreme levels in both time and volume. We search for the presence of such mantled bedrock landscapes near the alluvial fans in Mojave crater, which is addressed further at the end of the discussion.

The third factor, weathering that takes place after deposition, is related to the balance between the first two factors. Once material has been deposited on a low-angle fan surface, the lack of minor rain events makes it likely that material will remain there. The weathering processes described in the previous paragraph continue to act on material on the fan surface, breaking down what larger clasts may have passed through the system (Ewing et al., 2006; Placzek et al., 2010). As a result, older surfaces are not only more heavily indurated, but also finer grained. This affects the composition of the fan as it is preserved, removing what record there may have been of changes in available clast size or magnitude of mobilized sediment over time. We attempted to look for evidence of increased induration on older fan surfaces using nighttime THEMIS imagery (figures), using thermal conductivity as a proxy for grain size and induration, but the

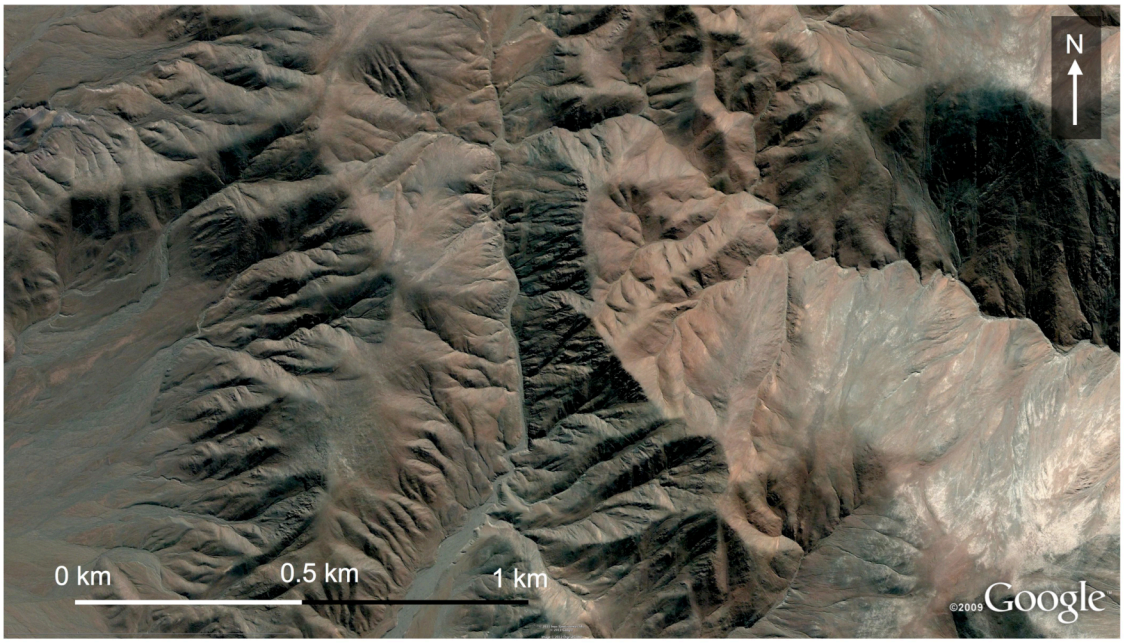

Figure 3.3. Example of extensively mantled bedrock with few bedrock exposures in the Coastal Cordillera near Mititus fans. QuickBird image from GoogleEarth Pro located at 23.009°S 70.237°W. Location contained within Study Area 2 box labeled on Figure 3.1A.

resolution is too coarse to distinguish between neighboring fans of the scale of those found in Mojave crater. It may be possible to do such an analysis on larger fans, but most of the larger fans were either formed by groundwater or are not close enough to a neighboring fan to determine relative age relationships. If higher resolution THEMIS imagery were to become available or direct observations of such fans were possible with a rover, it is likely that older fans would be both more finely grained and more heavily indurated than more recent deposits.

The THEMIS imagery was more revealing concerning factors one and two. Figures 3.4 and 3.5 show side-by-side comparisons of the visual and nighttime THEMIS imagery for a single fan and a set of bajadas in Mojave crater. Bedrock mantling and induration of fan surfaces appears to be evident in both cases, though in differing capacities. Figure

3.4 shows a single fan, flow to the north, with clear tributary channels originating from nearby topographic highs. In the nighttime THEMIS imagery, the bedrock has a lower temperature than the adjacent fan surfaces. This is consistent with what would be expected for the presence of a fine-grained mantle over the bedrock and indurated fan material. In Figure 3.5, most of the bedrock retains its heat at night, with the fans being colder than the bedrock, but warmer than the well-mantled crater floor. As can be seen in the visual imagery, however, most of the bedrock here does not appear to be extensively mantled. The exceptions that do appear to have mantling, outlined in yellow (Figure 3.5), appear colder than the surrounding bedrock on the THEMIS imagery. Though more work could theoretically be done comparing induration levels between neighboring fans, as stated before, the resolution of the current THEMIS imagery is too coarse to do so. On a first-order level, both in-place weathering of bedrock into fine material and induration of fan surfaces appear to be present in the fans observed in Mojave crater.

The presence of indurated fans and mantled bedrock on Mars suggest that similar processes may be aiding the formation and preservation of Martian fans during rare precipitation events, making the amount of precipitation necessary to activate the Atacama equivalents important to consider. Estimates have been made for how much water would be required to form the alluvial fans found on Mars, based primarily on the scaling of known events from fans in the arctic deserts or the American southwest (Hauber et al., 2009; Armitage et al., 2011; Irwin et al., 2008; Moore et al., 2003; Jerolmack et al., 2004). Since many of the estimates for larger fans include groundwater

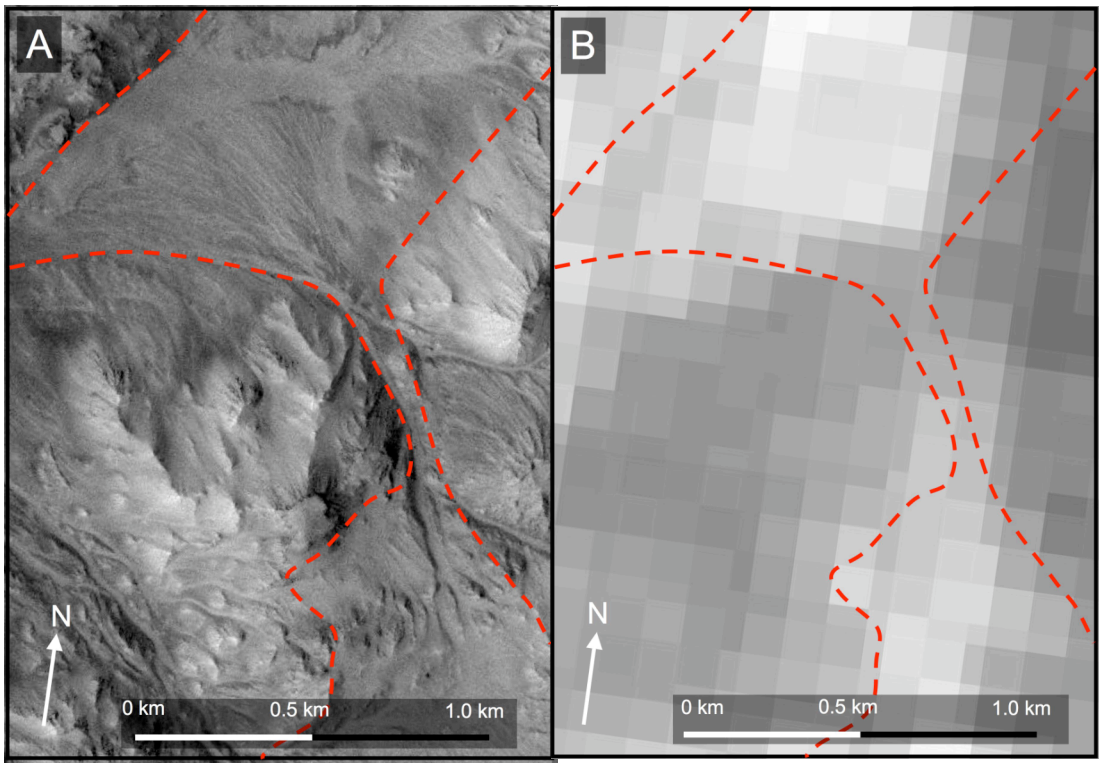

Figure 3.4. Side by side comparison of A) visual and B) nighttime THEMIS imagery for a single fan in Mojave Crater located at 7.334°N 327.432°E in MOC image R0601306:MOC. Red lines divide the depositional material of the fans from the surrounding bedrock. The fan deposit has a higher nighttime temperature (lighter color) than the neighboring well-mantled bedrock. The visual image is a portion of MOC image R0601306:MOC and the THEMIS imagery is from the THEMIS night IR 100 meter global mosaic v.13.

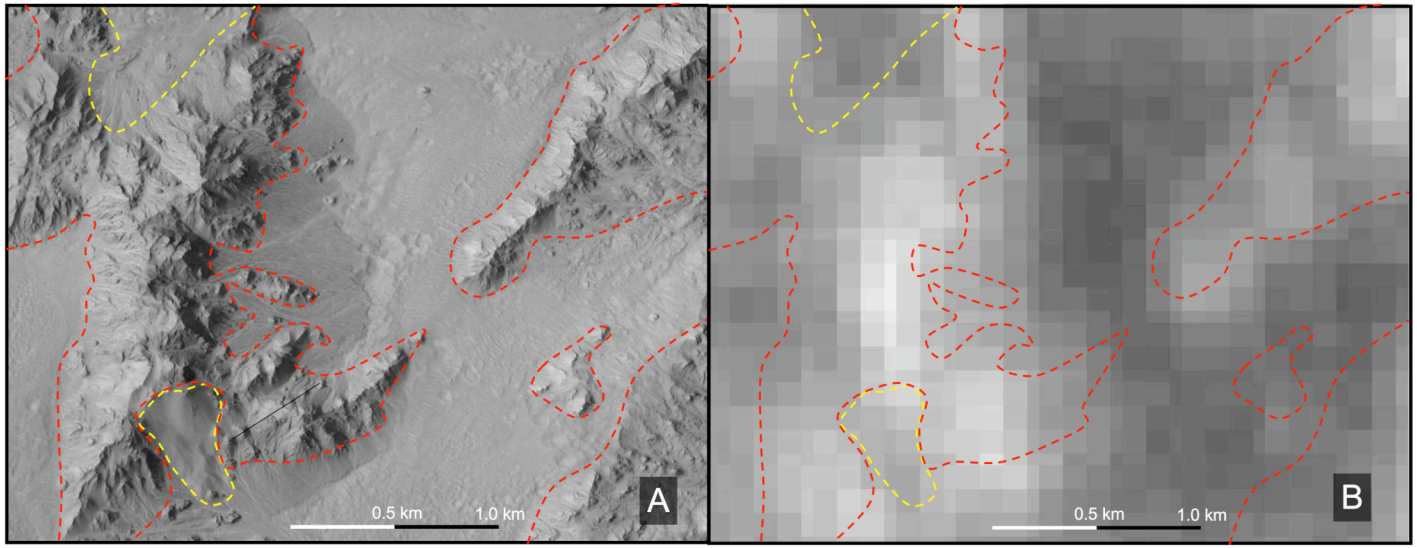

Figure 3.5. Side by side comparison of A) visual and B) nighttime THEMIS imagery for a bajada in Mojave Crater located at 7.736°N 326.627°E. Red lines divide the bedrock from the fans and crater floor. Yellow lines outline areas of well-mantled bedrock. The un-mantled bedrock has a higher nighttime temperature (lighter color) than the surrounding fans or crater floor. The indurated fans are warmer than the crater floor material. The mantled bedrock is noticeably cooler than the neighboring unmantled bedrock. The visual image is a portion of HiRISE image PSP_002167_1880 and the THEMIS imagery is from the THEMIS nighttime IR 100 meter global mosaic v.13.

components and would consider significant scaling, we focus on estimates for the small fans of Mojave crater. Based on measurements from alluvial fans in the White Mountains of California and Nevada, Williams and Malin (2008) approximate that it would require a total volume of ~$1.2x10^6 m^3$ of water from precipitation at a rate of 6-9cmh^{-1} to form a fan with a volume of ~$5.7x10^5 m^3$. The 1991 rain event in the Atacama mobilized a similar volume of sediment (~$6.0x10^5 m^3$) and can be used at least as a first-order comparison (Ramirez & Perez, 2011). Based on measurements throughout the coast a total volume of ~$1.7x10^5 m^3$ of water fell over 3 hours at a rate of 1.4cmh^{-1} (Ramirez & Perez, 2011). Both the total volume of water and precipitation rate are significantly less than those estimated based on the less-arid White Mountain fans.

Based on visual and nighttime THEMIS imagery of small alluvial fans in the Mojave crater on Mars, it seems likely that the induration and weathering processes facilitating the formation and preservation of precipitation-driven fans in the Coastal Cordillera are also facilitating the precipitation-driven activations on their Martian counterparts. These findings support the notion that the young alluvial fans on Mars could have been formed by exceedingly short-lived local precipitation events rather than requiring broader-scale climatic changes. The source of this post-Noachian precipitation is still a contested area of current research.

WORKS CITED

Armitage, J.J., Warner, N.H., Goddard, K. and Gupta, S. 2011. Timescales of alluvial fan development by precipitation on Mars. Geophysical Research Letters 38. L17203, doi: 10.1029/2011GL048907.

Baker, V.R. 2001. Water and the martian landscape. Nature 412, 228-236.

Baker V.R., Strom, R.G., Gulick, V.C., Kargel, J.S., Komatsu, G. and Kale, V.S. 1991. Ancient oceans, ice sheets, and the hydrological cycle on Mars. Nature 352, 589-594.

Banin, A., Han, F.X., Kan, I. and Cicelsky, A. 1997. Acidic volatiles and the Mars soil. Journal of Geophysical Research 102(E6), 13,341-13,356.

Breed, C.S., McCauley, J.F. and Grolier, M.J. 1982. Relict drainages, conical hills, and eolian veneer in southwestern Egypt: applications to Mars. Journal of Geophysical Research 87(B12), 9929-9950.

Carr, M.H. and Clow, G.D. 1981. Martian channels and valleys: their characteristics, distribution, and age. Icarus 48, 91-117.

Dunai, T.J., Gonzáles López, G.A., and Juez-Larré, J., 2005. Oligocene-Miocene age of aridity in the Atacama Desert revealed by exposure dating of erosion-sensitive landforms. Geology 33, 321-324.

Ewing, S.A., Sutter, B., Owen, J., Nishiizumi, K., Sharp, W., Cliff, S.S., Perry, K., Dietrich, W., McKay, C.P., and Amundson, R., 2006. A threshold in soil formation at Earth's arid-hyperarid transition. Geochimica Cosmochimica Acta 70, 5293-5322.

Golombek, M.P. and Bridges, N.T. 2000. Erosion rates on Mars and implications for climate change: constraints from the Pathfinder landing site. Journal of Geophysical Research 105, 1841-1853.

González, G.L., Dunai, T., Carrizo, D., and Allmendinger, R., 2006. Young displacements on the Atacama Fault System, Northern Chile from field observations and cosmogenic ^{21}Ne concentrations. Tectonics 25, TC3006.

Hall, S.R., Farber, D.L., Audin, L., Finkel, R.C., and Mériaux, A.-S., 2008. Geochronology

of pediment surfaces in southern Peru: implications for quaternary deformation of the Andean forearc. Tectonophysics 459, 186-205.

Hartley, A.J., Mather, A.E., Jolley, E., and Turner, P. 2005. Climate controls on alluvial-fan activity, Coastal Cordillera, northern Chile. In Harvey, A.M., Mather, A.E., and Stokes, M. (eds), *Alluvial Fans: Geomorphology, Sedimentology, Dynamics.* Geological Society, London, Special Publications: 251, 95-115.

Harvey, A.M. 1997. The role of alluvial fans in arid zone fluvial systems. In D.S.G. Thomas (ed), *Arid zone geomorphology: process, form and change in drylands,* 2nd edition. Wiley, Chichester, Wiley: 231-259.

Hauber, E. Preusker, F., Trauthan, F., Reiss, D., Carlsson, A.E., Hiesinger, H., Jaumann, R., Johansson, H.A.B., Johansson, L., Johnsson, A., McDaniel, S., Olvmo, M. and Zanetti, M. 2009. Morphometry of alluvial fans in a polar desert (Svalbard, Norway): implications for interpreting Martian fans. Lunar Planetary Science XL. Abstract 1658 (2009).

Haug, E.W., Kraal, E.R., Sewall, J.O., Van Dijk, M. and Chong Diaz, G., 2010. Climatic and geomorphic interactions on alluvial fans in the Atacama Desert, Chile. Geomorphology 121 (3-4), 184-196.

Hoke, G.D., Isacks, B.L., Jordan, T.E. and Yu, J.S., 2004. Groundwater-sapping origin for the giant quebradas of northern Chile. Geology 32, 605-608.

Hooke, R. le B. 1967. Processes on arid region alluvial fans. Journal of Geology 75, 438-460.

Houston, J. and Hartley, A., 2003. The central Andean west-slope rainshadow and its potential contribution to the origin of hyper-aridity in the Atacama Desert. International Journal of Climatology 23, 1453-1464.

Hynek, B.M. and Phillips, R.J. 2001. Evidence for extensive denudation of the martian highlands. Geology 29, 407-410.

Hynek, B.M., and Phillips, R.J. 2003. New data reveal mature, integrated drainage systems on Mars indicative of past precipitation. Geology 31(9), 757-760.

Irwin, R.P., Grant, J.A. and Howard, A.D. The alluvial fan complex in Holden crater: implications for the environment of early Mars. Lunar and Planetary Science XXXIX. Abstract 1869 (2008).

Ivanov, M.A. and Head, J.W. 2001. Chryse Planitia, Mars: topographic configuration, outflow channel continuity and sequence, and tests for hypothesized ancient bodies of water using Mars Orbiter Laser Altimeter (MOLA) data. Journal of Geophysical Research 106, 3275-3295.

Jerolmack, D.J., Mohrig, D., Zuber, M.T. and Byrne, S. 2004. A minimum time for the formation of Holden Northeast fan, Mars. Geophysical Research Letters 31, L21701, doi:10.1029/2004GL021326.

Kober, F., Ivy-Ochs, S., Schlunegger, F., Baur, H., Kubik, P.W., and Wieler, R., 2007. Denudation rates and a topography-driven rainfall threshold in northern Chile: multiple cosmogenic nuclide data and sediment yield budgets. Geomorphology 83, 97-120.

Kochel, R.C. 1990. Humid fans of the Appalachian Mountains. In A.H. Rachocki and M. Church (eds), *Alluvial fans: a field approach.* Wiley, Chinchester: 109-129.

Kochel, R.C. and Trop, J.M. 2008. Earth analog for high-latitude landforms and recent flows on Mars: icy debris fans in the Wrangell Volcanic Field, Alaska. Icarus 196, 63-77.

Kraal, E.R., Asphaug, E., Moore, J.M., Howard, A., and Bredt, A. 2008. Catalogue of large alluvial fans in Martian impact craters, Icarus 194, 101-110.

Malin, M.C. and Edgett, K.S. 2000. Evidence for recent groundwater seepage and surface runoff on Mars. Science 288, 2330-2335.

Malin, M.C. and Edgett, K.S. 2003. Evidence for persistent flow and aqueous sedimentation on early Mars. Science 302, 1931- 1934.

McLennan, S.M. and Grotzinger, J.P. Sulfur and the sulfur cycle on Mars. Lunar and Planetary Science XL. Abstract 2152 (2009).

Moore, J.M, Howard, A.D., Dietrich, W.E., and Schenk, P.M. 2003. Martian layered f

fluvial deposits: implications for Noachian climate scenarios. Geophysical Research Letters 30(24), 2292, doi:10.1029/2003GL019002.

Moore, J.M. and Howard, A.D. 2005. Large alluvial fans on Mars. Journal of Geophysical Research 110, E04005, doi:10.1029/2004JE002352.

Nishiizumi, K., Caffee, M.W., Finkel, R.C., Brimhall, G., and Mote, T., 2005. Remnants of a fossil alluvial fan landscape of Miocene age in the Atacama Desert of northern Chile using cosmogenic nuclide exposure age dating. Earth and Planetary Science Letters 237, 499-507.

Ori, G.G., Marinangeli, L. and Baliva, A. 2000. Terraces and Gilbert-type deltas in crater lakes is Ismenius Lacus and Memnonia (Mars). Journal of Geophysical Research 105, 17629-17641.

Placzek, C.J., Matmon, A., Granger, D.E., Quade, J., and Niedermann, S., 2010. Evidence for active landscape evolution in the hyperarid Atacama from multiple terrestrial cosmogenic nuclides. Earth and Planetary Science Letters 295, 12-20.

Pondrelli, M., Balvia, A., Di Lorenzo, S., Marinangeli, L. and Rossi, A.P. 2005. Complex evolution of paleolacustrine systems on Mars: an example from Holden crater. Journal of Geophysical Research 110. Doi:10.1029/2004JE002335.

Quinn, R.C., Zent, A.P., Ehrenfruend, P., Taylor, C.L., McKay, C.P., Garry, J.R.C., Grunthaner, F.J. Dry acid deposition and accumulation on the surface of Mars and in the Atacama Desert, Chile. Lunar Planetary Science XXXVI. Abstract 2282 (2005).

Ramirez, F.J. and Perez, P.C., 2011. Passing volume calculation system (PVCS): computer software for managing data on watersheds that produce mud flows and the case of Quebrada La Cadena, Antofagasta, Chile. Natural Hazards, doi: 10.1007/s11069-011-9744-5.

Rech, J.A., Currie, B.S., Michalski, G., and Cowan, A.M., 2006. Neogene climate change and uplift in the Atacama Desert, Chile. Geology 34, 761-764.

Rech, J.A., Quade, J., and Hart, W.S., 2003. Isotopic evidence for the source of Ca and S in soil gypsum, anhydrite and calcite in the Atacama Desert, Chile. Geochimica et Cosmochimica Acta 67, 575-586.

Reid, I. and Frostick, L.E. 1997. Channel form, flows and sediments in deserts. In D.S.G. Thomas (ed), *Arid zone geomorphology: process, form and change in drylands,* 2nd edition. Wiley, Chichester, Wiley: 206-230.

Settle, M. 1979. Formation and deposition of volcanic sulfate aerosols and Mars. Journal of Geophysical Research 84(B14). 8343-8354.

Sutter, B., Dalton, J.B., Ewing, S.A., Amundson, R., and McKay, C.P. Infrared spectroscopic analyses of sulfate, nitrate, and carbonate-bearing Atacama Desert soils: analogs for the interpretation of infrared spectra from the Martian surface. Lunar Planetary Science XXXVI. Abstract 2182 (2005).

Tosca, N. J., McLennan, S.M., Lindsley, D.H. and Schoonen, M.A.A. 2004. Acid-sulfate weathering of synthetic Martian basalt: The acid fog model revisited, Journal of Geophysical Research 109, E05003, doi:10.1029/2003JE002218

Williams, R.M.E., Edgett, K.S., Malin, M.C., Zimbelman, J.R. 2004. Unique fan-shaped Landforms in Mojave crater, Xanthe Terra, Mars. In: Workshop on Martian Valley Networks, August 11-14 2004.

Williams, R.M.E. and Malin, M.C. 2008. Sub-kilometer fans in Mojave Crater, Mars. Icarus 198, 365-383.

Williams, R.M.E., Malin, M.C., Edgett, K.S. Young fans in equatorial crater in Xanthe Terra, Mars. Lunar Planetary Science XXXV. Abstract 1415 (2004b).

APPENDIX A

SUPPLEMENTARY MATERIAL FOR CHAPTER 1

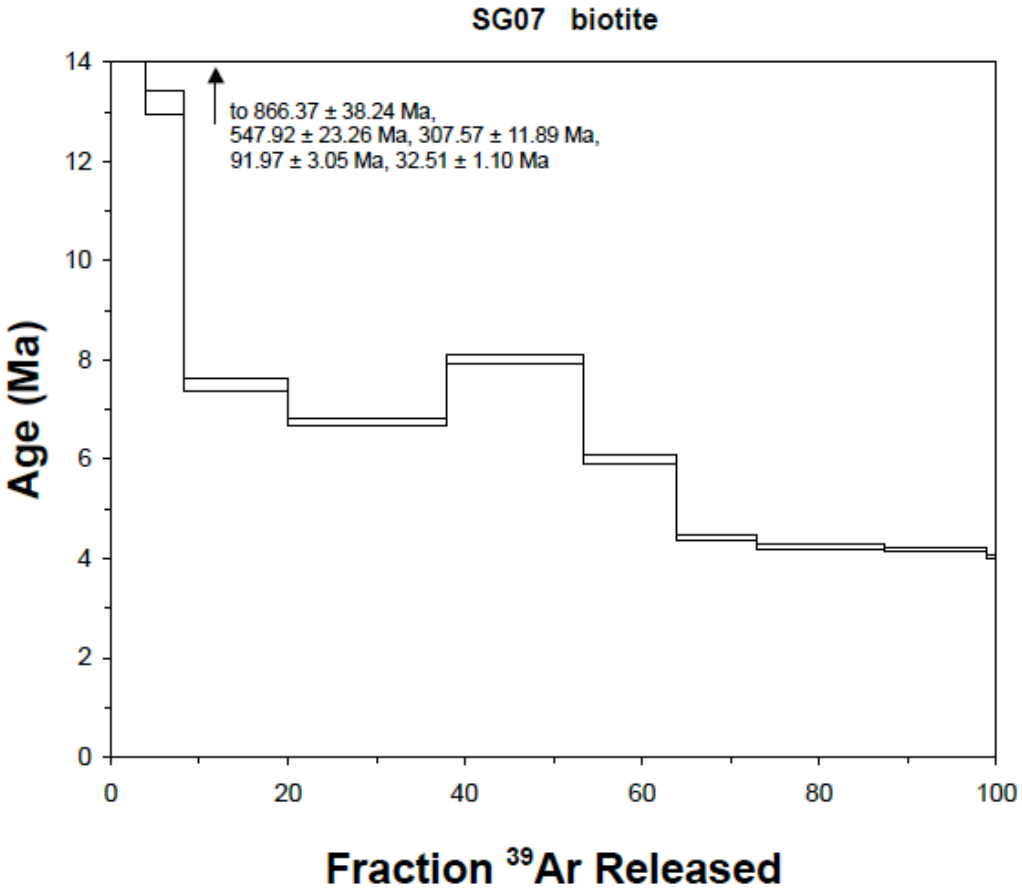

Figure A.1: Age spectrum for $^{40}Ar/^{39}Ar$ stepwise heating at the Nevada Isotope Geochronology Laboratory at the University of Nevada Las Vegas for biotite samples of the reworked tuffaceous beds at Punta de Lobos. The age spectrum lacks a plateau and there is a suggestion of excess argon. The total gas age of 10.09 ± 0.04 Ma is likely an overestimate. The samples lack sufficient sanidine, so biotite separates were dated.

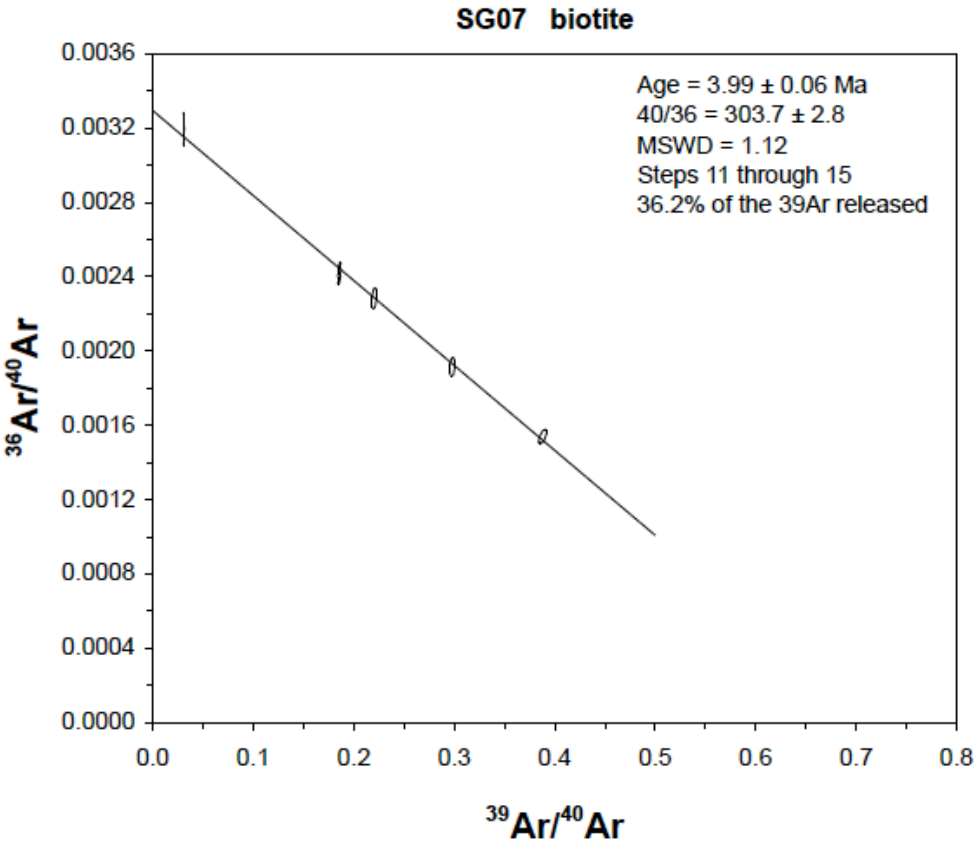

Figure A.2: An isochron age determined from about 36% gas release between heating steps 11 and 15, is well defined and yields an age of 3.99 ± 0.06 Ma. While this can hardly be considered a robust result, it is consistent with the surface ages as well as dated fans in similar settings elsewhere in the Coastal Cordillera and very tentatively suggests that at the head of the fan, ~3 m of coarse clastic sediment accumulated in about the last 4 million years.

Table A.1: Sample Processing Inputs and Corrections for ^{10}Be Samples

Chile samples

Sample Number	Target number	Qz wt (g)	Be carrier wt (g)	Carrier Name	Carrier Concentration (mg/g)	North Latitude (DD)	East Longitude (DD)	Altitude (m)	Sample thickness (cm)	10Be/9Be	error	# of Be-9 atoms	# of Be-10 atoms	error
Bajada1	76499	15.4616	0.5135	LBC 08	1.155	-21.0318	-70.1277	578	4	4.928E-13	*2.296E-14*	3.96317E+19	1.263E+06	*5.884E+04*
ActiveChannel1	83690	18.8316	0.4488	LBC 08	1.155	-21.0397	-70.1306	645	3	4.478E-13	*1.289E-14*	3.46382E+19	8.237E+05	*2.371E+04*
ActiveChannel3	76492	18.7146	0.5076	LBC 08	1.155	-21.0284	-70.1249	541	4	5.752E-13	*6.421E-14*	3.91764E+19	1.204E+06	*1.344E+05*
Fan1Channel	76491	14.4267	0.4611	LBC 08	1.155	-21.0376	-70.1257	611	3	7.035E-13	*2.965E-14*	3.55875E+19	1.735E+06	*7.314E+04*
Fan2ClastB	83691	16.7014	0.4765	LBC 08	1.155	-21.0378	-70.1259	609	5	2.167E-12	*4.955E-14*	3.67761E+19	4.771E+06	*1.091E+05*
Fan2Pebbles	76488	18.9183	0.3844	LBC 08	1.155	-21.0378	-70.1259	609	4.5	2.681E-12	*6.518E-14*	2.96679E+19	4.204E+06	*1.022E+05*
Fan3ClastA	76481	18.5738	0.4236	LBC 08	1.155	-21.0417	-70.1263	617	6	6.998E-13	*2.847E-14*	3.26933E+19	1.232E+06	*5.012E+04*
Fan1Pebbles	76487	19.2618	0.4223	LBC 08	1.155	-21.0377	-70.1282	624	4.5	1.198E-12	*6.889E-14*	3.2593E+19	2.027E+06	*1.166E+05*
Fan1ClastA	76495	20.3489	0.4514	LBC 08	1.155	-21.0377	-70.1282	624	6.5	1.776E-12	*6.682E-14*	3.48389E+19	3.040E+06	*1.144E+05*
Fan2ClastA	76493	19.2645	0.4138	LBC 08	1.155	-21.0378	-70.1259	609	4.5	2.742E-12	*1.003E-13*	3.19369E+19	4.546E+06	*1.663E+05*
Fan1ClastC	76484	20.0673	0.4191	LBC 08	1.155	-21.0377	-70.1282	624	8	9.146E-13	*1.042E-13*	3.2346E+19	1.474E+06	*1.680E+05*
Fan1ClastD	83694	20.6777	0.4221	LBC 08	1.155	-21.0377	-70.1282	624	7	9.799E-13	*2.899E-14*	3.25775E+19	1.544E+06	*4.567E+04*
Fan2ClastC	76480	16.4134	0.3856	LBC 08	1.155	-21.0378	-70.1259	609	4	2.768E-12	*3.328E-13*	2.97605E+19	5.019E+06	*6.035E+05*
Fan1ClastB	76497	20.6486	0.4136	LBC 08	1.155	-21.0377	-70.1282	624	7.5	9.603E-13	*5.404E-14*	3.19215E+19	1.485E+06	*8.354E+04*
Fan3ClastB	76489	9.8371	0.5364	LBC 08	1.155	-21.0417	-70.1263	617	8	2.145E-14	*3.383E-15*	4.13992E+19	9.027E+04	*1.424E+04*
ChileMT2	76498	11.6134	0.4719	LBC 08	1.155	-21.0485	-70.1378	857	2	1.461E-13	*1.735E-14*	3.64211E+19	4.582E+05	*5.442E+04*
SedSample2	76476	13.2139	0.4168	LBC 08	1.155	-21.0395	-70.1301	635	2	5.462E-13	*2.354E-14*	3.21685E+19	1.330E+06	*5.730E+04*
ChileMT1	76483	13.2240	0.4294	LBC 08	1.155	-21.0485	-70.1378	857	1.5	2.2071E-13	*1.30375E-14*	3.31409E+19	5.531E+05	*3.267E+04*
SedSample3	76482	9.0527	0.4301	LBC 08	1.155	-21.0443	-70.1380	741	2	4.1821E-13	*2.00816E-14*	3.3195E+19	1.534E+06	*7.364E+04*
SedSample1	76485	10.7424	0.4753	LBC 08	1.155	-21.0284	-70.1249	541	2	4.3831E-13	*1.63051E-14*	3.66835E+19	1.497E+06	*5.568E+04*
ActiveChannel2	76486	20.3416	0.4477	LBC 08	1.155	-21.0443	-70.1380	741	3	7.5441E-13	*7.74229E-14*	3.45533E+19	1.281E+06	*1.315E+05*
Fan3Pebbles	76479	18.6820	0.4653	LBC 08	1.155	-21.0417	-70.1263	617	2	2.7531E-13	*1.31919E-14*	3.59117E+19	5.292E+05	*2.536E+04*
ChileMT3	76475	17.8927	0.4283	LBC 08	1.155	-21.0473	-70.1386	814	3	7.0331E-13	*6.65078E-14*	3.3056E+19	1.299E+06	*1.229E+05*
ChileColluvium						-21.0377	-70.1311	680	5	*4.068E-13*	*1.102E-14*			

Table A.2: Blank Corrections for ^{10}Be Samples

	Be-10/Be-9 E-15			Be-10/Be-9 corrected	error
Chile MT3	706.4	66.8000	Chile MT3	703.31	66.50779728
Sed Sample 2	549.3	23.6700	Sed Sample 2	546.21	23.53684817
Fan 3 Pebbles	278.4	13.3400	Fan 3 Pebbles	275.31	13.1919375
Fan 2 Clast C	2771	333.2000	Fan 2 Clast C	2767.91	332.8284417
Fan 3 Clast A	702.9	28.6000	Fan 3 Clast A	699.81	28.4742723
Sed Sample 3	421.3	20.2300	Sed Sample 3	418.21	20.08162426
Chile MT1	223.8	13.2200	Chile MT1	220.71	13.03747185
Fan 1 Clast C	917.7	104.6000	Fan 1 Clast C	914.61	104.2477999
Sed Sample 1	441.4	16.4200	Sed Sample 1	438.31	16.30505256
Active Channel 2	757.5	77.7400	Active Channel 2	754.41	77.42288238
Fan 1 Pebbles	1201	69.0700	Fan 1 Pebbles	1197.91	68.89229284
Fan 2 Pebbles	2684	65.2600	Fan 2 Pebbles	2680.91	65.18486833
Fan 3 Clast B	24.54	3.8700	Fan 3 Clast B	21.45	3.382701711
Fan 1 Channel	706.6	29.7800	Fan 1 Channel	703.51	29.64977045
Active Channel 3	578.3	64.5500	Active Channel 3	575.21	64.20509338
Fan 2 Clast A	2745	100.4000	Fan 2 Clast A	2741.91	100.2869814
Fan 1 Clast A	1779	66.9400	Fan 1 Clast A	1775.91	66.82372985
Fan 1 Clast B	963.4	54.2100	Fan 1 Clast B	960.31	54.03612736
Chile MT2	149.2	17.7200	Chile MT2	146.11	17.35301072
Bajada 1	495.9	23.1000	Bajada 1	492.81	22.95606171
ChileColluvium	409.9	11.1000	ChileColluvium	406.81	11.01632349
Active Channel 1	450.9	12.9800	Active Channel 1	447.81	12.89104857
Fan 2 Clast B	2170	49.6200	Fan 2 Clast B	2166.91	49.54934295
Fan 1 Clast D	983	29.0800	Fan 1 Clast D	979.91	28.98858881
Blank 4	3.31	2.4800	75.0000		
Blank 3	3.39	1.3800	41.0000		
Blank 2	4.66	1.5500	33.0000		
Blank 1	1	0.5600	56.0000		
mean blank	3.0900	1.5244			

Table A.3: CRONUS Calculator Input for Determining Surface Exposure Ages

To paste into CRONUS

Sample name	Latitude (DD)	Longitude (DD)	Elevation (m)	Elv/pressure flag	Thickness (cm)	Density (g cm-2)	Shielding correction	Erosion rate (cm yr-1)	[Be-10] atoms g-1	+/- atoms g-1		[Al-26] atoms g-1	+/- atoms g-1	
Bajada1	-21.032	-70.128	578	std	4	2.7	1	0	1.263E+06	5.884E+04	07KNSTD	7.038E+06	3.566E+05	KNSTD
ActiveChannel1	-21.040	-70.131	645	std	3	2.7	1	0	8.237E+05	2.371E+04	07KNSTD	2.606E+06	2.497E+05	KNSTD
ActiveChannel3	-21.028	-70.125	541	std	4	2.7	1	0	1.204E+06	1.344E+05	07KNSTD	5.488E+06	3.192E+05	KNSTD
Fan1Channel	-21.038	-70.126	611	std	3	2.7	1	0	1.735E+06	7.314E+04	07KNSTD	9.878E+06	4.736E+05	KNSTD
Fan2ClastB	-21.038	-70.126	609	std	5	2.7	1	0	4.771E+06	1.091E+05	07KNSTD	2.197E+07	1.373E+06	KNSTD
Fan2Pebbles	-21.038	-70.126	609	std	4.5	2.7	1	0	4.204E+06	1.022E+05	07KNSTD	1.837E+07	8.424E+05	KNSTD
Fan3ClastA	-21.042	-70.126	617	std	6	2.7	1	0	1.232E+06	5.012E+04	07KNSTD	7.297E+06	3.080E+05	KNSTD
Fan1Pebbles	-21.038	-70.128	624	std	4.5	2.7	1	0	2.027E+06	1.166E+05	07KNSTD	1.019E+07	5.246E+05	KNSTD
Fan1ClastA	-21.038	-70.128	624	std	6.5	2.7	1	0	3.040E+06	1.144E+05	07KNSTD	1.545E+07	6.169E+05	KNSTD
Fan2ClastA	-21.038	-70.126	609	std	4.5	2.7	1	0	4.546E+06	1.663E+05	07KNSTD	2.197E+07	7.495E+05	KNSTD
Fan1ClastC	-21.038	-70.128	624	std	8	2.7	1	0	1.474E+06	1.680E+05	07KNSTD	8.475E+06	4.520E+05	KNSTD
Fan1ClastD	-21.038	-70.128	624	std	7	2.7	1	0	1.544E+06	4.567E+04	07KNSTD	8.554E+06	4.884E+05	KNSTD
Fan2ClastC	-21.038	-70.126	609	std	4	2.7	1	0	5.019E+06	6.035E+05	07KNSTD	2.136E+07	8.829E+05	KNSTD
Fan1ClastB	-21.038	-70.128	624	std	7.5	2.7	1	0	1.485E+06	8.354E+04	07KNSTD	8.292E+06	2.972E+05	KNSTD
Fan3ClastB	-21.042	-70.126	617	std	8	2.7	1	0	9.027E+04	1.424E+04	07KNSTD	3.184E+05	6.959E+04	KNSTD
ChileMT2	-21.048	-70.138	857	std	2	2.7	1	0	4.582E+05	5.442E+04	07KNSTD	2.601E+06	2.182E+05	KNSTD
SedSample2	-21.040	-70.130	635	std	2	2.7	1	0	1.330E+06	5.730E+04	07KNSTD	5.170E+06	3.725E+05	KNSTD
ChileMT1	-21.048	-70.138	857	std	1.5	2.7	1	0	5.531E+05	3.267E+04	07KNSTD	3.505E+06	2.610E+05	KNSTD
SedSample3	-21.044	-70.138	741	std	2	2.7	1	0	1.534E+06	7.364E+04	07KNSTD	6.417E+06	8.372E+05	KNSTD
SedSample1	-21.028	-70.125	541	std	2	2.7	1	0	1.497E+06	5.568E+04	07KNSTD	6.232E+06	3.651E+05	KNSTD
ActiveChannel2	-21.044	-70.138	741	std	3	2.7	1	0	1.281E+06	1.315E+05	07KNSTD	4.916E+06	4.487E+05	KNSTD
Fan3Pebbles	-21.042	-70.126	617	std	2	2.7	1	0	5.292E+05	2.536E+04	07KNSTD	3.053E+06	3.460E+05	KNSTD
ChileMT3	-21.047	-70.139	814	std	3	2.7	1	0	1.299E+06	1.229E+05	07KNSTD	6.176E+06	3.393E+05	KNSTD
	-21.038	-70.131	680		5									

Table A.4: Sample Processing Inputs and Corrections for ^{26}Al Samples

User ID	Quartz wt (g)	Quartz solution (g)	Al carrier wt (g)	Carrier concentration (mg/g)	Aliquot Al (g)	Al Concentration in Delivered Soln (ppm)	Amount of SiO2 in aliquot	Al in aliquot	Al in 1 gram of SiO2	# of atoms of Al in 1 g SiO2	CORRECTED RATIO Al-26/Al-27		FOR CRONUS #Al-26 in 1 gram	
Chile MT3	17.8927	102.1349	0.6012	1000	6.0019	23.3100	1.0515	0.000140	0.000133058	2.96769E+18	2081	114	**6.176E+06**	**3.393E+05**
Sed Sample 2	13.2139	107.8420	0.5623	1000	8.2805	20.0972	1.0146	0.000166	0.000164018	3.65822E+18	1413	102	**5.170E+06**	**3.725E+05**
Fan 3 Pebbles	18.6820	127.8524	0.6457	1000	7.1930	75.3800	1.0511	0.000542	0.000515872	1.15058E+19	265	30	**3.053E+06**	**3.460E+05**
Fan 2 Clast C	16.4134	154.9467	0.5700	1000	9.6147	14.3553	1.0185	0.000138	0.000135518	3.02255E+18	7067	292	**2.136E+07**	**8.829E+05**
Fan 3 Clast A	18.5738	163.4745	0.6032	1000	9.0686	15.0913	1.0304	0.000137	0.000132823	2.96245E+18	2463	104	**7.297E+06**	**3.080E+05**
Sed Sample 3	9.0527	52.7536	0.5644	1000	5.9857	35.5394	1.0272	0.000213	0.000207102	4.61914E+18	1389	181	**6.417E+06**	**8.372E+05**
Chile MT1	13.2240	107.1946	0.5357	1000	8.4678	18.9113	1.0446	0.000160	0.000153296	3.41907E+18	1025	76	**3.505E+06**	**2.610E+05**
Fan 1 Clast C	20.0673	125.0452	0.5072	1000	6.8939	20.9185	1.1063	0.000144	0.000130349	2.90727E+18	2915	155	**8.475E+06**	**4.520E+05**
Sed Sample 1	10.7424	90.6682	0.5790	1000	9.0037	24.5744	1.0668	0.000221	0.000207414	4.62609E+18	1347	79	**6.232E+06**	**3.651E+05**
Active Channel 2	20.3416	145.5013	0.5237	1000	7.5594	49.2665	1.0568	0.000372	0.000352398	7.85978E+18	625	57	**4.916E+06**	**4.487E+05**
Fan 1 Pebbles	19.2618	160.4219	0.5320	1000	8.4187	17.4645	1.0108	0.000147	0.000145453	3.24414E+18	3142	162	**1.019E+07**	**5.246E+05**
Fan 2 Pebbles	18.9183	160.9584	0.5673	1000	9.0629	30.7047	1.0652	0.000278	0.000261238	5.82657E+18	3153	145	**1.837E+07**	**8.424E+05**
Fan 3 Clast B	9.8371	80.9813	0.5741	1000	8.3337	19.7084	1.0123	0.000164	0.000162244	3.61864E+18	88	19	**3.184E+05**	**6.959E+04**
Blank 4	15.0000	102.7284	0.5579	1000	7.2008	5.5849	1.0514	0.000040	3.82485E-05	8.53082E+17	16.00	22.64	**1.365E+04**	**1.931E+04**
Fan 1 Channel	14.4267	151.0769	0.5715	1000	10.7883	13.8114	1.0302	0.000149	0.000144633	3.22586E+18	3062	147	**9.878E+06**	**4.736E+05**
Active Channel 3	18.7146	140.4571	0.5110	1000	7.4840	17.3448	0.9972	0.000130	0.000130176	2.90341E+18	1890	110	**5.488E+06**	**3.192E+05**
Fan 2 Clast A	19.2645	147.7677	0.4730	1000	8.0704	16.2359	1.0521	0.000131	0.000124537	2.77764E+18	7911	270	**2.197E+07**	**7.495E+05**
Blank 3	15.0000	133.1132	0.5681	1000	9.2960	4.3237	1.0475	0.000040	3.83691E-05	8.55774E+17	22.04	31.18	**1.886E+04**	**2.668E+04**
Fan 1 Clast A	20.3489	155.9400	0.5704	1000	7.7354	19.9480	1.0094	0.000154	0.000152868	3.40952E+18	4530	181	**1.545E+07**	**6.169E+05**
Blank 2	15.0000	127.6050	0.5152	1000	8.7622	4.0129	1.0300	0.000035	3.41379E-05	7.61402E+17	12.87	18.21	**9.799E+03**	**1.387E+04**
Fan 1 Clast B	20.6486	152.3861	0.5192	1000	7.8654	13.2914	1.0658	0.000105	9.80902E-05	2.18777E+18	3790	136	**8.292E+06**	**2.972E+05**
Chile MT2	11.6134	96.0526	0.5571	1000	8.5420	21.3373	1.0328	0.000182	0.000176477	3.9361E+18	661	55	**2.601E+06**	**2.182E+05**
Bajada 1	15.4616	153.9161	0.5780	1000	9.7280	14.9370	0.9772	0.000145	0.000148694	3.31643E+18	2122	108	**7.038E+06**	**3.566E+05**
Active Channel 1	18.8316	154.5184	0.5493	1000	8.8258	20.8864	1.0756	0.000184	0.000171379	3.82238E+18	682	65	**2.606E+06**	**2.497E+05**
Fan 2 Clast B	16.7014	137.2274	0.5655	1000	8.3467	149.3000	1.0158	0.001246	0.001226727	2.73605E+19	803	50	**2.197E+07**	**1.373E+06**
Blank 1	15.0000	129.5125	0.5447	1000	8.9636	4.2142	1.0382	0.000038	3.63858E-05	8.11538E+17	64.36	46.54	**5.223E+04**	**3.777E+04**
Fan 1 Clast D	20.6777	162.1076	0.5277	1000	8.1289	32.5672	1.0369	0.000265	0.000255318	5.69454E+18	1502	86	**8.554E+06**	**4.884E+05**
										BLANK	28.82	24.45493		

Table A.5: Compilation of TCN Surface Age Dates for the Atacama Desert

Citation	Sample Name	Latitude	Longitude	Elevation (m)	Sample Material	Nuclide	Age (Ma)	Error (Ma)	Erosion Rate (m/Ma)	Error (m/Ma)
Placzek et al 2010	ADSO-3	-24.0887	-70.0597	1057	boulder (diorite)	26Al/10Be	1.83	0.04	0.2	0.05
Placzek et al 2010	ADSO-6	-24.1153	-68.5956	2913	boulder (granite)	26Al/10Be	1.87	0.08	0.19	0.05
Placzek et al 2010	ADCRW-4	-24.5261	-70.5701	24	bedrock (diorite)	26Al/10Be	0.136	0.01	5.66	0.7
Placzek et al 2010	ADSO-6SD	-24.1153	-68.5956	2913	Alluvial Sediment	26Al/10Be	0.531	0.019	1.01	0.14
Placzek et al 2010	ADBA-2SD	-23.5335	-69.0796	2472	Alluvial Sediment	26Al/10Be	0.39	0.013	1.43	0.18
Placzek et al 2010	ADSA-3	-22.9147	-68.1193	2490	Cobble (granitic)	26Al/10Be	0.0146	0.0011	49.1	5.5
Placzek et al 2010	ADPC-3	-24.0698	-70.1997	1005	boulder (andesite)	26Al/10Be	2.14	0.07	0.16	0.05
Placzek et al 2010	ADSO-8CH	-24.1529	-68.547	3128	Channel Gravel	26Al/10Be	0.215	0.007	2.65	0.3
Placzek et al 2010	ADCRE-4	-24.4342	-70.3297	2207	Bedrock (andesite)	26Al/10Be	0.646	0.017	0.8	0.11
Placzek et al 2010	ASOI-SD	-24.0933	-70.1688	1040	Alluvial Sediment	26Al/10Be	0.9	0.04	0.55	0.09
Placzek et al 2010	ADSA-4BD	-23.223	-68.1193	2432	boulder (andesite)	26Al/10Be	0.128	0.041	4.7	1.9
Placzek et al 2010	ADSO-4SD	-24.0384	-69.8728	1034	Channel Gravel	26Al/10Be	0.84	0.04	0.6	0.1
Placzek et al 2010	ADCRW-3	-24.5682	-70.5411	134	Channel Gravel	26Al/10Be	0.079	0.02	10.6	3.2
Placzek et al 2010	ADCRW-7	-24.3197	-70.48	1059	bedrock (diorite)	26Al/10Be	0.225	0.021	2.78	0.42
Placzek et al 2010	ADSA-4CH	-23.2232	-68.5649	2440	Channel Gravel	26Al/10Be	0.173	0.016	3.48	0.5
Placzek et al 2010	ADCRE-1	-24.279	-70.2993	1830	Channel Gravel	26Al/10Be	0.8	0.07	0.63	0.12
Placzek et al 2010	ADBA-5SD	-23.4001	-69.4631	1517	Alluvial Sediment	26Al/10Be	0.642	0.02	0.82	0.11
Placzek et al 2010	ADCRE-8	-24.7089	-70.369	2104	Channel Gravel	26Al/10Be	0.766	0.016	0.67	0.1
Placzek et al 2010	ADSA-1SD	-23.7857	-68.1071	2364	Alluvial Sediment	26Al/10Be	0.389	0.028	1.44	0.21
Placzek et al 2010	ADSO-3SD	-24.0887	-70.0597	1057	Alluvial Sediment	26Al/10Be	0.93	0.08	0.52	0.11
Placzek et al 2010	ADBA-13CHsm	-23.5831	-69.2769	1857	Channel Gravel	26Al/10Be	1.57	0.03	0.25	0.05
Placzek et al 2010	ADSO-12	-24.2223	-68.8961	3246	Bedrock (quartz rich vein)	26Al/10Be	0.78	0.01	0.63	0.09
Placzek et al 2010	ADBA-12SDsm	-23.3978	-69.4624	1527	Alluvial Sediment	26Al/10Be	1.2	0.02	0.37	0.07
Placzek et al 2010	ADBA-27A	-22.8959	-70.1482	969	Cobble (quartz)	26Al/10Be	1.54	0.03	0.27	0.06
Placzek et al 2010	ADCRE-2	-24.2764	-70.3006	1918	Bedrock (andesite)	26Al/10Be	0.596	0.015	0.88	0.12
Placzek et al 2010	ADBA-25B	-22.9251	-70.1878	898	boulder (granite)	26Al/10Be	0.153	0.005	4.38	0.45
Placzek et al 2010	ADSO-13	-24.1978	-68.8114	3048	Bedrock (quartz rich vein)	26Al/10Be	0.83	0.03	0.59	0.09
Placzek et al 2010	ABBA-16	-23.6519	-68.7391	2662	bedrock (diorite)	26Al/10Be	0.93	0.02	0.51	0.08
Placzek et al 2010	ADBA-25A	-22.9252	-70.1887	989	boulder (granite)	26Al/10Be	0.086	0.0036	8.51	0.83
Placzek et al 2010	ADBA-25C	-22.9255	-70.1848	876	boulder (granite)	26Al/10Be	0.336	0.012	1.79	0.21
Placzek et al 2010	ADPC-1A	-24.0693	-70.1931	1047	boulder (andesite)	26Al/10Be	1.01	0.05	0.47	0.08
Placzek et al 2010	ADBA-5	-23.4001	-69.4631	1513	boulder (diorite)	26Al/10Be	2.63	0.07	0.11	0.04
Placzek et al 2010	ADBA-13SD	-23.5631	-69.2752	1862	Alluvial Sediment	26Al/10Be	2.4	0.05	0.13	0.04
Placzek et al 2010	ADBA-3	-23.4078	-69.4636	1740	bedrock (diorite)	26Al/10Be	1.07	0.03	0.43	0.08
Placzek et al 2010	ADBA-25CH	-22.8951	-70.1887	960	Channel Gravel	26Al/10Be	0.36	0.018	1.65	0.21
Placzek et al 2010	ADBA-4	-23.4037	-69.4623	1575	boulder (diorite)	26Al/10Be	0.82	0.02	0.61	0.09
Placzek et al 2010	ADBA-11	-23.4034	-69.4683	1513	boulder (diorite)	26Al/10Be	2.44	0.07	0.13	0.04
Placzek et al 2010	ADBA-27CH	-22.8951	-70.1482	960	Channel Gravel	26Al/10Be	1.01	0.03	0.47	0.08
Placzek et al 2010	ADSO-3	-24.0887	-70.0597	1057	boulder (diorite)	21Ne/10B	1.56	0.11	0.392	0.027
Placzek et al 2010	ADPC-3	-24.0698	-70.1997	1005	boulder (andesite)	21Ne/10B	2.84	0.16	0.215	0.012
Placzek et al 2010	ADSO-6	-24.1153	-68.5956	2913	boulder (granite)	21Ne/10B	2.15	0.1	0.285	0.014
Dunai et al 2005	PI03/1	-19.53	-70.11	957	amalgamation (vein quartz)	21Ne	23.15	0.11	-	-
Dunai et al 2005	PI03/1 duplicat	-19.53	-70.11	957	amalgamation (vein quartz)	21Ne	23.34	0.15	-	-
Dunai et al 2005	PI03/1 A	-19.53	-70.11	957	single clast (vein quartz)	21Ne	25	0.18	-	-
Dunai et al 2005	PI03/1 B	-19.53	-70.11	957	single clast (vein quartz)	21Ne	19.28	0.15	-	-
Dunai et al 2005	PI03/1 C	-19.53	-70.11	957	single clast (vein quartz)	21Ne	36.63	0.22	-	-
Dunai et al 2005	PI03/1 D	-19.53	-70.11	957	single clast (vein quartz)	21Ne	23.38	0.17	-	-
Dunai et al 2005	PI-06 A	-19.564	-70.12	925	single clast (vein quartz)	21Ne	25.34	0.17	-	-
Dunai et al 2005	PI-06 B	-19.564	-70.12	925	single clast (vein quartz)	21Ne	14.34	0.12	-	-
Dunai et al 2005	PI-06 C	-19.564	-70.12	925	single clast (vein quartz)	21Ne	8.88	0.08	-	-
Dunai et al 2005	PI-06 D	-19.564	-70.12	925	single clast (vein quartz)	21Ne	25.19	0.16	-	-
Dunai et al 2005	PI-07 A	-19.567	-70.11	931	single clast (vein quartz)	21Ne	14.27	0.1	-	-
Dunai et al 2005	PI-07 B	-19.567	-70.11	931	single clast (vein quartz)	21Ne	20.97	0.14	-	-
Dunai et al 2005	PI-07 C	-19.567	-70.11	931	single clast (vein quartz)	21Ne	26.99	0.18	-	-
Dunai et al 2005	PI-07 D	-19.567	-70.11	931	single clast (vein quartz)	21Ne	20.01	0.15	-	-
Dunai et al 2005	PI-11	-19.55	-70.07	1023	amalgamation (90cm depth)	21Ne	-	-	-	-
Dunai et al 2005	PI-12	-19.55	-70.07	1023	amalgamation(surface)	21Ne	0.155	0.04	-	-
Dunai et al 2005	PI-01	-19.57	-70.19	465	single clast (vein quartz)	21Ne	0.122	0.022	-	-
Nishiizumi et al 200	17	-26.26	-69.56	3201	bedrock	10Be	0.35	0.01	1.68	0.05
Nishiizumi et al 200	18	-26.26	-69.56	3201	bedrock	10Be	0.33	0.01	1.8	0.04
Nishiizumi et al 200	19	-26.26	-69.56	3212	bedrock	10Be	0.32	0.01	1.93	0.09
Nishiizumi et al 200	20	-26.22	-69.54	2701	bedrock	10Be	0.1	0.01	6.03	0.15
Nishiizumi et al 200	21	-26.2	-69.59	2295	erosional surface (cobbles)	10Be	2.22	0.05	0.17	0.02
Nishiizumi et al 200	22	-26.2	-69.59	2295	erosional surface (cobbles)	10Be	2.63	0.06	0.1	0.03
Nishiizumi et al 200	23	-26.25	-69.58	2421	alluvial fan (cobbles)	10Be	3.49	0.24	0.06	0.02
Nishiizumi et al 200	24	-26.25	-69.58	2423	alluvial fan (cobbles)	10Be	3.08	0.19	0.12	0.04
Nishiizumi et al 200	72	-26.5	-69.74	1950	incised channel	10Be	0.36	0.01	1.67	0.04
Nishiizumi et al 200	73	-26.5	-69.74	1950	alluvial fan (cobbles)	10Be	1.14	0.03	0.36	0.09
Nishiizumi et al 200	74	-26.5	-69.74	1950	alluvial fan (cobbles)	10Be	4.41	0.29	0.03	0.01
Nishiizumi et al 200	251	-26.25	-69.57	2710	bedrock	10Be	0.34	0.01	1.67	0.04
Carrizo et al 2008	SG-1A	20.58.48	69.38.26	-	peniplanicie	21Ne	18.2	1.1	-	-
Carrizo et al 2008	SG-1B	20.58.47	69.38.26	-	peniplanicie	21Ne	19	0.1	-	-
Carrizo et al 2008	SG-2	21.07.38	69.44.11	-	paleocanal	21Ne	3.98	0.11	-	-
Carrizo et al 2008	SG-3	21.00.29	70.02.27	-	peniplanicie	21Ne	4.94	0.3	-	-
Carrizo et al 2008	SG-4	21.00.07	70.02.02	-	peniplanicie	21Ne	4.12	0.25	-	-
Carrizo et al 2008	SG-5	20.58.26	70.01.15	-	abanico aluvial	21Ne	2.17	0.13	-	-
Carrizo et al 2008	SG-6	20.57.55	70.02.00	-	paleocanal	21Ne	6.93	0.42	-	-
Carrizo et al 2008	SG-7	21.03.10	69.39.09	-	peniplanicie	21Ne	15.5	0.6	-	-
Carrizo et al 2008	SG-8	20.52.42	69.39.54	-	peniplanicie	21Ne	10.3	0.4	-	-
Carrizo et al 2008	SG-9	20.38.35	69.39.54	-	peniplanicie	21Ne	15	0.6	-	-
Carrizo et al 2008	SG-10	21.05.26	69.51.48	-	peniplanicie	21Ne	24.1	1	-	-
Carrizo et al 2008	SG-12	21.01.33	70.00.58	-	abanico aluvial	21Ne	2.6	0.11	-	-
Carrizo et al 2008	SG-14	20.37.58	69.48.49	-	peniplanicie	21Ne	18	0.7	-	-
Kober et al 2007	203	-19.12	-70.15	500	boulder (granite)	21Ne/10B	22.45	9.3	0.04	0.02
Kober et al 2007	203	-19.12	-70.15	500	boulder (granite)	21Ne	12.5	0.5	0	0.001
Kober et al 2007	203	-19.12	-70.15	500	boulder (granite)	26Al	4.39	1.35	0.01	0.04
Kober et al 2007	203	-19.12	-70.15	500	boulder (granite)	10Be	1.76	0.09	0.26	0.01
Kober et al 2007	36	-19.33	-70.05	1150	boulder (granite)	21Ne	1.36	0.15	0.5	0.06
Kober et al 2007	36	-19.33	-70.05	1150	boulder (granite)	26Al	0.53	0.04	1.07	0.09
Kober et al 2007	36	-19.33	-70.05	1150	boulder (granite)	10Be	0.81	0.04	0.76	0.05
Kober et al 2007	7	-18.37	-69.56	1620	boulder (andesite)	21Ne	2.53	0.38	0.27	0.04
Kober et al 2007	8b	-18.25	-69.51	1670	boulder (ignimbrite)	21Ne	1.04	0.07	0.65	0.05

Table A.5: Continued

Kober et al 2007	8b	-18.25	-69.51	1670	boulder (ignimbrite)	10Be	0.78	0.04	0.8	0.05
Kober et al 2007	1c	-18.28	-69.54	1930	boulder (ignimbrite)	21Ne/10B	2.52	0.08	0.31	0.03
Kober et al 2007	1c	-18.28	-69.54	1930	boulder (ignimbrite)	21Ne	1.5	0.07	0.45	0.02
Kober et al 2007	1c	-18.28	-69.54	1930	boulder (ignimbrite)	10Be	1.34	0.04	0.39	0.02
Kober et al 2007	301	-18.44	-69.41	2185	bedrock (ignimbrite)	21Ne/10B	2.48	0.1	0.34	0.03
Kober et al 2007	301	-18.44	-69.41	2185	bedrock (ignimbrite)	21Ne	1.41	0.04	0.48	0.01
Kober et al 2007	301	-18.44	-69.41	2185	bedrock (ignimbrite)	26Al	1.3	0.28	0.27	0.09
Kober et al 2007	301	-18.44	-69.41	2185	bedrock (ignimbrite)	10Be	1.26	0.06	0.42	0.02
Kober et al 2007	302	-18.44	-69.39	2590	bedrock (ignimbrite)	21Ne/10B	2.48	0.2	0.48	0.05
Kober et al 2007	302	-18.44	-69.39	2590	bedrock (ignimbrite)	21Ne	1.16	0.03	0.58	0.01
Kober et al 2007	302	-18.44	-69.39	2590	bedrock (ignimbrite)	26Al	0.63	0.05	0.84	0.08
Kober et al 2007	302	-18.44	-69.39	2590	bedrock (ignimbrite)	10Be	1.05	0.04	0.55	0.03
Kober et al 2007	19	-18.43	-69.41	2730	bedrock (ignimbrite)	21Ne/10B	5.35	0.24	0.1	0.02
Kober et al 2007	19	-18.43	-69.41	2730	bedrock (ignimbrite)	21Ne	3.67	0.12	0.18	0.01
Kober et al 2007	303	-18.43	-69.39	3070	bedrock (ignimbrite)	21Ne	1.13	0.05	0.49	0.03
Kober et al 2007	310	-18.21	-69.37	3220	bedrock (ignimbrite)	21Ne	0.17	0.06	4.02	0.13
Kober et al 2007	310	-18.21	-69.37	3220	bedrock (ignimbrite)	21Ne/10B	0.25	0.04	2.25	0.25
Kober et al 2007	104A	-18.22	-69.4	3235	bedrock (ignimbrite)	21Ne/10B	1.25	0.08	0.28	0.08
Kober et al 2007	104A	-18.22	-69.4	3235	bedrock (ignimbrite)	21Ne	0.96	0.05	0.7	0.03
Kober et al 2007	5	-18.42	-69.37	3260	bedrock (ignimbrite)	21Ne/10B	3.58	0.29	0.32	0.03
Kober et al 2007	5	-18.42	-69.37	3260	bedrock (ignimbrite)	21Ne	1.7	0.09	0.39	0.01
Kober et al 2007	16	-18.21	-69.37	3270	amalgamated (conglomerate)	21Ne	1.23	0.07	0.55	0.04
Kober et al 2007	23	-18.23	-69.4	3280	bedrock (ignimbrite)	21Ne/10B	2.08	0.03	0.05	0.02
Kober et al 2007	23	-18.23	-69.4	3280	bedrock (ignimbrite)	21Ne	1.92	0.09	0.35	0.01
Kober et al 2007	111F	-18.14	-69.49	3435	bedrock (ignimbrite)	21Ne/10B	2.05	0.34	0.5	0.07
Kober et al 2007	111F	-18.14	-69.49	3435	bedrock (ignimbrite)	21Ne	1.05	0.07	0.65	0.03
Kober et al 2007	201	-18.22	-69.5	3440	bedrock (ignimbrite)	21Ne/10B	3.05	0.13	0.15	0.03
Kober et al 2007	201	-18.22	-69.5	3440	bedrock (ignimbrite)	21Ne	2.2	0.09	0.31	0.02
Kober et al 2007	305	-18.11	-69.43	3670	bedrock (ignimbrite)	21Ne/10B	0.32	0.01	-	-
Kober et al 2007	305	-18.11	-69.43	3670	bedrock (ignimbrite)	21Ne	0.32	0.01	2.1	0.08
Kober et al 2007	112	-18.05	-69.41	3920	bedrock (ignimbrite)	21Ne/10B	0.85	0.08	4.17	0.17
Kober et al 2007	112	-18.05	-69.41	3920	bedrock (ignimbrite)	21Ne	0.16	0.01	4.23	0.22
Kober et al 2007	308	-18.33	-69.17	4150	bedrock (Andesite)	21Ne	0.08	0.03	8.35	3
Kober et al 2007	26	-20.18	-68.55	4205	bedrock (ignimbrite)	21Ne	0.4	0.02	1.67	0.08
Kober et al 2007	307	-18.19	-69.27	4420	bedrock (volcanic)	21Ne	0.21	0.02	3.18	0.27
Kober et al 2007	309	-18.14	-69.09	4510	bedrock (ignimbrite)	21Ne/10B	0.051	0.01	3.9	1
Kober et al 2007	309	-18.14	-69.09	4510	bedrock (ignimbrite)	21Ne	0.43	0.003	15.6	0.9
Kober et al 2007	113	-18.1	-69.3	4560	bedrock (ignimbrite)	21Ne/10B	0.104	0.097	34	2
Kober et al 2007	113	-18.1	-69.3	4560	bedrock (ignimbrite)	21Ne	0.02	0.004	34.5	4.8
Gonzalez et al 2006	FSC-19	-23.525	-70.247	682	alluvial fan (pebbles)	21Ne	0.351	0.181	-	-
Gonzalez et al 2006	FSC-18A	-23.575	-70.269	616	alluvial fan (pebbles)	21Ne	0.55	0.234	-	-
Gonzalez et al 2006	FSC-14	-23.675	-70.292	685	alluvial fan (pebbles)	21Ne	0.424	0.151	-	-
Gonzalez et al 2006	FSC-7	-23.723	-70.29	533	alluvial fan (pebbles)	21Ne	0.538	0.092	-	-
Evenstar et al 2009	11/24	-19.82694	-69.68111	1254	planation surface boulders	3He	1.3	-	-	-
Evenstar et al 2009	12/24	-19.82694	-69.68111	1254	planation surface boulders	3He	1.2	-	-	-
Evenstar et al 2009	14/24	-19.82694	-69.68111	1254	planation surface boulders	3He	1.3	-	-	-
Evenstar et al 2009	22/24	-19.7066	-69.6292	1480	planation surface boulders	3He	7.3	-	-	-
Evenstar et al 2009	23/24	-19.7066	-69.6292	1480	planation surface boulders	3He	6.8	-	-	-
Evenstar et al 2009	24/24	-19.7066	-69.6292	1480	planation surface boulders	3He	7.1	-	-	-
Evenstar et al 2009	04/26	-19.6881	-69.6183	1523	planation surface boulders	3He	10.1	-	-	-
Evenstar et al 2009	03/02a	-19.6489	-69.58	1684	planation surface boulders	3He	14.6	-	-	-
Evenstar et al 2009	03/02b	-19.6489	-69.58	1684	planation surface boulders	3He	14.8	-	-	-
Evenstar et al 2009	05/02	-19.6489	-69.58	1684	planation surface boulders	3He	16.5	-	-	-
Evenstar et al 2009	09/02	-19.6458	-69.5811	1703	planation surface boulders	3He	2.6	-	-	-
Evenstar et al 2009	11/26	-19.5342	-69.5342	1811	planation surface boulders	3He	3	-	-	-
Evenstar et al 2009	13/26	-19.5342	-69.5342	1811	planation surface boulders	3He	2.8	-	-	-
Evenstar et al 2009	15/26	-19.5342	-69.5342	1811	planation surface boulders	3He	2.6	-	-	-
Evenstar et al 2009	21/26	-19.6181	-69.5336	1901	planation surface boulders	3He	14.8	-	-	-
Evenstar et al 2009	22/26	-19.6181	-69.5336	1901	planation surface boulders	3He	14.7	-	-	-
Evenstar et al 2009	23/26	-19.6181	-69.5336	1901	planation surface boulders	3He	22	-	-	-
Evenstar et al 2009	04/27	-19.5272	-69.3989	2582	planation surface boulders	3He	6.8	-	-	-
Evenstar et al 2009	05/27	-19.5272	-69.3989	2582	planation surface boulders	3He	3	-	-	-
Evenstar et al 2009	06/27	-19.5272	-69.3989	2582	planation surface boulders	3He	7.6	-	-	-
Evenstar et al 2009	12/02	-19.5228	-69.3731	2739	planation surface boulders	3He	2.6	-	-	-
Evenstar et al 2009	12/27	-19.5281	-69.3786	2727	planation surface boulders	3He	5.2	-	-	-
Evenstar et al 2009	13/27	-19.5281	-69.3786	2727	planation surface boulders	3He	5.2	-	-	-
Evenstar et al 2009	07/04	-19.2878	-69.3967	3077	Tana lava	3He	0.0077	-	-	-
Hall et al 2008	PL04-5	-14.611	-75.177	387	Pediment	10Be	0.219	0.006	-	-
Hall et al 2008	PL04-6	-14.611	-75.177	387	Pediment	10Be	0.239	0.007	-	-
Hall et al 2008	PL04-7	-14.611	-75.178	387	Pediment	10Be	0.162	0.005	-	-
Hall et al 2008	PL04-8	-14.611	-75.177	387	Pediment	10Be	0.201	0.01	-	-
Hall et al 2008	PL04-1	-14.613	-75.176	409	Pediment	10Be	1.06	0.032	-	-
Hall et al 2008	PL04-2	-14.613	-75.177	408	Pediment	10Be	0.999	0.028	-	-
Hall et al 2008	PL04-4	-14.613	-75.176	409	Pediment	10Be	1.216	0.035	-	-
Hall et al 2008	QC04-7	-17.46	-70.681	1198	Pediment	10Be	0.3	0.008	-	-
Hall et al 2008	QC04-8	-17.46	-70.681	1198	Pediment	10Be	0.29	0.008	-	-
Hall et al 2008	QC04-9	-17.46	-70.681	1198	Pediment	10Be	0.294	0.008	-	-
Hall et al 2008	C04-10	-17.46	-70.681	1199	Pediment	10Be	0.247	0.007	-	-
Hall et al 2008	C04-11	-17.46	-70.681	1198	Pediment	10Be	0.311	0.009	-	-
Hall et al 2008	QC04-1	-17.454	-70.664	1299	Pediment	10Be	0.36	0.009	-	-
Hall et al 2008	QC04-2	-17.454	-70.664	1302	Pediment	10Be	0.26	0.007	-	-
Hall et al 2008	QC04-3	-17.454	-70.664	1302	Pediment	10Be	0.232	0.006	-	-
Hall et al 2008	QC04-5	-17.454	-70.664	1305	Pediment	10Be	0.288	0.008	-	-
Hall et al 2008	QC04-6	-17.454	-70.664	1305	Pediment	10Be	0.257	0.007	-	-
Hall et al 2008	PG05-08	-17.474	-70.581	1504	Pediment	10Be	0.106	0.003	-	-
Hall et al 2008	PG05-09	-17.474	-70.581	1504	Pediment	10Be	0.107	0.003	-	-
Hall et al 2008	PG05-19	-17.474	-70.581	1504	Pediment	10Be	0.148	0.004	-	-
Hall et al 2008	RL05-01	-17.562	-70.663	841	Strath	10Be	0.198	0.006	-	-
Hall et al 2008	RL05-02	-17.562	-70.663	841	Strath	10Be	0.148	0.003	-	-
Hall et al 2008	RL05-03	-17.562	-70.663	841	Strath	10Be	0.126	0.003	-	-
Hall et al 2008	RL05-04	-17.562	-70.663	841	Strath	10Be	0.171	0.006	-	-
Hall et al 2008	PC05-2 (T1)	-17.56	-70.508	1798	Strath	10Be	0.029	0.001	-	-
Hall et al 2008	PC05-5 (T1)	-17.56	-70.508	1798	Strath	10Be	0.043	0.002	-	-
Hall et al 2008	PC05-8 (T2)	-17.561	-70.51	1804	Strath	10Be	0.225	0.005	-	-
Hall et al 2008	PC05-11 (T3)	-17.562	-70.51	1813	Pediment	10Be	0.519	0.019	-	-
Hall et al 2008	PC05-1012 (T3)	-17.562	-70.51	1813	Pediment	10Be	0.626	0.016	-	-

Table A.5: Continued

Baker (this work)	Fan2ClastB	-21.038	-70.126	609	quartz cobble	10Be	0.85	0.14	-	-
Baker (this work)	Fan2Pebbles	-21.038	-70.126	609	composite clasts quartz	10Be	0.69	0.11	-	-
Baker (this work)	Fan3ClastA	-21.042	-70.126	617	quartz cobble	10Be	0.213	0.024	-	-
Baker (this work)	Fan1Pebbles	-21.038	-70.128	624	composite clasts quartz	10Be	0.182	0.045	-	-
Baker (this work)	Fan1ClastA	-21.038	-70.128	624	quartz cobble	10Be	0.41	0.072	-	-
Baker (this work)	Fan2ClastA	-21.038	-70.126	609	quartz cobble	10Be	0.781	0.131	-	-
Baker (this work)	Fan1ClastC	-21.038	-70.128	624	quartz cobble	10Be	0.082	0.043	-	-
Baker (this work)	Fan1ClastD	-21.038	-70.128	624	quartz cobble	10Be	0.092	0.03	-	-
Baker (this work)	Fan2ClastC	-21.038	-70.126	609	quartz cobble	10Be	0.91	0.23	-	-
Baker (this work)	Fan1ClastB	-21.038	-70.128	624	quartz cobble	10Be	0.083	0.032	-	-
Baker (this work)	Fan3ClastB	-21.042	-70.126	617	quartz cobble	10Be	0.017	0.003	-	-
Baker (this work)	Fan3Pebbles	-21.042	-70.126	617	composite clasts quartz	10Be	0.09	0.01	-	-
Baker (this work)	Fan2ClastB	-21.038	-70.126	609	quartz cobble	26Al	0.83	0.19	-	-
Baker (this work)	Fan2Pebbles	-21.038	-70.126	609	composite clasts quartz	26Al	0.57	0.11	-	-
Baker (this work)	Fan3ClastA	-21.042	-70.126	617	quartz cobble	26Al	0.218	0.026	-	-
Baker (this work)	Fan1Pebbles	-21.038	-70.128	624	composite clasts quartz	26Al	0.19	0.041	-	-
Baker (this work)	Fan1ClastA	-21.038	-70.128	624	quartz cobble	26Al	0.423	0.077	-	-
Baker (this work)	Fan2ClastA	-21.038	-70.126	609	quartz cobble	26Al	0.78	0.15	-	-
Baker (this work)	Fan1ClastC	-21.038	-70.128	624	quartz cobble	26Al	0.14	0.034	-	-
Baker (this work)	Fan1ClastD	-21.038	-70.128	624	quartz cobble	26Al	0.142	0.035	-	-
Baker (this work)	Fan2ClastC	-21.038	-70.126	609	quartz cobble	26Al	0.73	0.14	-	-
Baker (this work)	Fan1ClastB	-21.038	-70.128	624	quartz cobble	26Al	0.13	0.03	-	-
Baker (this work)	Fan3ClastB	-21.042	-70.126	617	quartz cobble	26Al	0.014	0.003	-	-
Baker (this work)	Fan3Pebbles	-21.042	-70.126	617	composite clasts quartz	26Al	0.095	0.015	-	-
Baker (this work)	Fan 1 Channel	-21.03755	-70.12571	611	composite quartz	10Be	0.338	0.039	-	-
Baker (this work)	Fan 1 Channel	-21.03755	-70.12571	611	composite quartz	26Al	0.303	0.039	-	-
Baker (this work)	Sed Sample 1	-21.02844	-70.12486	541	sediment	10Be	0.303	0.345	-	-
Baker (this work)	Sed Sample 1	-21.02844	-70.12486	541	sediment	26Al	0.192	0.024	-	-
Baker (this work)	Sed Sample 2	-21.02844	-70.12486	541	sediment	10Be	0.247	0.028	-	-
Baker (this work)	Sed Sample 2	-21.02844	-70.12486	541	sediment	26Al	0.144	0.019	-	-
Baker (this work)	Sed Sample 3	-21.04432	-70.138	741	sediment	10Be	0.263	0.031	-	-
Baker (this work)	Sed Sample 3	-21.04432	-70.138	741	sediment	26Al	0.168	0.030	-	-
Baker (this work)	MT 1	-21.04845	-70.13783	857	bedrock	10Be	0.085	0.010	-	-
Baker (this work)	MT 1	-21.04845	-70.13783	857	bedrock	26Al	0.083	0.011	-	-
Baker (this work)	MT 2	-21.04845	-70.13783	857	bedrock	10Be	0.070	0.011	-	-
Baker (this work)	MT 2	-21.04845	-70.13783	857	bedrock	26Al	0.062	0.008	-	-
Baker (this work)	MT 3	-21.04734	-70.13862	814	bedrock	10Be	0.207	0.030	-	-
Baker (this work)	MT 3	-21.04734	-70.13862	814	bedrock	26Al	0.151	0.018	-	-
Baker (this work)	AC1	-21.03969	-70.13058	645	composite quartz	10Be	0.149	0.016	-	-
Baker (this work)	AC1	-21.03969	-70.13058	645	composite quartz	26Al	0.074	0.011	-	-
Baker (this work)	AC2	-21.04432	-70.138	741	composite quartz	10Be	0.217	0.033	-	-
Baker (this work)	AC2	-21.04432	-70.138	741	composite quartz	26Al	0.129	0.018	-	-
Baker (this work)	AC3	-21.02844	-70.12486	541	composite quartz	10Be	0.244	0.039	-	-
Baker (this work)	AC3	-21.02844	-70.12486	541	composite quartz	26Al	0.171	0.021	-	-
Baker (this work)	Bajada1	-21.03175	-70.12771	578	composite quartz	10Be	0.239	0.027	-	-
Baker (this work)	Bajada1	-21.03175	-70.12771	578	composite quartz	26Al	0.214	0.026	-	-

APPENDIX B

SUPPLEMENTARY MATERIAL FOR CHAPTER 2

Table B.1: Scanline Data for Mitius Fan Surfaces

F1B09

Waypoint	Halfwidth (cm)	edge width	Orientation	depth (cm)	Type/ Description	Photos		Latitude	Longitude	Altitude (m)	Eastings	Northings
811					starting point			-23.06095	-70.19288	702.4	377800.63	7449234.73
812	20		50		E2/C4 almost invisible, but there, depth only grains where present			-23.06108	-70.19251	703.8	377838.66	7449220.64
813		*2	37		B2 type just fresh in loost material, so not vertical walls			-23.06125	-70.1922	705.5	377870.57	7449202.08
814	110	*	34	5	fresh crack, sandy fill varying with C2, very wide, fresh only on eastern edge	MT09 12		-23.06134	-70.19207	704.8	377883.97	7449192.23
815	15		14		B4 with fresh across channel, see crusty edges, but total fill	MT09 13		-23.06161	-70.1916	707.2	377932.36	7449162.72
816		*1	8		B1/2 type just fresh in loose material			-23.06165	-70.19141	707.2	377951.87	7449158.45
817		*1	48		B1/2 type just fresh in loose material		zone of strong drainage	-23.06167	-70.18969	710.5	378128.10	7449157.67
818		*2	13		B2 fresh only like previous			-23.06168	-70.18965	710.3	378132.21	7449156.60
819	22		42		C2 subtle depression, cuts terrain but some cange of width			-23.06172	-70.18939	711	378158.88	7449152.39
820	19		343		C2/3 mild depression that cuts surfaces and has variable width, partially due to fill in shallow feature			-23.06177	-70.18919	711.7	378179.41	7449147.02
821		*1	14		B2 fresh only in loose material			-23.06175	-70.18911	712.5	378187.59	7449149.30
822	6		349		E2 no depression, just fill/sorting, consistant width			-23.06183	-70.18876	712.9	378223.52	7449140.73
823	4		357		C2 mild depression, but clearer visible edges			-23.0619	-70.1883	714.9	378270.71	7449133.37
824	26		344		C2 same as previous			-23.06196	-70.18806	715.6	378295.35	7449126.92
825	14		1		C2 same as previous	MT09 14		-23.06212	-70.18743	718.7	378360.04	7449109.73
826	12		6		C2 like previous			-23.06217	-70.18723	719.2	378380.58	7449104.36
827	22		3		B4 like previous with some depth			-23.0622	-70.18699	719.7	378405.19	7449101.24
828	24		13		B4 like 827 and sooooo subtle			-23.06217	-70.18691	720.4	378413.36	7449104.63
829		*2	15		B2 fresh in loose *overall level of induration much less than PDL			-23.06218	-70.18686	720.4	378418.49	7449103.56
830	33		6		poor, as poor as I would give a B			-23.06221	-70.18669	721.3	378435.93	7449100.38
831	13		5		B 2/3 visible depression, some crusty bound			-23.06221	-70.18644	721.6	378461.55	7449100.59
832	10		17		E3 distribution ok clasts/fill, but laterally continuous			-23.06222	-70.18614	723.8	378492.29	7449099.73
833	24		357		A4 clear walls with fill	MT09 15	very proximal to F4	-23.0622	-70.18597	724.7	378509.69	7449102.09
834	39		14		B3 w/fresh, visible, but depressed			-23.06224	-70.18579	725.2	378528.17	7449097.81
835	24	*	7		fresh in C2		getting into drainage/channel area clasts and sediment getting thicker, slope getting steeper	-23.06221	-70.18565	725.9	378542.48	7449101.25
836	65	28	351		B3 w/ A2 in middle	MT09 16		-23.06206	-70.18468	730	378641.72	7449118.66
837	77	31 *	351		B3 w/A2 inside, fresh down center, except through circlar collapse feature			-23.06199	-70.18453	730.2	378657.03	7449126.54
838			11		C4... holes w/no clear crack connecting them			-23.06195	-70.18444	730.7	378666.21	7449131.04
839		*1.5	24		A1 fresh only			-23.06196	-70.18432	731.4	378678.52	7449130.03
840	50	20	24		A2 inside of B3			-23.06192	-70.18378	733.6	378733.80	7449134.91
841	**19**		357		A2 but not clear enough for actual		getting into steeper part of top of fan	-23.06188	-70.18339	734.8	378773.72	7449139.66
842	11		47		D2, otherwise depressed and constant width			-23.06177	-70.18197	743.7	378919.10	7449153.02
843	19		2		B2 continuous into F4	MT09 17, MT09 18		-23.06176	-70.18163	743.7	378953.93	7449154.40
844					ending point			-23.06176	-70.18162	744.4	378954.95	7449154.41

Opening cm	688.5	6.885
length m	1157.11204	
e	0.005985775	
%e	0.598577477	

Table B.1: Continued

F2C09

Waypoint	Halfwidth (cm)	edge width	Orientation	depth (cm)	Type/ Description	Photos	Latitude	Longitude	Altitude (m)	Eastings	Northings
909					starting point		-23.06331	-70.17842	762.2	379284.18	7448985.45
910	**90**		31	19	A2	MT09 29	-23.06329	-70.17846	761.2	379280.06	7448987.63
911	32		314		B2/B1 subtlty, fill, not as long as previous, but doesn't appear to be drainage		-23.06329	-70.17854	761.2	379271.86	7448987.56
912	**86**		344	10	A3/ B2 subtlty close to too shallow		-23.06326	-70.17873	760.3	379252.37	7448990.73
913	**35**		343		B2 subtle depression, but clear		-23.06325	-70.17881	758.8	379244.17	7448991.77
914	**19**		3	12	A3 due to rounding		-23.06326	-70.17899	758.4	379225.73	7448990.51
915	13		6		C2 varying width, but still some depression		-23.06327	-70.17937	756.4	379186.81	7448989.09
916	**75**		345	11	D1 perfect, but might be drainage		-23.06327	-70.17939	756.2	379184.76	7448989.07
917	**80**		0	12	B1/B2 subtle, practically no fill	MT09 30	-23.06332	-70.17959	756	379164.32	7448983.37
918	**44**		26	10	A2/3 rounding, practically no fill straighter sides in some places		-23.06337	-70.1802	752.4	379101.87	7448977.33
919	11		22		B3 very broad		-23.06337	-70.18034	751.2	379087.53	7448977.22
920	**37**		11		B2 gentle but very clear		-23.06338	-70.1806	749.7	379060.90	7448975.90
921	**90**		4	15	B2 same as previous		-23.06334	-70.18075	749.5	379045.50	7448980.20
922	7		9		B3 more broad		-23.06335	-70.18082	749.2	379038.33	7448979.03
923	**80**		16	12	A2 rounding		-23.06334	-70.18104	747.3	379015.79	7448979.96
924	**75**		21	14	A3 rounding		-23.06333	-70.18121	746.6	378998.36	7448980.93
925	**57**		344	9	A3/B1 rounding, little fill		-23.06331	-70.18145	746.1	378973.76	7448982.94
926		16-23	24		B1	MT09 31	-23.06337	-70.18181	743.9	378936.93	7448976.00
927	14		7		B3 subtlty and fill		-23.06334	-70.18248	738.7	378868.26	7448978.77
928	15		4		C2 subtle and changes slope		-23.06331	-70.18295	737.7	378820.08	7448981.70
929		5	63		fresh only B2		-23.06329	-70.18303	737	378811.87	7448983.85
930		3	12		B2 fresh only		-23.06326	-70.18334	734.8	378780.08	7448986.91
931	16		2		B2 subtle but clear		-23.06323	-70.18347	734.6	378766.74	7448990.13
932	28		341		B3 subtlty and fill		-23.06327	-70.1837	733.6	378743.21	7448985.51
933		6	16		Fresh only B3, broad in fill		-23.06327	-70.18384	732.9	378728.87	7448985.39
934	9		346		C2/C1 variable, collapses, walls, then non		-23.06331	-70.18417	731.4	378695.09	7448980.69
935		*3	12		B3 very subtle fresh		-23.06336	-70.18456	730	378655.18	7448974.83
936		*1	25		Fresh only B2		-23.06348	-70.18521	725.4	378588.70	7448961.00
937		*2	4		Fresh only B1		-23.0635	-70.18558	723.8	378550.81	7448958.48
938		*1	33		Fresh only B2		-23.06353	-70.18579	722.1	378529.32	7448954.99
939	9		7		B3 very subtle		-23.0636	-70.18603	720.9	378504.80	7448947.04
940	55		357		B3 w/ crustys on either side		-23.06363	-70.18616	720.9	378491.51	7448943.61
941					ending point		-23.06365	-70.18617	720.6	378490.50	7448941.38

Opening cm	1019	10.19
length m	794.8965865	
e	0.012985745	
%e	1.298574547	

F2A 09

Waypoint	Halfwidth (cm)	edge width	Orientation	depth (cm)	Type/ Description	Photos	Latitude	Longitude	Altitude (m)	Eastings	Northings
942					starting point	polygonal ground here will make subtle cracks difficult	-23.06152	-70.17673	774	379455.72	7449185.02
943	**44**		28		A2/3 rounding		-23.06134	-70.17732	768	379395.11	7449204.47
944	**21**		13		A3 rounding reall hard to see in poolygons		-23.06126	-70.17751	765.6	379375.58	7449213.17
945		*3	33		Fresh only		-23.06083	-70.17884	753.3	379238.93	7449259.68
946					ending point		-23.06019	-70.17944	746.8	379176.89	7449330.04

Opening cm	68	0.68
length m	314.285374	
e	0.00216833	
%e	0.216833019	

F3 scanline 1

Total Length 128.64

Waypoint	Halfwidth (cm)	edge width	Orientation	depth (cm)	Type/ Description	Photos	Latitude	Longitude	Altitude (m)
285					starting point		-23.06618	-70.18005	757.2
286	42	*	27				-23.06604	-70.18014	754.8
287	9	*	35				-23.0659	-70.18034	753.1
288	18		14				-23.06559	-70.18082	750.7
289	17		16				-23.06548	-70.181	750.4
290					ending point		-23.06549	-70.18106	749

F4E09

Waypoint	Halfwidth (cm)	edge width	Orientation	Depth	Type/ Description	Photos	Latitude	Longitude	Altitude (m)	Eastings	Northings
772					starting point		-23.07351	-70.18272	1395.9	378852.78	7447852.58
773	16		74		B2 photo of crack, subtle depression	MT09 1	-23.07347	-70.18273	1395.2	378851.72	7447857.00
774	22		63		A3 rounded but with notable depth		-23.07343	-70.18275	1395	378849.64	7447861.41
775	34		42		B3 rounded subtle fill		-23.07311	-70.18299	1394.7	378824.76	7447896.64
776	**33**		67		B3		-23.0731	-70.183	1394	378823.73	7447897.74
777	**35**		64		B3 lot of fill, sinuous, but with overall orient	MT09 2	-23.07303	-70.18312	1394.3	378811.37	7447905.39
778	18	*	47		B3 with fresh		-23.07274	-70.18355	1391.6	378767.06	7447937.14
779	**105**	*	44		A3 rounding with fresh 20cm depth	MT09 3 - MT09 4	-23.07257	-70.1837	1390.9	378751.55	7447955.84
780	**85**		48		B2 subtle, but clear appears save fluid has traveled down, 12cm deep		-23.07253	-70.1838	1389.7	378741.27	7447960.18

Table B.1: Continued

781	55		47		B2/A3 clear depth, but very rounded	MT09 5	drainage orientation	-23.07229	-70.18401	1389.7	378719.54	7447986.58
782	220		14		A2 rounding, but clearly a fault	MT09 6-MT09 11	65 cm deep	-23.07166	-70.1849	1384.9	378627.80	7448055.59
783	37		327		D2 ok, but curves dramatically to become drainage			-23.07137	-70.18547	1383	378569.15	7448087.23
784	22	*	46		B3/C2 w/fresh, varies much along width			-23.07105	-70.18591	1381	378523.78	7448122.29
785	18	*	27		fresh only cutting drainage, very hard to see in groove, very subtle B2			-23.07089	-70.18618	1379.4	378495.98	7448139.78
786	17		356		B2 becomes drainage to norh			-23.0708	-70.18635	1378.2	378478.48	7448149.61
787	39		336		C3/ E2 practically impossible to see due to sublety			-23.07064	-70.18651	1377.9	378461.95	7448167.19
788		*3mm	21		fresh crank only in drainage, not extending to surrounding surface	actually a series of those within drainage just not along		-23.06901	-70.18824	1368.6	378283.26	7448346.22
789					ending point			-23.06845	-70.18901	1364.5	378203.87	7448407.58

Opening cm	756	7.56
length m	853.8804271	
e	0.008932787	
%e	0.893278687	

n channel, still appears quite fresh

F5D09

Waypoint	Halfwidth (cm)	edge width	Orientation	depth (cm)	MT09 25 Type/ Description	Photos		Latitude	Longitude	Altitude (m)	Eastings	Northings
902					starting point			-23.06982	-70.1847	746.1	378646.64	7448259.48
903	**79**		33	13	A3 rounding			-23.06965	-70.18493	745.1	378622.92	7448278.11
904	57	*	2		A3/B2 subtlty w/fresh			-23.06937	-70.18531	743.2	378583.74	7448308.80
905	81	*	9		C1/C2 otherwise clear w/fresh			-23.06924	-70.18543	741.8	378571.33	7448323.09
906	67	*	46	10	A4 see photo for flat-bottomed fill, cuts clearly across terrain	MT09 27	MT09 28	-23.0692	-70.18549	742.5	378565.15	7448327.47
907	29		31		B3 subtle with fill			-23.06875	-70.18605	739.4	378507.38	7448376.83
908					ending point			-23.06218	-70.19253	706.7	377837.60	7449098.84

Opening cm	313	3.13
length m	1165.789894	
e	0.002692103	
%e	0.269210284	

F6F09

Waypoint	Halfwidth (cm)	edge width	Orientation	ype/ Description	Photos	Latitude	Longitude	Altitude	Eastings	Northings
790				starting point		-23.07016	-70.19033	718.2	378070.18	7448217.15
791	7		7	t no depth, but present		-23.07007	-70.19041	718	378061.91	7448227.05
792	24		37	but 9cm deep hole along length		-23.07006	-70.19042	718	378060.87	7448228.15
793	26		43	subtlty of depth		-23.06996	-70.19049	718	378053.61	7448239.16
794	31		24	lear edges but fill		-23.06978	-70.1906	717.5	378042.18	7448259.00
795	16		22	C3 very subtle		-23.0695	-70.19069	717.3	378032.71	7448289.92
796	6	*	58	resh, really hard to see		-23.06942	-70.19069	717.7	378032.64	7448298.78
797	26		47	o depth but clear		-23.06916	-70.1907	717.7	378031.38	7448327.56
798	12		54	2 almost no depth		-23.06906	-70.19074	716.8	378027.19	7448338.60
799				oops		-23.06906	-70.19076	718	378025.14	7448338.58
800	2		53	rface material only		-23.06894	-70.1909	719.9	378010.69	7448351.75
801	12		34	2 very unclear		-23.06855	-70.19131	718.9	377968.33	7448394.59
802	31		359	B3 subtle		-23.06853	-70.19133	718.5	377966.27	7448396.79
803	36		351	ainage, but clear elsewhere		-23.06827	-70.19162	718.5	377936.32	7448425.33
804	70		351	ge, other drainages in same orient		-23.06799	-70.19183	717	377914.56	7448456.16
805	36		359	possible drainage		-23.06768	-70.1922	716.1	377876.37	7448490.17
806				drainage		-23.06723	-70.19276	714.9	377818.60	7448539.52
807	27		357	some fill, clear edges w/depth		-23.06659	-70.19344	713.7	377748.36	7448609.81
808	3		53	nvisible as they come		-23.06649	-70.19356	713.4	377735.97	7448620.79
809	18		355	depth allows for spreading		-23.06622	-70.1938	712.5	377711.14	7448650.48
810				ending point		-23.066	-70.19399	712.5	377691.48	7448674.68

Opening cm	383	3.83
length m	593.9292343	
e	0.006490434	
%e	0.649043377	

F7G09

Waypoint	Halfwidth (cm)	edge width	Orientation	depth (cm)	Type/ Description	Photos	Latitude	Longitude	Altitude (m)	Eastings	Northings
845					starting point		-23.07599	-70.18486	762.9	378635.78	7447576.22
846	22		28		B3 subtle, rounded, but depressed		-23.07587	-70.18502	760.5	378619.28	7447589.37
847	24		42		B3 expressed here in drainage more subtlty than in surrounding		-23.07584	-70.1851	759.6	378611.06	7447592.63
848	27		6		B3 subtle, buut distinct seems to continue into neighboring part		-23.07579	-70.18517	758.6	378603.85	7447598.11
849	7		36		B3	MT09 19	-23.0755	-70.18571	755.5	378548.27	7447629.77
850	6		26		B4 so subtle, but consistant width		-23.07539	-70.18586	753.8	378532.80	7447641.82
851	10		24		C3/4 crappy variable		-23.07528	-70.18605	752.8	378513.24	7447653.84
852	29		351		B3 subtle depth, broad, fill		-23.07519	-70.18618	751.9	378499.84	7447663.70
853	22		34		B2 more depressed		-23.07506	-70.18652	751.6	378464.90	7447677.81

Table B.1: Continued

					D2 potential drainage, definitely leads into						
854	23		33		one		-23.07503	-70.18659	750.9	378457.70	7447681.07
855	70	70	41	8	A3 rounding, but measurable depth	MT09 20, MT09 21	-23.07488	-70.18685	749.7	378430.93	7447697.46
					B2 with collapses of A3 quality along						
856	120	collapse 25, 28, 36	353		length	MT09 22	-23.07472	-70.18705	746.8	378410.30	7447715.01
857	48		353		D2 drainage potentially very soft fill		-23.07458	-70.18739	745.6	378375.34	7447730.23
858	34		3		D2 potential drainage, ends in one		-23.07409	-70.18821	743	378290.90	7447783.80
859	3	1	48		B2 super subtle, but w/ fresh		-23.07358	-70.18894	740.6	378215.66	7447839.66
860	**125**		4	9	B2/A3 crosses drainages		-23.07333	-70.18938	739.1	378170.36	7447866.97
861	**100**		24	10	C1/2 depth, but variable		-23.07325	-70.18962	738.4	378145.70	7447875.63
862	**160**		16	15	A3 rounding, crusting on edge		-23.07302	-70.19016	737.2	378090.18	7447900.64
863	145		12		B2 sublty		-23.07282	-70.19046	735.8	378059.26	7447922.53
864	28		53		E only just visible, no depression		-23.07247	-70.19088	733.6	378015.92	7447960.94
					B4 subtlest possible, but with constant						
865	9	*	76		with fresh		-23.07233	-70.19114	732.4	377989.16	7447976.22
866	75		32		C3 varying width, little depression		-23.07224	-70.19131	732.2	377971.66	7447986.04
867	**18**		8		C2 defined with depth but width varies		-23.07211	-70.19152	731.4	377950.03	7448000.26
868	19		19		B3 rounded subtle		-23.07193	-70.19185	730.2	377916.07	7448019.91
869	2		29		A1 fresh throuogh indurated material		-23.07191	-70.19191	730.5	377909.90	7448022.08
870	5	*	21		B2 subtle but clear edges with fresh		-23.07179	-70.19214	729.3	377886.23	7448035.17
871	7	*	25		B2 subtlty, fill w/ fresh		-23.07167	-70.19237	728.8	377862.56	7448048.26
872	14	*3	45		B2 w/ fresh		-23.07136	-70.19315	726.2	377782.37	7448081.94
873		*2	17		B2 fresh only		-23.07124	-70.19352	725.4	377744.36	7448094.91
874	21		1		subtlty w/fill		-23.07116	-70.19373	724	377722.78	7448103.59
875		*1	42		A2/3 fresh only, breaking down some		-23.07105	-70.194	723.5	377695.02	7448115.55
					B3 w/fresh crack, fresh cracks continue and fork here, on slight raise in terrain, fresh is B2 now on west side up block of						
876	46	*8	33		fault		-23.0709	-70.19441	722.6	377652.88	7448131.81
877	24		37		B4 but clearly cuts topo		-23.07083	-70.19455	722.1	377638.48	7448139.44
878		*3	48		B2 fresh only in some loose		-23.07079	-70.19477	720.6	377615.90	7448143.69
879	50	*2	27		B3 but cuts topo w/fresh		-23.07067	-70.1952	718.9	377571.74	7448156.61
880		*1	66		Fresh only B1		-23.07063	-70.19532	719.7	377559.41	7448160.94
881	23		56		C2 unclear, width shallow		-23.07058	-70.19546	718.7	377545.03	7448166.36
882	16	*	33		B4 but cuts topo, with >1cm fresh		-23.07039	-70.19601	716.8	377488.51	7448186.94
883	17		9		D2 potential drainage, unclear if cuts topo		-23.07037	-70.19612	716.1	377477.22	7448189.06
884		*4	34		Fresh only B2 breaking down		-23.0703	-70.19634	715.8	377454.62	7448196.62
885		*2	32		B2 fesh only in loose		-23.07025	-70.1965	714.9	377438.18	7448202.03
886	21		6		B3 cuts drainage, subtle, crusty edges		-23.07019	-70.19687	714.6	377400.23	7448208.36
887	17		354		B3 cuts drainage, crusty edges		-23.07014	-70.19702	714.1	377384.81	7448213.77
888	12		14		C2 cuts drainage though		-23.0701	-70.19714	713.9	377372.48	7448218.10
889	16		2		B2 crusty edges, more consistent		-23.07007	-70.19729	713.2	377357.09	7448221.29
890	15		14		C2 width varies		-23.07003	-70.19742	713.2	377343.74	7448225.61
891	23		356		B2 more clear w/ crusty edges		-23.06994	-70.19769	711.3	377315.99	7448235.35
892	24		10		B3 fill		-23.06991	-70.19781	711.5	377303.67	7448238.57
893	19	*2	17		C3 width changes, very shallow with fresh		-23.0699	-70.19792	711.3	377292.40	7448239.59
894		*1	56		B2 fresh only with some breakdown		-23.06979	-70.19817	709.8	377266.69	7448251.56
					B4 crusty edges visible, but completely						
895	15		10		filled		-23.06968	-70.19847	709.1	377235.85	7448263.48
896			69		E4 just there		-23.06936	-70.19932	707.4	377148.48	7448298.20
					B4 with fill, width constant, mostly fresh						
897	20	*1	57		crack		-23.06928	-70.19944	706.7	377136.12	7448306.95
898	6		64		C2/3 hard to see		-23.06912	-70.19971	706.2	377108.31	7448324.44
899	23		5		C2 cuts topo, with fill		-23.06904	-70.19992	705.5	377086.73	7448333.12
900	11		47		C3 cuts topo, more varied here		-23.06888	-70.2002	704.3	377057.90	7448350.60
901					ending point	MT09 23, MT09 24	-23.06886	-70.20023	704.5	377054.80	7448352.79

Opening cm	1581	15.81
length m	1761.40637	
e	0.009057077	
%e	0.905707658	

F8I 09	n fact, drainages										
Waypoint	Halfwidth (cm)	edge width	Orientation	Depth	Type/ Description	Photos	Latitude	Longitude	Altitude (m)	Eastings	Northings
967					starting point		-23.11341	-70.19603	720.4	377525.46	7443423.84
968		*2	18		Fresh only B1		-23.11315	-70.19707	715.3	377418.72	7443451.75
969		*2	2		Fresh only B1		-23.11305	-70.1973	713.4	377395.07	7443462.63
970		*2	297		Fresh only B1		-23.11301	-70.19739	712.5	377385.82	7443466.99
					C2 (recorded min and max along length,						
971	68	27 *	8		subtly and fill width change		-23.11287	-70.19781	711.3	377342.68	7443482.13
972	**84**		3	11	B2/A3 depth and fill		-23.11277	-70.19811	710.3	377311.86	7443492.95
973	42		316		D1/2 beautiful, but drainage... crusty edges		-23.11275	-70.19817	710.3	377305.70	7443495.12
974	20		33		B2/3 subtlty and fill		-23.11257	-70.1988	707.2	377241.02	7443514.52

Table B.1: Continued

975	**125**		18	13-25	B2 actually fault, west side up, damming drainage	MT09 34		-23.11247	-70.19909	704.3	377211.23	7443525.34
976	44		47		C3 oor, but opening visible in crusty material			-23.1123	-70.19948	703.8	377171.13	7443543.84
977	24		27		B4 width consistent, but totally filled	MT09 35		-23.11213	-70.20007	700.9	377110.55	7443562.16
978	34		28		B3/4 a little less fill than preivious			-23.11194	-70.20052	699.7	377064.30	7443582.82
979	21		32		B4 like 977			-23.11187	-70.20071	699.7	377044.77	7443590.41
980	43		15		B4/C3 like previous, but losing width definition			-23.11168	-70.20129	697.1	376985.20	7443610.96
981	27		0		C3/4 poor			-23.11152	-70.20173	695.4	376939.99	7443628.30
982	37		5		C4 poor almost invisible once on it			-23.11148	-70.20187	694.2	376925.62	7443632.61
983	11		11		C4/E3 very poor, here losing any depression at all			-23.11141	-70.2024	692.3	376871.28	7443639.92
984	14		12		B4 edges w/ fill			-23.11137	-70.20255	691.3	376855.88	7443644.22
985	14		33		C2/3 same depression, very poor width			-23.11128	-70.20284	690.1	376826.10	7443653.94
986	80		6		C2 depression clear, but varying width			-23.11107	-70.2034	687.2	376768.55	7443676.72
987	22		12		C2 same as previous			-23.11101	-70.20378	685.8	376729.58	7443683.04
988	38		358		B2 depressed, but very rounded and filled			-23.111	-70.20388	684.3	376719.33	7443684.06
989	**85**		336	22	west side up fault again, crusty edges on both sides, much larger and deeper than anything around			-23.11102	-70.2042	682.9	376686.58	7443681.58
990	**70**		354		B2/3 joins back up w/ fault (fill)			-23.11102	-70.20445	682.9	376660.97	7443681.36
991	40		339		B3 subtlty and fill			-23.11101	-70.20459	682.7	376646.63	7443682.35
992	77		356		B3 subtlty and fill, more west side up across this feature		fault at 16 degrees	-23.11098	-70.20488	681.7	376616.90	7443685.43
993	**39**		334		C1/2 depressed, but width clearly varies, cuts topo			-23.11101	-70.20528	680.3	376575.96	7443681.77
994					ending point			-23.11084	-70.20669	675.9	376431.40	7443699.40

Opening cm	1065	10.65
length m	1128.227995	
e	0.009529536	
%e	0.952953623	

F9H 09

Waypoint	Halfwidth (cm)	edge width	Orientation	Depth	Type/ Description	Photos		Latitude	Longitude	Altitude	Eastings	Northings
947					starting point			-23.1083	-70.19721	690.8	377399.98	7443988.62
948	22		60		C2 unclear, but cuts drainage		polygons in this terrain make it somewhat hard	-23.10805	-70.19805	687.9	377313.72	7444015.59
949	70		27		A4/B3 subtle but due to fill			-23.10791	-70.19857	687	377260.34	7444030.66
950	11		26		B3 very subtle and sinuous, w/ fresh			-23.10788	-70.19861	687	377256.21	7444033.94
951	18		11		C2 variable width due to shallowness			-23.10781	-70.19879	686.5	377237.71	7444041.54
952	**80**		20	7	B2/3 with fill and fresh	MT09 33		-23.10779	-70.19886	685.8	377230.53	7444043.70
953	6	*1	49		C2 w/ fresh, cuts drainage clearly			-23.10776	-70.19901	685.5	377215.14	7444046.89
954	13	*1	33		B2 w/ B1 fresh crack in center			-23.10774	-70.19904	686	377212.05	7444049.08
955		*1	30		just B1 fresh			-23.10769	-70.19917	685.5	377198.69	7444054.51
956	43		26		B3 rounding			-23.10768	-70.19921	684.8	377194.58	7444055.58
957	**48**		27	8	A3/B2 rounding and fill			-23.10763	-70.19938	684.6	377177.13	7444060.98
958	**46**	*2	59	7	A3/B2 rounding and fill w/ fresh			-23.1076	-70.19958	683.6	377156.61	7444064.13
959		*1	42		B1 fresh only			-23.10754	-70.19977	682.7	377137.10	7444070.61
960		*1	41		B1 fresh only (not any notable change in nature of surface where void of cracks, exists, just polygons			-23.10706	-70.20119	677.1	376991.23	7444122.56
961	14		8		B3 subtlty of depth, fill			-23.10667	-70.20267	671.8	376839.30	7444164.49
962	8	*1	20		B3 same as above with fresh			-23.1066	-70.20289	670.9	376816.71	7444172.06
963	22		356		C2 unclear, hard to see, but cuts drainage			-23.10657	-70.20298	670.4	376807.46	7444175.30
964	**20**		351		B2 w/ some collapses			-23.10625	-70.20396	667.5	376706.80	7444209.90
965	**36**		19	~3	B2 w/ fresh and some depth			-23.10617	-70.20451	665.6	376650.40	7444218.30
966					ending point			-23.10575	-70.20596	663.4	376501.51	7444263.57

Opening cm	460	4.6
length m	939.5949423	
e	0.004919813	
%e	0.491981271	

F10 Scanline 2

Waypoint	Halfwidth (cm)	edge width	Orientation	Depth	Type/ Description	Photos	Latitude	Longitude	Altitude (m)
386					starting point		-23.08598	-70.19019	729.8
387	<1	*	55				-23.08578	-70.1904	729.5
388	<1		30				-23.08525	-70.19083	728.1
389					194 endpoint		-23.08446	-70.19127	728.6

F10 Scanline 3

Waypoint	Halfwidth (cm)	edge width	Orientation	Depth	Type/ Description	Photos	Latitude	Longitude	Altitude (m)
391	too small		320				-23.08657	-70.19271	713.4

Table B.1: Continued

392	too small		4				-23.08663	-70.19276	712.2
F10 Scanline 4									
Waypoint	Halfwidth (cm)	edge width	Orientation	Depth	Type/ Description	Photos	Latitude	Longitude	Altitude (m)
393					starting point		-23.08821	-70.20294	679.3
394	28		350				-23.08828	-70.20304	679.1
395	<1	*	330				-23.08849	-70.20338	678.8
396	18		314				-23.08893	-70.20415	675.9
397	28	*	336				-23.08899	-70.20419	675.9
398	<1	*	34				-23.08922	-70.20453	675.4
399	75		331				-23.08915	-70.2045	674.5
400	<1	*	53				-23.08929	-70.20474	675.2
401	<1	*	294				-23.08938	-70.20484	675.7
402	74		320				-23.08948	-70.20505	674.2
403	<1	*	46				-23.08961	-70.20531	671.6
404	130		300				-23.08979	-70.20562	672.1
F11 Scanline 1									
Waypoint	Halfwidth (cm)	edge width	Orientation	Depth	Type/ Description	Photos	Latitude	Longitude	Altitude (m)
405					starting point		-23.10622	-70.19683	697.8
406	20	*	10				-23.10604	-70.19814	690.1
407	15		36				-23.1048	-70.20232	668
408	27		14				-23.1047	-70.20244	669.7
409	97		26				-23.10446	-70.2033	667.3
410	70		34				-23.10418	-70.20376	665.8
411	<1	*	14				-23.1041	-70.20405	666.1
412							-23.10325	-70.20679	661
F12 Scanline 1									
Waypoint	Halfwidth (cm)	edge width	Orientation	Depth	Type/ Description	Photos	Latitude	Longitude	Altitude (m)
418					starting point		-23.10595	-70.19751	702.1
419	20		45		ending point		-23.10422	-70.20116	681.7
F12 Scanline 2									
Waypoint	Halfwidth (cm)	edge width	Orientation	Depth	Type/ Description	Photos	Latitude	Longitude	Altitude (m)
420					starting point		-23.10096	-70.20202	672.1
421	<1		29				-23.1014	-70.20138	672.1
422	<1		354				-23.10393	-70.19844	689.9
423							23.10436	70.19782	693
F13 Scanline 1									
Waypoint	Halfwidth (cm)	edge width	Orientation	Depth	Type/ Description	Photos	Latitude	Longitude	Altitude (m)
413					starting point		-23.10177	-70.20566	670.2
414	53		8				-23.10294	-70.20275	678.3
415	62		15				-23.10305	-70.20228	678.6
416	26		13				-23.10345	-70.20125	681.7
417					ending point		-23.10412	-70.19934	690.3

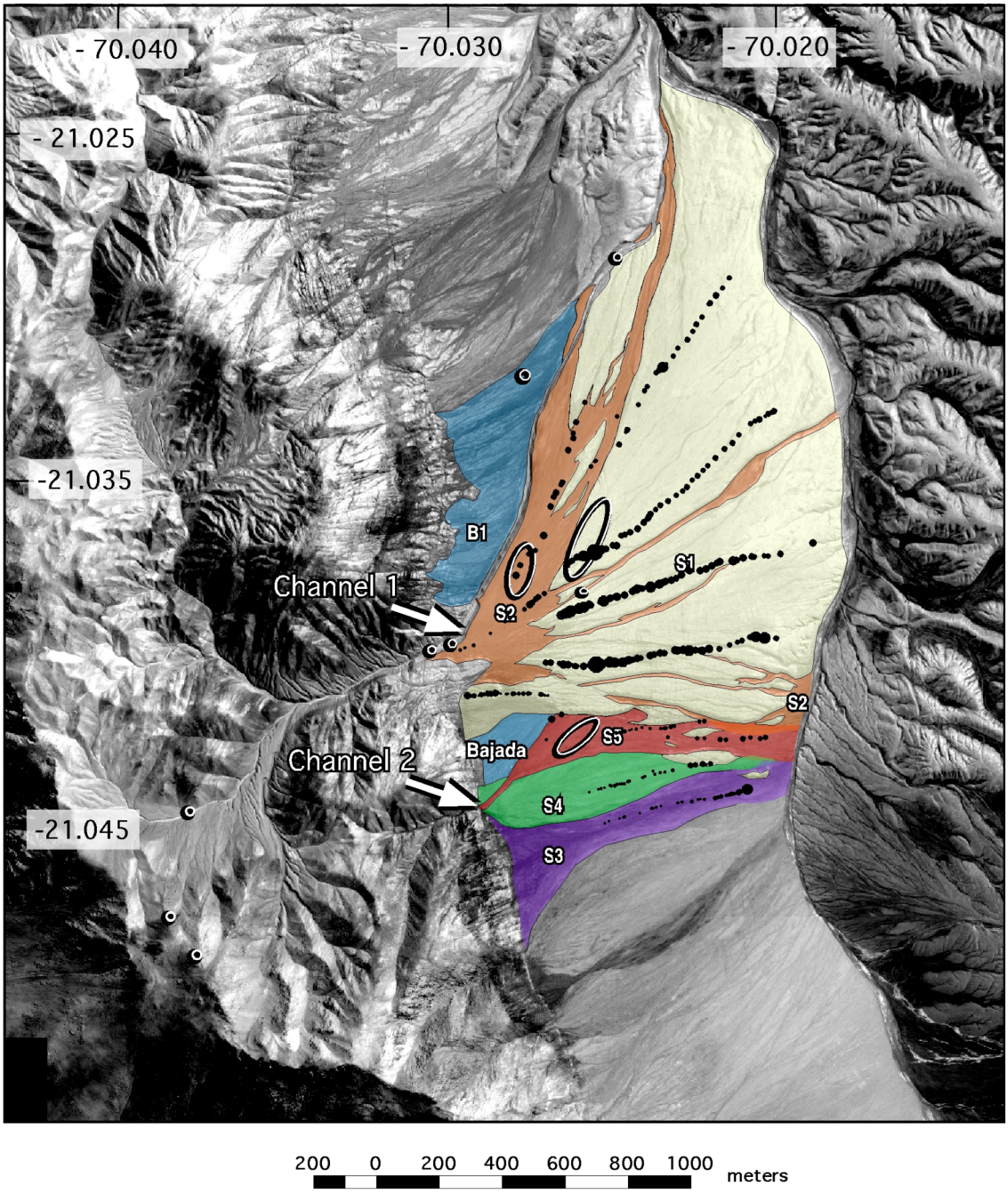

Figure B.1: IKONOS imagery of Punta de Lobos fan site with morphostratigraphic overlay. Ovals contain sampling locations. Each black dot represents a single crack with the size of the dot scaling with the width of opening.

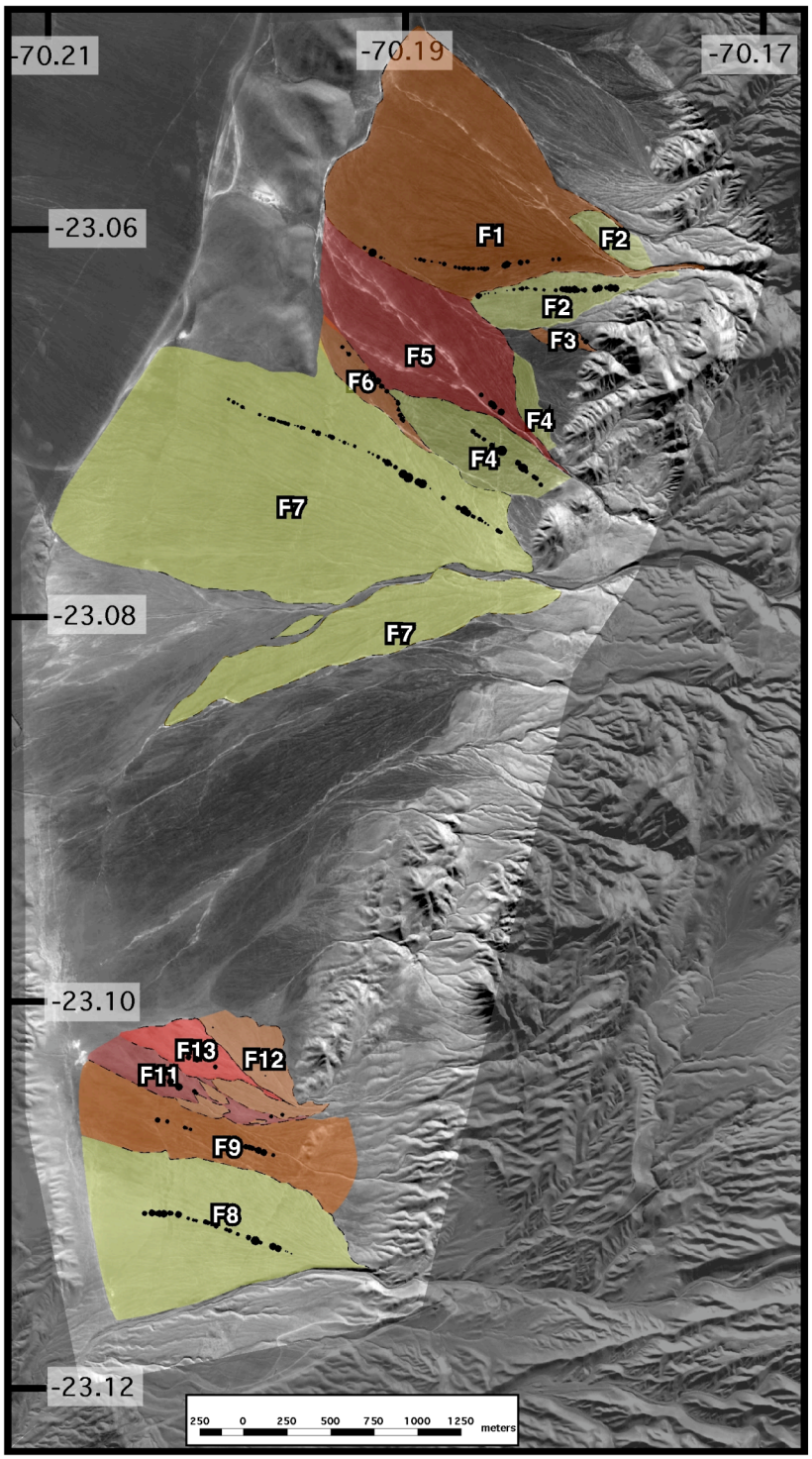

Figure B.2: Quickbird imagery of MItitus fan site with morphostratigraphic overlay. Each black dot represents a single crack with the size of the dot scaling with the width of opening.

Table B.2: Scanline Data for Punta de Lobos Fan Surfaces

F109 A

Waypoint	Halfwidth (cm)	actual	Orientation	Type/ Description	Photos		Latitude	Longitude	Altitude (m)	Eastings	Northings
267				starting point			-21.03865	-70.12894	639.2	382695.16	7673159.93
268	80		12	B3 very broad, poor edges, subtle depression			-21.03775	-70.1281	627.1	382781.75	7673260.17
269	60		20	B3-C2 so gentle, hard to see			-21.03746	-70.12797	625.7	382795.03	7673292.36
270	35	*3	6	B3 fresh, super subtle	pdl09 59		-21.03707	-70.12765	621.4	382827.98	7673335.77
271	25		19	B3-C2 so hard to see			-21.03715	-70.12772	621.6	382820.77	7673326.86
272	30		37	B3-C2			-21.03715	-70.12772	621.9	382820.77	7673326.86
273	45		23	B3-C2 only regard as a soft depresssion			-21.03704	-70.12751	619.7	382842.51	7673339.19
274	80		24	B3-C3	pdl09 60	alligned with drainages	-21.03661	-70.12725	616.1	382869.19	7673386.98
275	65		33	really unclear almost D3			-21.03578	-70.12703	608.9	382891.40	7673479.01
276	60		2	C3, D3 bc runs into drainage			-21.0355	-70.12693	607	382901.58	7673510.08
277	65		2	D2-D3 questionable if drainage, very poorly definred	pdl09 61		-21.03538	-70.12686	606.2	382908.76	7673523.41
278	40		3	C3-D3			-21.03515	-70.1267	603.6	382925.20	7673548.99
279	50		355	D2 these are all so questionable			-21.03509	-70.12666	603.6	382929.31	7673555.66
280	70		7	D3 questionable could be either			-21.03416	-70.12648	594.9	382947.29	7673658.73
281	60		7	B3-C2 we are turning away from drainages	pdl09 62		-21.03382	-70.12632	592.1	382963.65	7673696.48
282	45		14	C2	pdl09 63		-21.03368	-70.12632	590.4	382963.54	7673711.98
283	55		354	C2 varying width but not badly ~B3			-21.03336	-70.12623	587.5	382972.65	7673747.47
284	40		4	B2 clearer bounds less fill some F2 may be showing through			-21.03279	-70.12596	581.7	383000.26	7673810.76
285				ending point			-21.03253	-70.12582	579.3	383014.61	7673839.64

F109 B

Waypoint	Halfwidth	Orientation	Type/ Description	Photos	Latitude	Longitude	Altitude (m)	Eastings	Northings
286			starting point		-21.03307	-70.1249	578.8	383110.64	7673780.54
287	30	39	B3 unclear edges, cracks clear in F2 on either side of channel, but nothing in channel itself		-21.0332	-70.12497	579.6	383103.46	7673766.10
288	20	320	C3 from F2 directly		-21.03448	-70.12563	588.9	383035.87	7673623.93
289	12	322	C3 blotchy and unclear from F2		-21.0345	-70.12567	589.6	383031.73	7673621.69
290	30	339	B2 directly from F2 into channel		-21.03464	-70.12578	591.3	383020.41	7673606.11
291			ending point		-21.03632	-70.12698	606.5	382897.02	7673419.28

F109 C

Waypoint	Halfwidth		Orientation	Type/ Description	Photos	Latitude	Longitude	Altitude (m)	Eastings	Northings
292				starting point		-21.03991	-70.12989	644.2	382597.43	7673019.76
293	25		241	B3 vague		-21.03989	-70.12983	643.7	382603.65	7673022.02
294	13	*	7	B3 very vaque rounded, fresh		-21.03983	-70.12968	643	382619.19	7673028.77
295	19		33	B3 rounded		-21.03976	-70.12941	640.4	382647.19	7673036.72
296	15		24	B3		-21.03942	-70.1289	633.6	382699.92	7673074.73
297	18		350	B3 all about the same here		-21.03907	-70.12845	628.8	382746.41	7673113.80
298	30		352	cuts more clearly into distance		-21.03898	-70.1283	626.9	382761.93	7673123.87
299	30	*11	354	A3, B2 - open crack	pdl09 64, pdl09 65	-21.03873	-70.12785	622.1	382808.50	7673151.88
300	80	*	353	A3 rounded, goes into F2 fresh		-21.0386	-70.12769	619.5	382825.02	7673166.38
301	55	*	4	A3 with fresh (rounded edges) into F2		-21.03854	-70.12761	619.7	382833.29	7673173.08
302	50		338	B2 with fresh deep but rounded into F2		-21.03844	-70.1275	618.2	382844.64	7673184.23
303	60	45	3	A2-A3 into F2		-21.03838	-70.12742	617.5	382852.91	7673190.93
304	40		324	B2 with fresh (not into F2)		-21.03828	-70.12724	615.6	382871.53	7673202.13
305				ending point		-21.03821	-70.1271	614.4	382886.03	7673209.98

Table B.2: Continued

F209 A

Waypoint	Halfwidth (cm)	edge width	Orientation	Type/ Description	Photos	Latitude	Longitude	Altitude	Eastings	Northings
6				Starting point		-21.02902	-70.12141	539.9	383470.17	7674231.38
7	45		322	D3 short, poor boundaries		-21.02924	-70.12151	541.6	383459.95	7674206.96
8	45		350	C2 turns into channel		-21.02953	-70.12172	543	383438.35	7674174.71
9	65		224	B3 sinunous		-21.02974	-70.12192	545.4	383417.73	7674151.31
10	50		298	C3 short		-21.02996	-70.1221	547.1	383399.19	7674126.83
11	45		18	D2 possible drainage		-21.02998	-70.12213	547.6	383396.09	7674124.60
12	40		25	D1 becomes drainage		-21.03036	-70.12235	549.8	383373.53	7674082.37
13	50		352	C3 eventually drainage, but only at toe		-21.03057	-70.12253	552.2	383354.98	7674059.00
14	40		325	B3 rounded sides and sinuous		-21.03077	-70.12264	553.8	383343.71	7674036.78
15	55		149	B2-B3 rounded, but fill		-21.03101	-70.1228	555	383327.27	7674010.10
16	45		6	C2-C3 rounded		-21.03125	-70.1231	557.2	383296.28	7673983.31
17	40		5	A2-3 but narrow	PDL09 5	-21.03148	-70.12324	560.1	383281.91	7673957.75
18	25		345	B3 but very subtle sides		-21.03171	-70.12345	561.3	383260.26	7673932.14
19	140	150	11	A2-A3	pdl09 6, pdl09 7	-21.0318	-70.12356	563	383248.90	7673922.10
20	65	70	10	A2 sinuous	pdl09 8. Pdl09 9	-21.03188	-70.12367	564.2	383237.53	7673913.16
21	40		34	D3 lack of edges, potential drainage		-21.03195	-70.12377	564.7	383227.19	7673905.34
22	45		21	D3 lack of edges, potential drainage		-21.03235	-70.12404	568.3	383199.45	7673860.87
23	40		26	A3 (but close to edge, maybe drainage)		-21.03247	-70.12413	569.5	383190.19	7673847.52
24	45		325	C3-C4 really short		-21.03287	-70.12432	572.6	383170.75	7673803.10
25	55		317	B3 very subtle sides		-21.03359	-70.12466	579.3	383135.98	7673723.16
26	20		342	D2 subtle depression, otherwise good (C3?)		-21.03365	-70.12471	580.3	383130.83	7673716.48
27	55		318	B2-B3, subtle edges		-21.03401	-70.12492	583.4	383109.29	7673676.48
28				ending point		-21.03401	-70.12493	583.4	383108.25	7673676.47

F209 B

Waypoint	Halfwidth	edge width	Orientation	Type/ Description	Photos	Latitude	Longitude	Altitude	Eastings	Northings
29				starting point		-21.0375	-70.12658	610.6	382939.51	7673288.96
30	75	60	4	A2 mostly because of fill	pdl09 12	-21.03747	-70.12654	610.3	382943.64	7673292.31
31	60	50	287	C3		-21.03737	-70.12643	609.1	382955.00	7673303.46
32	55		357	C2 no fill, but bad boundaries		-21.03734	-70.12637	609.1	382961.21	7673306.82
33	70	60	354	A3		-21.03724	-70.12623	607.9	382975.68	7673317.99
34	85	50-90	35	A3 (maybe A2) with fill		-21.03723	-70.12615	607.2	382983.98	7673319.16
35	85	75	29	A3 because of rounding		-21.03723	-70.1261	606.7	382989.18	7673319.19
36	125	130	18	A1 (with some fill)	pdl09 13	-21.03721	-70.12602	606.5	382997.48	7673321.47
37	170	150	18	A2-A3 (rounded sides)	pdl09 14	-21.03711	-70.12568	603.8	383032.73	7673332.78
38	105	125	13	A1-A3 ranges from vertical to rounded		-21.03703	-70.12547	602.4	383054.49	7673341.79
39	75	75	8	A2 vertical with fill		-21.03701	-70.12534	601.7	383067.99	7673344.10
40	70	70	32	A2 vertical with fill		-21.03691	-70.12513	600.5	383089.73	7673355.33
41	85	70	20	A1-A2 (fill) but extremely constant width	pdl09 15	-21.03692	-70.12502	600.2	383101.17	7673354.30
42	50		10	B3 small		-21.03663	-70.12487	598.3	383116.53	7673386.51
43	60	50	358	A2-A3 sides degraded in places, cuts F1 drainage	pdl09 16	-21.0366	-70.12476	596.9	383127.94	7673389.91
44	75	65	26	B2 wit some vertical sides		-21.03654	-70.1246	595.2	383144.52	7673396.67
45	85		11	C2 boundaries come and go		-21.03644	-70.12437	594.2	383168.34	7673407.91
46	70	60	350	A3 cuts F1 drainage		-21.03626	-70.12418	592.3	383187.95	7673427.97
47	75	80	343	A3 cuts F1 drainage		-21.03614	-70.12405	591.3	383201.36	7673441.35

Table B.2: Continued

48	70	70	341	B2-B3 (photo for measurements match)	pdl09 17	-21.03611	-70.12403	590.6	383203.42	7673444.68
49	65	60	352	B2-B3		-21.03602	-70.12397	590.4	383209.58	7673454.69
50	45	40	349	B3		-21.03589	-70.12381	588.9	383226.11	7673469.19
51	55		358	A3		-21.03577	-70.12367	587.5	383240.56	7673482.58
52	60		335	B3		-21.03565	-70.12343	583.9	383265.41	7673496.04
53	40		359	B3		-21.03548	-70.12318	582.9	383291.26	7673515.04
54	40		352	C3- poor boundaries		-21.03536	-70.12298	580.5	383311.95	7673528.47
55	55		306	C2 little fill, poor boundaries		-21.03525	-70.12285	580.5	383325.37	7673540.74
56	40		336	B3		-21.03505	-70.12269	579.3	383341.84	7673562.99
57	50		353	C4 sinuous, poor, very rounded		-21.03493	-70.12252	577.6	383359.42	7673576.40
58	40		345	C4 poor, very very rounded		-21.03477	-70.12235	577.4	383376.96	7673594.23
59	40		351	C3-C4 rounded, discontinuous		-21.03464	-70.12221	575.5	383391.40	7673608.73
60	55		310	C3-C4 rounded, loses width (wide round)		-21.03442	-70.12197	572.8	383416.17	7673633.25
61	60		5	C3 very broad anad unclear		-21.03416	-70.12169	570.9	383445.07	7673662.24
62	50	50	11	B3		-21.03399	-70.12145	569	383469.88	7673681.23
63	40		342	C3 very poor boundaries	*reaching overlapping F1 channel , loose material	-21.03376	-70.12125	567.5	383490.48	7673706.83
64	40	35	344	C2 rounded but clear		-21.03344	-70.12089	562.3	383527.65	7673742.52
65	45		25	C3 very subtle almost lost in overlap		-21.03336	-70.12075	561.8	383542.13	7673751.47
66	65		49	D3 (drainage?)		-21.03332	-70.12062	562	383555.61	7673756.00
67	25		304	C4 very poorly defined		-21.03322	-70.12043	560.6	383575.28	7673767.20
68	50		15	B3 filled completely, but clear edge		-21.03316	-70.12034	560.6	383584.58	7673773.91
69	40		294	C4 really sinuous		-21.03312	-70.12024	560.3	383594.95	7673778.41
70	55		20	A3 fill, but preserves boundaries		-21.03308	-70.12016	559.8	383603.23	7673782.90
71				ending point		-21.03308	-70.12012	560.6	383607.39	7673782.93

F209 C

Waypoint	Halfwidth		Orientation	Type/ Description	Photos	Latitude	Longitude	Altitude	Eastings	Northings
72				starting point		-21.03891	-70.12676	619.5	382921.91	7673132.75
73	105	80	9	A3 wide with clear-nonvertical edges		-21.03891	-70.12673	618.7	382925.02	7673132.77
74	120	160	354	A2-A3 not vertical, but clear bounds		-21.03887	-70.1266	618.5	382938.50	7673137.30
75	130	150	11	A3 clear extensive, rounded		-21.03885	-70.12652	618	382946.80	7673139.57
76	60	45	14	A4 perfect, but ~20m long		-21.03883	-70.12648	618.2	382950.94	7673141.81
77	155	130	1	A2 somewhat rounded		-21.0388	-70.12643	616.3	382956.11	7673145.17
78	90	90	17	A3 rounded		-21.03877	-70.12632	617.5	382967.52	7673148.57
79	50	40	355	B2		-21.03876	-70.12626	617.8	382973.75	7673149.72
80	130	140	356	A3 rounded		-21.03872	-70.12617	616.6	382983.07	7673154.22
81	110	110	262	B3 rounded		-21.0387	-70.12609	616.1	382991.37	7673156.49
82	130		1	C2 loses width, little fill		-21.03869	-70.12604	616.1	382996.56	7673157.63
83	100		9	B3 unclear bounds		-21.03861	-70.12587	615.4	383014.16	7673166.61
84	70		324	B3		-21.03863	-70.12582	615.1	383019.37	7673164.43
85	55		345	C2 varying width little fill		-21.03854	-70.12553	612.7	383049.44	7673174.61
86	130	110	13	C2 varying width little fill, sinuous		-21.03851	-70.12542	612.2	383060.84	7673178.01
87	85		2	C2 varying width little fill		-21.03843	-70.12523	611	383080.53	7673187.00
88	45	80	16	A2-C2, varying along length, disappears		-21.0384	-70.12512	610.1	383091.93	7673190.41
89	100	90	18	C2 varying width, ~B3		-21.03839	-70.12502	609.6	383102.32	7673191.59
90	80	90	337	B2 some vertical sides		-21.03834	-70.12479	608.6	383126.18	7673197.29
91	80	75	13	B2 though not constant along length		-21.03824	-70.12454	606	383152.08	7673208.54
92	90	85	17	C1 variable width with vertical sides		-21.03819	-70.12447	606	383159.31	7673214.13
93	105	115	0	A2 somewhat filled		-21.03817	-70.1244	605	383166.57	7673216.39
94	75	90	347	B2 somewhat variable fit		-21.03815	-70.12431	604.6	383175.91	7673218.67
95	70	75	10	A1		-21.03816	-70.12424	604.1	383183.19	7673217.62
96	125	130	20	A2-A3 somewhat rounded		-21.03812	-70.12398	602.6	383210.18	7673222.23

Table B.2: Continued

97	110 125	24	A1-A2	pdl01 20, pdl09 21	-21.03804	-70.12372	600.5	383237.14	7673231.28
98	85 90	20	A2	pdl09 22	-21.038	-70.12362	600	383247.50	7673235.78
99	80 60	19	A2		-21.03796	-70.12352	599	383257.86	7673240.28
100	80 80	24	B2		-21.03792	-70.12335	598.3	383275.49	7673244.83
101	75	350	B1 rounded no fill		-21.03787	-70.1232	597.1	383291.04	7673250.48
102	75	357	B2		-21.03788	-70.1232	597.6	383291.05	7673249.37
103	80	342	A2-A3 rounded edges		-21.03777	-70.12304	595.2	383307.59	7673261.66
104	90 100	349	B2 varying amounts of fill		-21.03766	-70.12279	594.5	383333.48	7673274.02
105	85 80	15	A1-A2 varying fill steep sides		-21.03766	-70.12246	592.5	383367.78	7673274.26
106	80 80	8	A3		-21.03761	-70.12228	591.6	383386.44	7673279.93
107	85 80	320	B1		-21.03752	-70.1221	589.6	383405.08	7673290.02
108	70 70	22	B1 sharp, but varying path		-21.03744	-70.12195	587.7	383420.60	7673298.99
109	80	330	A1-A2 (gets wider)		-21.0374	-70.12186	587.7	383429.92	7673303.48
110	105 110	347	A1-A3 varying along length		-21.03738	-70.12146	585.3	383471.48	7673305.99
111	70	338	B3-B4 poor definition		-21.03736	-70.12135	585.3	383482.89	7673308.28
112	75 80	22	B3 unclear boundaries		-21.03729	-70.12116	583.9	383502.58	7673316.17
113	90 80	341	A3 sinuous		-21.03729	-70.12114	583.4	383504.66	7673316.18
114	70 60	19	C2 varying width		-21.03726	-70.12088	581.2	383531.65	7673319.69
115	50 45	6	B3/C2		-21.03727	-70.12081	580.8	383538.94	7673318.64
116	45 50	19	B2 laterally limited		-21.03724	-70.1205	579.3	383571.13	7673322.18
117	45 30	37	B3 unclear bounds		-21.03725	-70.12038	577.9	383583.61	7673321.16
118	75 80	22	B2-B3 bounds unclear, little fill		-21.03719	-70.12	575.2	383623.05	7673328.08
119	90	344	C2-C3 varying width, little fill		-21.03688	-70.11901	568.3	383725.69	7673363.12
120			ending point		-21.03687	-70.11899	568	383727.76	7673364.24

F209 D

Waypoint	Halfwidth	Orientation	Type/ Description	Photos	Latitude	Longitude	Altitude	Eastings	Northings
121			starting point		-21.03961	-70.11991	576	383634.28	7673060.28
122	60	15	E4 deep		-21.03962	-70.12015	576.2	383609.35	7673059.00
123	155 180	349	A3		-21.03961	-70.1205	577.9	383572.97	7673059.85
124	140	1	A1-A2 vertical with fill		-21.03957	-70.12077	579.3	383544.88	7673064.08
125	50 45	45	C2 variable width, no fill		-21.03958	-70.12095	580	383526.18	7673062.84
126	50 40	34	B2 rounded		-21.03968	-70.1212	581.5	383500.28	7673051.59
127	40	0	D2 no fill just depression		-21.03972	-70.12134	582.7	383485.77	7673047.06
128	45	336	B3 very rounded		-21.0398	-70.12158	582.7	383460.89	7673038.03
129	55 40	25	A3 well defined rounded		-21.03991	-70.12189	585.1	383428.76	7673025.63
130	100 100	9	A2 fill		-21.03991	-70.12221	587	383395.51	7673025.39
131	100 110	22	A2 fill		-21.03996	-70.12241	588.4	383374.76	7673019.71
132	75 95	44	A3-A4 lack of length		-21.03996	-70.12248	588.9	383367.49	7673019.66
133	85 90	6	A4-B3		-21.03994	-70.12263	588.9	383351.89	7673021.77
134	125 140	24	A3		-21.03996	-70.12282	590.6	383332.16	7673019.41
135	95 105	25	A2 near vertical with fill		-21.03993	-70.123	590.4	383313.43	7673022.60
136	100 110	8	B2-B3 rounded with varying fill		-21.03995	-70.12318	591.8	383294.74	7673020.26
137	95 90	11	A3 fill		-21.03994	-70.12324	591.8	383288.50	7673021.32
138	75	8	D2 barely visible depression no fill		-21.04002	-70.12358	593.3	383253.23	7673012.22
139	90	16	D2 fresh crack with little fill		-21.04002	-70.12371	594.9	383239.72	7673012.12
140	75	0	C1 varying width with clear bounds		-21.04006	-70.12389	595.4	383221.04	7673007.56
141	90 85	16	A1-A2 some fill		-21.04009	-70.12401	596.9	383208.60	7673004.15
142	50	5	B2 rounded		-21.04016	-70.1243	598.3	383178.52	7672996.19
143	15	351	B2 fresh, almost tiny, subtle		-21.04016	-70.12434	597.3	383174.36	7672996.16
144	30	5	B2 subtle, small fresh		-21.04016	-70.12434	598.5	383174.36	7672996.16
145	90 100	344	A3		-21.04016	-70.1244	598.5	383168.13	7672996.12
146	55	13	A4-B3		-21.04021	-70.12454	599.5	383153.62	7672990.48
147	50	4	C2 blotchy depths		-21.04021	-70.12459	599	383148.42	7672990.45
148	55 45	15	A1-A2 along length		-21.04021	-70.12459	599.3	383148.42	7672990.45
149	70 50	9	B2 fresh		-21.0402	-70.12464	599.5	383143.22	7672991.52
150	95 80	2	C1 deep narrow, varying fresh		-21.04022	-70.12468	600	383139.08	7672989.27
151	120	351	C1 deep, varying, no fill		-21.04028	-70.12485	600.9	383121.46	7672982.51
152	100	337	C2		-21.04029	-70.1249	600.5	383116.27	7672981.36
153	80	357	C2 varying little fill		-21.04029	-70.12495	600.5	383111.07	7672981.33
154	120	337	C2-D2 borad and non-descript		-21.04029	-70.12509	601.4	383096.53	7672981.23
155	130	354	D1 no fill broad subtle depression		-21.04027	-70.12525	603.3	383079.88	7672983.32
156	160	21	A3 fresh, one side steep, other narrow		-21.04033	-70.12554	605.8	383049.79	7672976.47
157	190	35	D4 not really any clear bounds		-21.04034	-70.12566	607.2	383037.33	7672975.27
158	110	25	B4 rounded but variable enough for C		-21.04035	-70.1258	607.4	383022.79	7672974.06

Table B.2: Continued

				A2 frersh crack where crosses F1						
159	20	*5	14	Channel	pdl09 23	-21.04036	-70.12591	608.4	383011.37	7672972.88
				A4 vertical sides peek through but						
160	85	70	21	filled	pdl09 24	-21.04038	-70.12605	609.1	382996.84	7672970.56
161	60	65	28	A2, turns into A1		-21.04038	-70.12628	610.6	382972.94	7672970.39
				A1 perfect with fresh where across						
162		*15-115	24	channel	pdl09 25 - pdl09 31	-21.04038	-70.12632	611	382968.78	7672970.36
163		*15	46	A2 mild depression		-21.04034	-70.12639	611	382961.47	7672974.74
164	80		10	C2 broad varying, little fill		-21.04033	-70.12652	611.5	382947.96	7672975.75
165	100		22	C2 fresh broad, varying, little fill		-21.04033	-70.12667	612.2	382932.37	7672975.64
166	60	55	26	A2		-21.04031	-70.12672	612.7	382927.16	7672977.82
167		*45	40	A1-A2		-21.0403	-70.12679	613.7	382919.88	7672978.87
168	65	70	12	fresh A3		-21.04027	-70.12706	615.6	382891.80	7672981.99
169	60	55	357	A2-A3 varyiable degrading		-21.04028	-70.12706	615.6	382891.80	7672980.89
170		*70	12	A2 but often covered by F1 material		-21.04027	-70.12721	616.8	382876.21	7672981.88
171				ending point		-21.04031	-70.12744	618.5	382852.34	7672977.29

F209 E

Waypoint	Halfwidth		Orientation	Type/ Description	Photos	Latitude	Longitude	Altitude	Eastings	Northings
306				starting point	pdl09 66, pdl09 67	-21.0412	-70.12965	644.7	382623.38	7672877.15
307	85		347	A3 very rounded, little fill		-21.0412	-70.12962	644	382626.50	7672877.17
308	40	*	6	A3 very rounded		-21.0412	-70.1296	643	382628.58	7672877.19
309	25	*	7	C1 realy subtle no fill		-21.04121	-70.12952	642	382636.90	7672876.14
310	8		3	C2 really more subtle		-21.04121	-70.12943	641.6	382646.25	7672876.21
				B3 rounded but depressed and						
311	45		2	constant		-21.04121	-70.12941	641.1	382648.33	7672876.22
312		*3	23	fresh only		-21.04121	-70.12927	639.6	382662.88	7672876.32
313	45		355	B2 rounded but clear		-21.04118	-70.12919	638.7	382671.17	7672879.70
314	18		9	depression, very rounded B3		-21.04117	-70.12911	637.5	382679.47	7672880.87
315	55		354	A3 bc of rounding		-21.04115	-70.12899	636.8	382691.93	7672883.17
316	55	60	30	A2-A3 varies		-21.04116	-70.1289	635.3	382701.29	7672882.13
317		27	0	A2 well-defined (some A1)		-21.04115	-70.12887	635.3	382704.40	7672883.26
318						-21.04115	-70.12882	634.6	382709.59	7672883.30
319	60	*	19	B3 rounded with fresh		-21.04114	-70.12876	633.4	382715.82	7672884.45
320	70	*	4	B3 rounded with fresh		-21.04114	-70.12876	633.9	382715.82	7672884.45
321	25		4	C2 unclear/varying		-21.04113	-70.12869	632.2	382723.09	7672885.60
322		*1	9	fresh only A1		-21.04115	-70.1286	631.9	382732.45	7672883.46
323	9	*2	27	B3 with fresh, boundaries unclear		-21.04117	-70.12842	630	382751.17	7672881.38
324		*2	34	fresh A1		-21.04116	-70.12838	629.1	382755.32	7672882.51
325		*2	29	fresh A1		-21.04116	-70.12826	627.9	382767.79	7672882.60
326	35	30	26	A2		-21.04116	-70.12823	628.1	382770.91	7672882.62
327	20	*	337	B3 with fresh		-21.04116	-70.12817	627.9	382777.14	7672882.67
328	19	*	9	B3 with fresh		-21.04116	-70.12804	626.9	382790.65	7672882.76
329		13 *	354	A2 with fresh		-21.04116	-70.12794	625.9	382801.05	7672882.83
330	33		1	B3-C2 some varying		-21.04116	-70.1279	625.7	382805.20	7672882.86
331	30		2	B2		-21.04116	-70.12775	624	382820.79	7672882.97
332	9		6	B2-B3 subtle		-21.04116	-70.12769	624	382827.02	7672883.02
333	35		39	B1 rounded subtle, no fill		-21.04118	-70.12738	621.6	382859.25	7672881.03
334		32	24	A2		-21.04119	-70.12734	620.7	382863.42	7672879.95
335	12		37	B2		-21.04121	-70.12725	619.7	382872.79	7672877.81
336		*2	23	A1 fresh only		-21.04122	-70.12716	619.5	382882.15	7672876.77
337	2		24	fresh only A1		-21.04121	-70.12715	619.5	382883.18	7672877.88
338				ending point		-21.04122	-70.12714	619.9	382884.22	7672876.78

Table B.2: Continued

F309 A

Waypoint	Halfwidth	actual	Orientation	Type/ Description	Photos	Latitude	Longitude	Altitude	Eastings	Northings
229				starting point		-21.04246	-70.12025	576.2	383601.16	7672744.57
230	45		22	C3 subtle but varying width	pdl09 51	-21.04247	-70.1205	578.6	383575.19	7672743.28
231	45		37	C3 round areas with narrower connections verying width along		-21.0425	-70.12066	578.8	383558.59	7672739.84
232	30	*4	10	B3 with fresh openings deeper and narrower than previous		-21.04247	-70.12096	579.6	383527.39	7672742.94
233	55		4	A4 obvious depression, very rounded, continues in in to F2 surface		-21.0425	-70.12119	581.7	383503.52	7672739.46
234	35		31	B2-B3 we are now clearly to north of F2 island where crack continues		-21.04253	-70.12171	584.6	383449.50	7672735.75
235	45		13	C3 hard to see varies width		-21.04252	-70.12189	586	383430.79	7672736.73
236	25		339	B3 obscured somewhat by larger clasts	pdl09 52, pdl09 53	-21.04248	-70.12237	589.4	383380.88	7672740.81
237	35		346	B2-B3 along length, rounding, into F2	pdl09 54, pdl09 55, pdl09 spillover onto F	-21.04248	-70.12259	590.1	383358.02	7672740.65
238	25		356	B4 poor in F3, clear in abutting F2, super subte		-21.04244	-70.12349	596.4	383264.47	7672744.42
239				ending point		-21.04264	-70.12422	601.9	383188.76	7672721.74

F309 B

Waypoint	Halfwidth		Orientation	Type/ Description	Photos	Latitude	Longitude	Altitude	Eastings	Northings
240				starting point		-21.04254	-70.12554	612.2	383051.52	7672731.84
241	20		341	C2 subtle, hard to see, inconsistant, little fill		-21.04231	-70.12507	606.7	383100.18	7672757.65
242	20		0	B3-C3 (becomes more variable along length)		-21.04229	-70.12496	606.2	383111.59	7672759.94
243	12		15	A2 fresh		-21.04228	-70.1249	605.3	383117.82	7672761.09
244	25		14	continues into F2 A3-B2		-21.04227	-70.12483	605.8	383125.09	7672762.25
245	20		1	B3, barely there, ~40m long but comes up against very blocky material to south		-21.04226	-70.1248	604.6	383128.20	7672763.38
246		*2	9	A1 only discernible thing is fresh crack, lost in blockier material		-21.04223	-70.12466	604.1	383142.72	7672766.80
247		*1	4	A1 only fresh		-21.04221	-70.1246	602.9	383148.94	7672769.06
248	10	*1	351	A3 very clear but very rounded		-21.0422	-70.12445	602.4	383164.52	7672770.28
249	13		28	B2		-21.04216	-70.12428	602.1	383182.16	7672774.83
250	12	9	18	A3 slightly degraded with fresh		-21.04219	-70.12403	601.4	383208.16	7672771.69
251	14		325	B2-B3 continues through only a little into F2		-21.04219	-70.1237	599	383242.45	7672771.93
252	15		353	B2-B3 no clear continuation in F2		-21.04219	-70.12361	598.1	383251.80	7672772.00
253	20		355	C2 only visible ~40m		-21.04218	-70.12355	597.8	383258.03	7672773.15
254				now no larger material overlay, fine grains		-21.04215	-70.12342	598.3	383271.51	7672776.57
255	28		17	B3 yes into F2		-21.04215	-70.1234	598.1	383273.59	7672776.58
256	20		19	B3 yes into F2		-21.04213	-70.12329	597.8	383285.01	7672778.88
257	17		324	C2 yes into F2		-21.042	-70.12252	593	383364.92	7672793.83
258	27		358	B3 yes into F2, fresh		-21.04199	-70.12237	591.3	383380.50	7672795.04
259				ending point		-21.04199	-70.12234	591.6	383383.62	7672795.07

F309 C

Waypoint	Halfwidth		Orientation	Type/ Description	Photos	Latitude	Longitude	Altitude	Eastings	Northings
260				starting point		-21.0417	-70.12541	613.4	383064.37	7672824.92
261	11		40	A2-A3 obscured by large blocks		-21.04249	-70.12721	631.9	382877.94	7672736.15
262				ending point		-21.04286	-70.12771	639.6	382826.28	7672694.83

Table B.2: Continued

F309 D

Waypoint	Halfwidth		Orientation	Type/ Description	Photos		Latitude	Longitude	Altitude	Eastings	Northings
263				starting point			-21.04278	-70.12778	639.2	382818.94	7672703.64
264	80		44	A3 clear but rounded, too round for direct measure	pdl09 58		-21.0419	-70.12704	627.1	382895.15	7672801.59
265	60		34	D1 may be drainage but goes into F2 crack			-21.04177	-70.12674	624	382926.22	7672816.20
266				ending point			-21.0417	-70.12658	622.1	382942.79	7672824.06

F409 A

Waypoint	Halfwidth	actual	Orientation	Type/ Description	Photos		Latitude	Longitude	Altitude	Eastings	Northings
202				starting point	pdl09 41, pdl0942		-21.04402	-70.12594	618	383011.11	7672567.73
203		*2	4	B4 very subtle, points of A1 exposed			-21.04401	-70.12591	618	383014.22	7672568.86
204		*1-2	344	A1 fresh only			-21.04393	-70.12563	613	383043.25	7672577.92
205	6	*1-2	345	B2 subtle with some fresh openings along			-21.04391	-70.12555	613.9	383051.55	7672580.19
206	3	*1	347	A2			-21.04388	-70.12544	612.5	383062.96	7672583.59
207	10	*2	340	A2 with fresh	pdl09 43		-21.04382	-70.12527	610.6	383080.58	7672590.36
208	10	*2	342	B2 with fresh			-21.04383	-70.12523	610.3	383084.74	7672589.28
209	20	20 *2	0	A3 with fresh			-21.04382	-70.12512	610.1	383096.16	7672590.47
210	12	*1	1	B2 with fresh			-21.04379	-70.12505	609.4	383103.41	7672593.84
211	10	*1	358	B2 with fresh			-21.04378	-70.12497	608.9	383111.72	7672595.01
212	9	*	346	B3			-21.04377	-70.1249	607.7	383118.98	7672596.17
213	14		350	B3 with fresh, long but subtle	pdl09 44		-21.04377	-70.12483	607.2	383126.26	7672596.22
214	7	*	4	B4 really subtle			-21.04371	-70.12473	606	383136.60	7672602.93
215	6	*	347	B4 almost invisible with fresh			-21.0437	-70.12468	605.3	383141.79	7672604.08
216	14		339	B3 with fresh			-21.0436	-70.12427	601.9	383184.32	7672615.44
					numerous cracks iike this here (less than 30)						
217	14	*	338	C3 - 15m long	similar morphology		-21.04357	-70.1242	601.2	383191.57	7672618.82
218	10	*	354	B4 almost invisible			-21.04341	-70.12395	598.5	383217.42	7672636.71
219	6	*	308	D3 may be drainage with fresh			-21.0435	-70.1239	599	383222.69	7672626.78
220	15	*	10	B3 very rounded edges			-21.04346	-70.12373	597.3	383240.32	7672631.34
221	8		345	B3 very rounded edges			-21.04344	-70.12359	596.1	383254.85	7672633.65
222	17		347	B3 segmets of fresh			-21.0434	-70.12334	595.2	383280.80	7672638.26
						clearl affected by surrounding					
223	55	50	0	A2 goes directly into neighboring fan	pdl09 45, pdl09 46	material	-21.04326	-70.1228	591.3	383336.81	7672654.15
224		45	359	A2	pdl09 47		-21.04324	-70.12265	590.1	383352.38	7672656.48
225	60 (16)		2	A3 some perfect opening, but varied along strike	pdl09 48		-21.04322	-70.12243	588.2	383375.22	7672658.85
226	10		4	B2 does not continue into F2 island			-21.04324	-70.12232	587.5	383386.67	7672656.72
227		40	23	A2 does continue into F2 island			-21.04321	-70.12219	587.2	383400.15	7672660.14
228				ending point	pdl09 49, pdl09 50		-21.0432	-70.12208	587	383411.58	7672661.32

total opening	404	0.0012
Total length r	411.2567389	2.91789E-06
e	0.009921007	
%e	0.992100671	

Table B.2: Continued

S09 A Waypoint	Halfwidth	actual	Orientation	Type/ Description	Photos		Latitude	Longitude	Altitude	Eastings	Northings
172				starting point			-21.04393	-70.12096	578.8	383528.53	7672581.34
173	130	70	355	B2 lose definition along length, fresh	pdl09 34 pdl09 35		-21.04396	-70.12106	579.8	383518.16	7672577.94
174	45	20 *	6	goes from fresh only to A3 in F2/F4	pdl09 36		-21.04397	-70.12116	579.6	383507.78	7672576.76
175	20-60	*	14	B2-B3 fresh, fill hard to tell from surface material	pdl09 37		-21.04402	-70.12129	580.3	383494.31	7672571.13
176	60	*	13	B2 going from fresh only (A1) to rounded, wider crack			-21.04405	-70.12134	579.6	383489.13	7672567.78
177		20	40	A1			-21.04408	-70.12147	581.5	383475.65	7672564.36
178	35		32	C2 loses width, wobbly			-21.04409	-70.12155	582.2	383467.34	7672563.20
179	20	*	12	A1(fresh)- A3 degraged			-21.04411	-70.12162	582.4	383460.09	7672560.93
180	25	*	353	A3 degraded			-21.04413	-70.12171	582.9	383450.75	7672558.65
181	35		358	B3-B4 very subtle			-21.04416	-70.12187	584.1	383434.15	7672555.21
182	20		18	B2-B3 surrounding material extremely blocky	pdl09 38		-21.04418	-70.12197	585.6	383423.77	7672552.93
183	30		6	A2 but blocky surrounding can obscure	pdl09 39	thicker material	-21.0442	-70.12206	586.3	383414.43	7672550.65
184	10	*	341	A1-A2			-21.04424	-70.12238	587.7	383381.21	7672545.99
185		3	359	A1 open	pdl09 40		-21.04423	-70.1225	587.7	383368.74	7672547.01
186		14	1	A2-A4 along strike			-21.04424	-70.12258	589.9	383360.43	7672545.84
187	25	20	30	A2-B2 along strike			-21.0443	-70.12277	590.9	383340.73	7672539.06
188		10	358	A1 but only visible ~30m			-21.04431	-70.12307	593.3	383309.57	7672537.73
				blockiness and slope increasing			-21.04433	-70.1232	594.7	383296.07	7672535.42
190		6	13	B1 but only because of length			-21.04433	-70.1232	594.9	383296.07	7672535.42
191	5		338	B2 subtle but otherwise visible			-21.04442	-70.12372	599.7	383242.11	7672525.08
192	10		337	B2 same as above			-21.04445	-70.12386	600.9	383227.58	7672521.66
193		6	338	really short A2			-21.04448	-70.12397	600.7	383216.18	7672518.26
194		*3	342	A1-A2 only fresh ~30m long, some minor variation			-21.04449	-70.12402	601.9	383210.99	7672517.11
195		*2	353	fresh onl A1			-21.04462	-70.12436	604.8	383175.76	7672502.48
196	10		354	fresh-A2 maybe B2 because of subtlty			-21.04472	-70.12483	608.9	383127.00	7672491.06
197		*2	4	A1 fresh only			-21.04474	-70.12487	608.9	383122.86	7672488.82
198		*1-2	359	A1 fresh only, continue at least 30m			-21.04477	-70.12498	610.3	383111.45	7672485.42
199		*2-3	337	fresh A2 - mildly degraded			-21.04485	-70.12531	613.2	383077.22	7672476.32
200		*2	352	fresh, only 20m long A1 otherwise			-21.04491	-70.12544	615.4	383063.76	7672469.58
201				ending point			-21.0449	-70.12547	616.1	383060.64	7672470.67

total opening	573	0.012
Total length r	480.8012446	2.4959E-05
e	0.01206138	
%e	1.206138043	

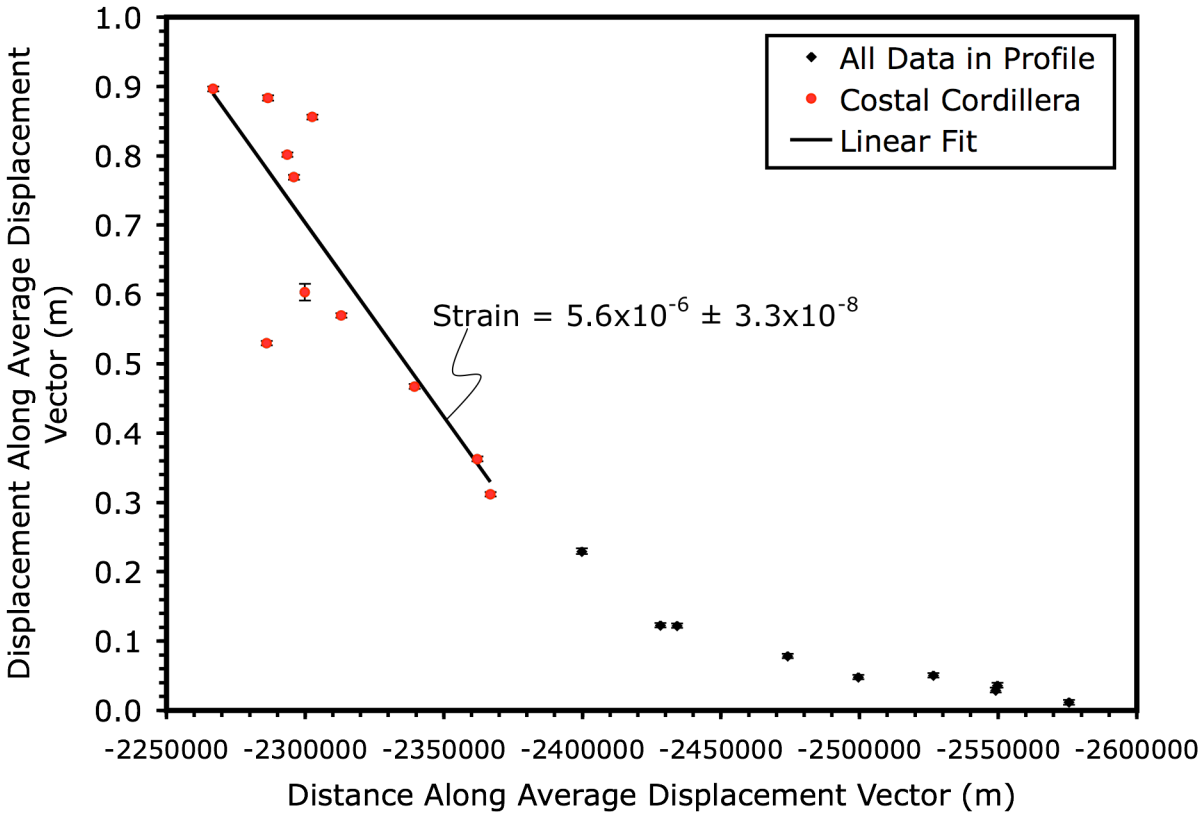

Figure B.3: 1D Coseismic extensional strain for 1995 Antofagasta earthquake from Klotz et al. (1999).

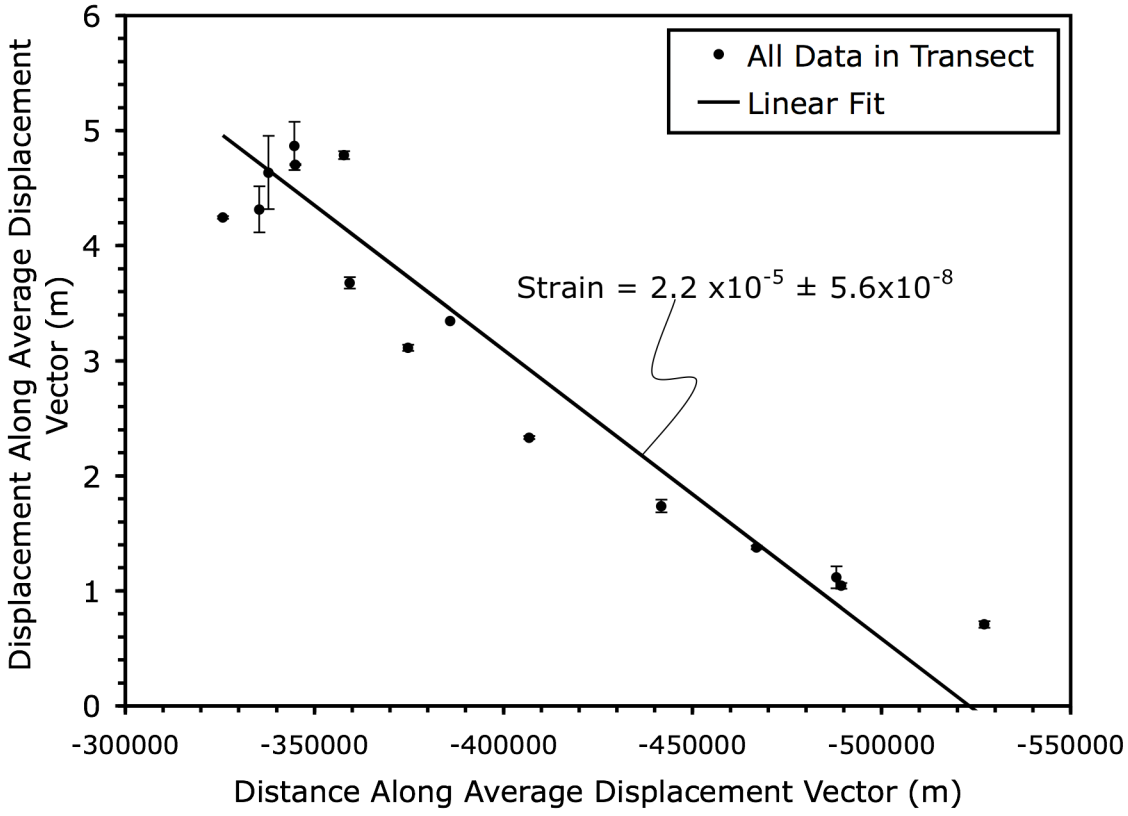

Figure B.4: 1D Coseismic extensional strain for 2010 Maule earthquake from Vigny et al. (2011).

Coseismic Extension Calculation for Tocopilla Earthquake

using Delaunay Triangulation

2012-01-16 03:39:13 +0000. 2D Strain calculation:

Reference frame = Undeformed configuration

Total number of stations = 3

Stations name: JRGN - MCLA - VLZL

Chi squared for least squares fit = 0.000000 (1 sigma errors shown below)

Cartesian components of translation vector:
-5.388265e+00 ± 6.121571e-02 -2.998861e+00 ± 6.121571e-02

Displacement gradient tensor:
1.005795e-06 ± 8.267618e-09 6.543224e-07 ± 8.351018e-09
1.860561e-06 ± 8.267618e-09 2.978191e-07 ± 8.351019e-09

Lagrangian strain tensor:
1.005797e-06 1.257442e-06
1.257442e-06 2.978194e-07

Magnitude and orientation (trend and plunge) of principal extensions:
emax: 1.958125e-06 ± 1.629844e-08 52.86° ± 0.05° 0.0°
emin: -6.545108e-07 ± 3.201986e-10 322.86° ± 0.05° 0.0°

Maximum shear strain magnitude:
2.612634e-06 ± 1.597821e-08 at 45.00 ± 0.00° to maximum principal strain axis

Volume strain (dilatation; -ve = excess shortening):
1.303613e-06 ± 1.661863e-08

Infinitesimal rotation axis (clockwise +ve):
Trend = 90.00°; Plunge = 90.00°; Magnitude = -3.455618e-05 ± 2.389236e-09

JRGN	-70.5749	-23.2889	327.8000	-0.1899	-0.1574	0.2361
MCLA	-70.2475	-22.7458	1033.2000	-0.1172	-0.0780	0.2664
VLZL	-69.9647	-23.1172	1555.3000	-0.1145	-0.0356	-0.0404

==========

Table B.3: 21Ne Surface Age Dating Results for Select Samples from the Punta de Lobos Fans

Sample Name		22Ne mol	er	20Ne/22Ne	er	21Ne/22Ne	er		Weight mg	21Ne cosmo mol/g		Age (yr) 20	er atoms/g/yr
S2P	Ne13305_F1P-200T200	7.1E-17	5.5E-18	9.86	1.01	0.0284	0.0027						
S2P	Ne13306_F1P-350T350	1.7E-16	6.8E-18	9.69	0.43	0.0414	0.0016						
S2P	Ne13307_F1P-550T550	1.4E-15	3.3E-17	9.99	0.09	0.0324	0.0004						
S2P	Ne13308_F1P-625T625	$	9.7E-18	9.48	9.68	0.0281	0.0293	Blank					
		1.6E-15	3.4E-17	9.95	0.30	0.0332	0.0010		222	3.1E-17	3.9E-18	9.4E+05	1.2E+05
AC1	Ne13310_AC1-200T200	3.7E-17	5.2E-18	9.71	1.95	0.0291	0.0054						
AC1	Ne13311_AC1-350T350	1.7E-16	6.7E-18	9.74	0.43	0.0383	0.0015						
AC1	Ne13312_AC1-550T550	9.8E-16	2.4E-17	9.92	0.10	0.0317	0.0004						
AC1	Ne13313_AC1-625T625	$	9.7E-18	9.25	6.52	0.0247	0.0189	Blank					
		1.2E-15	2.6E-17	9.89	0.31	0.0326	0.0010		241.2	1.8E-17	3.1E-18	5.5E+05	9.3E+04
AC3	Ne13328_AC3-200T200	1.1E-17	5.0E-18	9.93	6.02	0.0306	0.0171						
AC3	Ne13329_AC3-350T350	1.4E-16	6.4E-18	9.56	0.47	0.0342	0.0015						
AC3	Ne13330_AC3-550T550	1.2E-15	3.4E-17	9.88	0.09	0.0321	0.0004						
AC3	Ne13331_AC3-625T625	1.6E-16	1.0E-17	9.75	0.79	0.0314	0.0025						
AC3	Ne13333_AC3-625RT625	$	9.3E-18	9.49	8.97	0.0258	0.0261	Blank					
		1.5E-15	3.6E-17	9.84	0.33	0.0320	0.0011		241	2.1E-17	4.7E-18	6.4E+05	1.4E+05
AC2	Ne13334_AC2-200T200	3.3E-17	5.0E-18	10.19	2.13	0.0311	0.0060						
AC2	Ne13335_AC2-350T350	6.2E-17	5.2E-18	9.72	1.10	0.0403	0.0038						
AC2	Ne13336_AC2-550T550	7.8E-16	2.2E-17	9.88	0.11	0.0327	0.0005						
AC2	Ne13337_AC2-650T650	9.7E-17	9.7E-18	9.64	1.29	0.0324	0.0042						
AC2	Ne13338_AC2R-650T650	$	9.3E-18	9.68	6.02	0.0301	0.0187	Blank					
		9.7E-16	2.5E-17	9.85	0.38	0.0321	0.0013		237.3	1.7E-17	4.4E-18	5.2E+05	1.3E+05
S5P	Ne13342_F3P-200T200	8.7E-18	4.9E-18	8.52	7.31	0.0226	0.0187						
S5P	Ne13343_F3P-380T380	5.3E-17	5.1E-18	9.60	1.27	0.0422	0.0045						
S5P	Ne13344_F3P-580T580	8.5E-16	2.4E-17	9.92	0.11	0.0305	0.0004						
S5P	Ne13345_F3P-650T650	6.8E-17	9.5E-18	9.62	1.85	0.0301	0.0058						
S5P	Ne13346_F3P-650RT650	$	9.3E-18	9.35	6.25	0.0287	0.0193	Blank					
		9.8E-16	2.7E-17	9.87	0.40	0.0308	0.0013		218.6	9.3E-18	4.4E-18	2.8E+05	1.3E+05
S1P	Ne13348_F2P-200T200	8.7E-19	4.9E-18	7.74	70.32	0.0452	0.2894	Blank					
S1P	Ne13349_F2P-400T400	8.1E-17	5.5E-18	9.29	0.83	0.0566	0.0039						
S1P	Ne13350_F2P-580T580	9.9E-16	2.8E-17	9.83	0.10	0.0347	0.0005						
S1P	Ne13351_F2P-650T650	4.0E-17	9.3E-18	9.32	3.06	0.0369	0.0109						
S1P	Ne13352_F2P-650RT650	$	9.3E-18	10.22	8.27	0.0229	0.0221	Blank					
		1.1E-15	3.0E-17	9.77	0.38	0.0364	0.0014		155.9	5.5E-17	7.3E-18	1.6E+06	2.2E+05

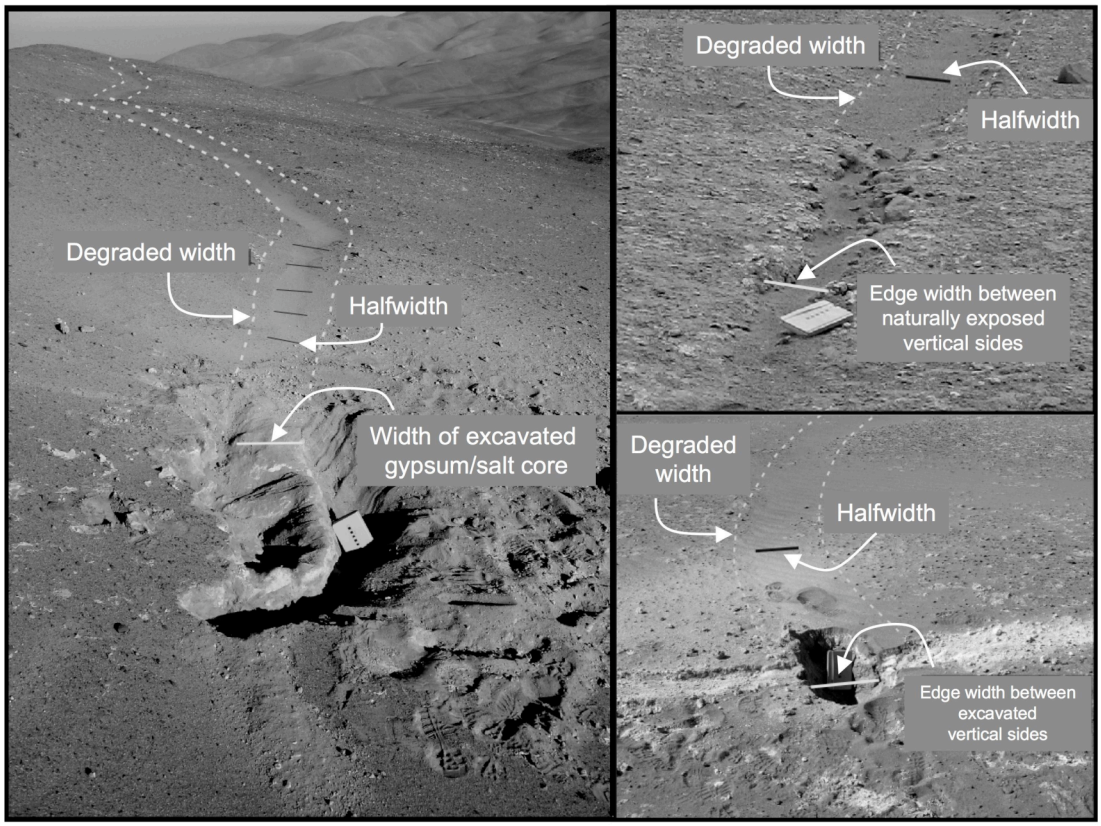

Figure B.5: Photos of excavated cracks used for comparison between halfwidth and true width for Figure 2.4. Three types of cracks were used: soft fill with hard core (left), naturally exposed edges (upper right), and soft fill and hard surrounding material (lower right). Measurements were completed using a cm-ruled tape measure.

Calculating Strain from Scanline Measurements

Strain for fan surfaces was determined using scanlines. Lines were walked approximately perpendicular to the crack population along the longest transects of each fan surface. Opening for each crack was determined using halfwidth and the total length of the line was determined using GPS. The measure of strain reported is extension, calculated as change in length / original length. For the scanline,s, that calculation is as follows:

$$\text{strain} = \text{extension} = \frac{\text{sum of opening from cracks}}{(\text{scanline length}) - (\text{sum of opening})}$$

APPENDIX C

SUPPLEMENTARY MATERIAL: TOOLS FOR INTERPRETING FIELD NOTES

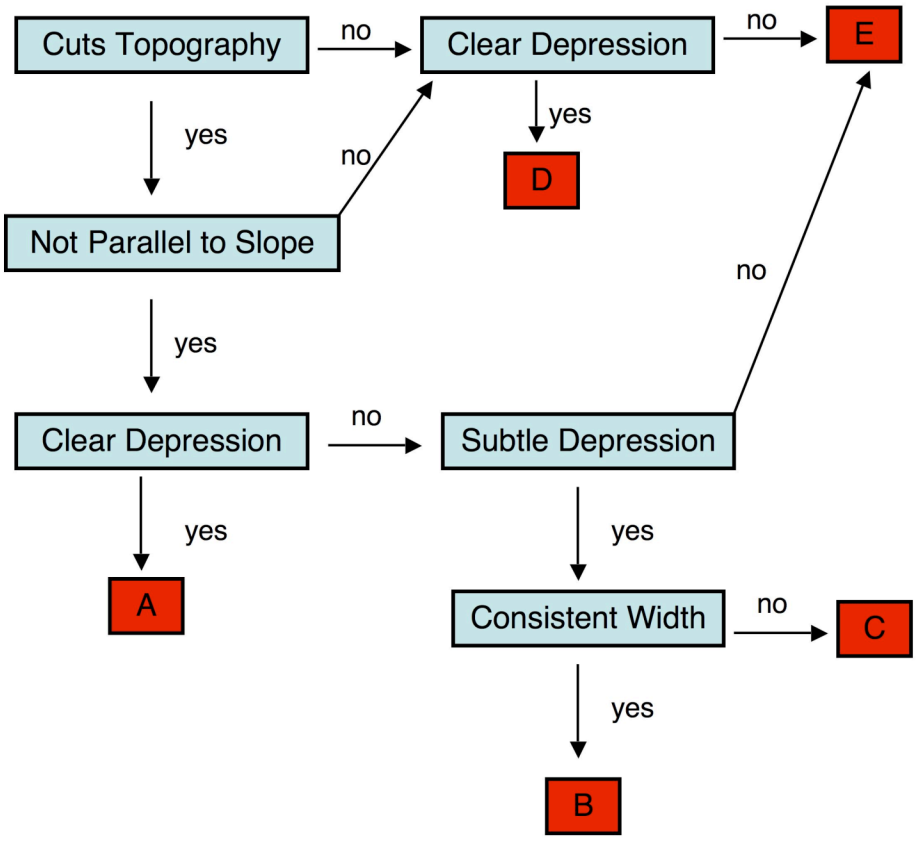

Figure C.1: Flow chart for crack qualification scheme as used in scanline and other field studies.

Table C.1: Detailed descriptions for crack qualification scheme as used in scanline and other field studies.

	A	B	C	D	E
1	• Little to no fill • Vertical Sides • Straight for 10's of meters • Continuous fo 50+ meters	• Little to no fill • Vertical to slightly degraded sides • Straight for 10's of meters • Continuous fo 50+ meters	• Little to no fill • Discernable boundaries • Straight for 10's of meters • Continuous fo 50+ meters	• Little to no fill • Straight for 10's of meters • Continuous fo 50+ meters	• Consistent width • Straight for 10's of meters • Continuous fo 50+ meters
2	• Little to mild fill •Slightly degraded sides • Straight for 10's of meters • Continuous fo 50+ meters	• Mild to moderate fill •Slightly degraded sides, mild rounding • Straight for 10's of meters • Continuous fo 50+ meters	• Mild to moderate fill •Discernable boundaries • Straight for 10's of meters • Continuous fo 50+ meters	• Mild to moderate fill • Straight for 10's of meters • Continuous fo 50+ meters	• Varying width • Straight for 10's of meters • Continuous fo 50+ meters
3	• Significant fill • Degraded sides, but clear boundary • Straight for 10's of meters • Continuous fo <50 meters	• Significant fill • Rounded crack sides, edges unclear • Straight for 10's of meters • Continuous fo <50 meters	• Significant fill • Boundaries unclear • Straight for 10's of meters • Continuous fo <50 meters	• Significant fill • Straight for 10's of meters • Continuous fo <50 meters	• Varying width • Straight for <10m • Continuous fo 50+ meters
4	• Fill reaching top of crack • Obscured crack edges • Straight for meters • Continuous fo <50 meters	• Fill reaching top of crack • Completely rounded crack sides • Straight for 10's of meters • Continuous fo <50 meters	• Fill reaching top of crack • Unlcear boundaries • Straight for 10's of meters • Continuous fo <50 meters	• Fill reaching top of crack • only mildest depression • Straight for 10's of meters • Continuous fo <50 meters	• Varying width • Straight for <10m • Continuous fo <50 meters

Table C.2: Fan surface labels for Punta de Lobos in field notes versus final figures

Name of Surface in Field Notes and Old Tables	Name of Surface Based on Stratigraphic Relationship
F2	S1
F1	S2
S	S3
F4	S4
F3	S5
B1	B1
Bajada	Bajada
Active Channel	Channel 1